UNIVERSITÀ DI PADOVA FACOLTÀ DI INGEGNERIA

DIPARTIMENTO DI INGEGNERIA DELL'INFORMAZIONE

SCUOLA DI DOTTORATO IN INGEGNERIA DELL'INFORMAZIONE

INDIRIZZO IN SCIENZA E TECNOLOGIA DELL'INFORMAZIONE

XXVII Ciclo

Efficient Spectrum Management as an Enabler Towards 5G Cellular Systems

Dottorando

FRANCESCO GUIDOLIN

Supervisore:

Chiar.mo Prof. Leonardo Badia

Direttore della Scuola:

Chiar.mo Prof. Matteo Bertocco

Anno Accademico 2014/2015

To my family
and to those who made this possible.

In memory of Giovanni.

Abstract

Advanced spectrum sharing and resource management techniques are needed in future wireless cellular networks to ensure high data rates to the end users. New system architectures will be required, taking into account aspects such as like spectrum resources availability, deployment and operational costs, as well as power consumption. Thus, it becomes key for the development of the fifth generation of cellular networks (5G) to pursue an efficient exploitation of the wireless medium, in the sense of both using advanced physical (PHY) layer techniques, and also seeking coordination among operators. In this thesis, we analyze the problem of spectrum management within the next generation of cellular networks and we propose new algorithms for spectrum sharing and for interference coordination.

In the first part of the thesis, we focus on the spectrum sharing between operators. Firstly, we develop a Long Term Evolution (LTE) standard compliant simulation environment extending the open-source network simulator ns3 to support multi-input multi-output (MIMO) systems and advanced beamforming systems. Then, we present a mathematical analysis for the network performance of non-orthogonal spectrum sharing, connecting it directly with the statistics of the radio channel and we develop some spectrum sharing algorithms considering different aspects of the operators coexistence. The analysis is further extended to the performance evaluation of more complex digital beamforming techniques developed in a multi-input-single-output (MISO) system allowing to reach a Pareto equilibrium between the operators. Finally, we consider also an orthogonal spectrum sharing scenario investigating the impact of asymmetries and dynamics of the user demands on the implementation of spectrum sharing techniques.

In the second part of the thesis, we extend the concept of spectrum management to two different scenarios. In the first scenario, we consider coordination between multiple cells, e.g. coordinated multipoint (CoMP). In particular, thanks to the exploitation of digital

beamforming techniques, we present a novel distributed clustering algorithm that adapts the cluster configuration according to the users distribution and the average cluster size. In the second scenario, we extend the concept of spectrum sharing to the coexistence between different communications system in order to study the feasibility of the deployment of the cellular systems within the mmWave spectrum. In particular, we analyze the impact of the novel cellular networks on the fixed satellite system (FSS).

In the last part of the thesis, we focus on the mobility management of the users in a heterogeneous network. Firstly, we focus on the average performance experienced by a mobile user while crossing a pico/femtocell, as a function of the handover parameters to provide an approximate expression of the average Shannon capacity experienced by a mobile user when crossing the femtocell. Then, we propose a Markov-based framework to model the user state during the handover process and, based on such a model, we derive an optimal context-dependent handover criterion.

Sommario

I futuri sistemi di comunicazione cellulare dovranno affrontare nei prossimi anni un rapido aumento della domanda di traffico dati mobile rendendo necessario l'utilizzo di avanzate tecniche di condivisione dello spettro e gestione delle risorse. Sarà quindi fondamentale lo sviluppo di nuove tecnologie che dovranno considerare aspetti quali la disponibilità di risorse spettrali, i costi di realizzazione ed il consumo di energia. La chiave per lo sviluppo della quinta generazione di sistemi cellulari (5G), sarà quindi la ricerca di un uso più efficiente delle risorse wireless, sfruttando nello stesso tempo le più avanzate tecniche a livello fisico e la coordinazione tra gli operatori. In questa tesi, vengono analizzati i problemi relativi alla gestione delle risorse spettrali nelle reti cellulari di nuova generazione proponendo nuovi algoritmi per la condivisione dello spettro e la gestione delle interferenze.

Nella prima parte di questa tesi vengono analizzate tematiche relative alla condivisione dello spettro tra operatori. In primo luogo è stata implementata un'estensione del simulatore di rete ns3, basata sullo standard Long Term Evolution (LTE) al fine di supportare l'analisi di sistemi multi antenna (MIMO) e di avanzate tecniche di beamforming. È stata quindi effettuata un'analisi matematica delle performance ottenibili dalla condivisione di spettro non ortogonale connessa direttamente al comportamento statistico del canale radio. Sono stati quindi sviluppati alcuni algoritmi di condivisione dello spettro considerando diversi aspetti della coesistenza tra operatori. L'analisi è stata quindi estesa alla valutazione di tecniche di beamforming digitale sviluppate in uno scenario multi-input-single-output (MISO) e atte a realizzare un equilibrio di Pareto tra gli operatori. Al termine di questa sezione sono inoltre stati analizzati alcuni scenari di condivisione ortogonale delle risorse, al fine di studiare l'impatto delle dinamiche degli utenti sulla implementazione delle tecniche di gestione delle risorse spettrali.

Nella seconda parte di questa tesi il concetto di gestione delle risorse è stato esteso a

due ulteriori scenari. Nel primo scenario, si è considerata la coordinazione tra celle diverse (CoMP). Nello specifico, grazie all'uso di tecniche di beamforming digitale, è stato ideato un nuovo algoritmo di clustering delle celle capace di adattare la configurazione dei clusters in relazione alla distribuzione degli utenti e alla dimensione dei cluster stessi. Nel secondo scenario, il concetto di condivisione di spettro è stato esteso alla coesistenza tra diversi sistemi di comunicazione, al fine di fornire uno studio di fattibilità sullo sviluppo dei sistemi cellulari all'interno dello spettro delle onde millimetriche. In particolare, è stato analizzato l'impatto delle nuove reti cellulari su sistemi satellitari fissi (FSS).

Nell'ultima parte delle tesi vengono invece trattati aspetti riguardanti la gestione della mobilità degli utenti all'interno delle reti eterogenee. Inizialmente, sono state analizzate le performance ottenute da un utente mobile nell'attraversare una pico/femto cella in funzione dei parametri di handover, al fine di fornire un espressione della capacità di Shannon media dell'utente. E' stato quindi proposto un modello basato su una catena dI Markov atto a studiare lo stato dell'utente durante il processo di handover e, sfruttando tale modello, è stato derivato un criterio di handover ottimale basato sulle condizioni del contesto.

Contents

List of Figures

Chapter 1

Introduction

In the last few years, a widespread diffusion of mobile phones, the appearance of novel applications for multi-media communications and the mobile Internet have caused a great demand for wireless connectivity all over the world. Cellular phones are nowadays seen as a universal gateway to be constantly connected and exploit a number of useful web-based applications. This has led to a tremendous improvements of the transmission capabilities of wireless cellular systems thank to the development of efficient standards, which exploit advanced modulation schemes and channel-aware transmission scheduling to achieve high data rates. For example, users of the current generation of cellular networks, such as the Long Term Evolution (LTE) of the Universal Mobile Telecommunications System (UMTS) [1], consider it normal to perform heavy traffic exchanges, e.g. , involving multimedia communications, through the wireless channel. In accordance with the forecast provided by the major global mobile operators the demand of high rate connectivity is still growing due to the diffusion of smarter end-user devices and machine to machine (M2M) communications. This evolution of the wireless network will bring together people, process, data and things to make networked connections more relevant and valuable but, at the same time, it will led to a huge increase of the number of required connections and signalling. For example, Fig. 1.1 shows the expected grow of data traffic by 2018 that will reach 15.9 exabytes per month by 2018, nearly a 11-fold increase over 2013 [2].

This connectivity hunger poses a great challenge to mobile operators and Internet service providers, in light of the strong limitations of resources available. For example, the NGNM (Next Generation Mobile Networks) Alliance has addressed the requirements on new gener-

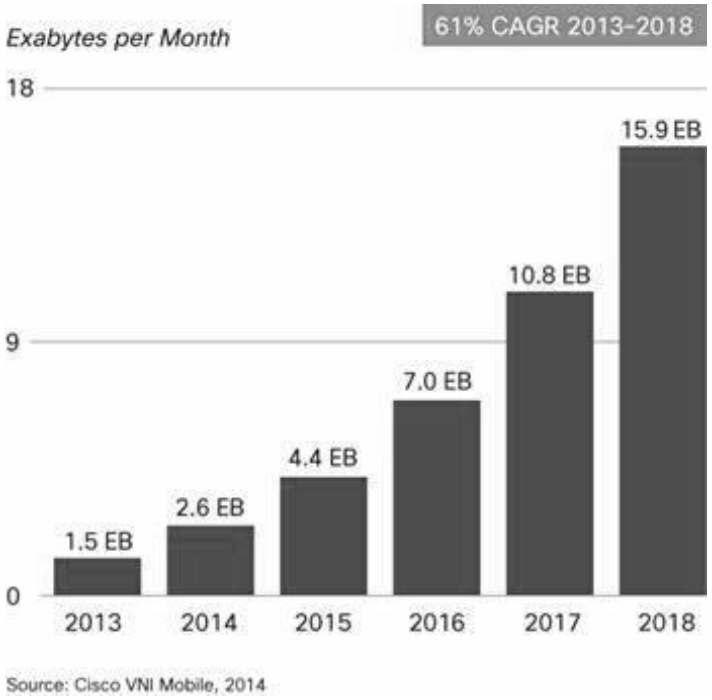

Figure 1.1. *Cisco forecast 15.9 Exabytes per month of mobile data traffic by 2018.*

ation mobile networks [3], which include increased spectral efficiency and re-use of existing infrastructure. New system architectures will be required, taking into account the power consumption of the terminals, the operational cost, and the constraints on the spectrum resources. In particular, heterogeneous networks (HetNets) have emerged as one promising configuration of NGMNs. While classical cellular networks have a ”flat hierarchy”, since wireless coverage is guaranteed by one layer of homogeneous Base Stations (BSs), HetNets utilize a higher density of BSs, also with different roles. In particular, ”pico” or ”femto” base stations (i.e., smaller nodes with reduced power and coverage) can be introduced to locally increase access to the network, even though this may also imply an overlap with existing top-layer BSs and therefore an increase of interference, that has to be properly managed [4]. In this scenario, some techniques for interference management, such as Statical Fractional Frequency Reuse (SFFR), can be employed, but they only mitigate the problem, without solving it. In the end, partitioning the frequency assignment into sub-allocations with exclusive usage may lead to improving the signal to interference plus noise ratio (SINR) perceived by the users, but at the price of decreasing the available bandwidth [5].

Therefore, many researchers advocate the need for an improvement in the radio spec-

trum usage, reached by *sharing*, as opposed to simply re-distributing, the available resources. Several papers, projects, and initiatives, have been aimed in the last years at quantifying how theoretical performance limits can pushed forward by sharing spectrum resources among the involved operators; this leads to estimating the achievable gains from both points of view of technical and also economic performance [6] [7] [8] [9]. This scenario has been investigated by the EU-funded project SAPHYRE [10] [11] with the aim to quantify the gain obtained by sharing resources in an inter-operator scenario. The aim of the project is not only to quantify if and how much the efficiency of resource usage can be improved, but also to identify new business models that can facilitate competition among the mobile networks and enhance the overall societal benefit. With a higher degree of competition on both spectrum and infrastructure, less regulation is needed, benefiting end users and society in general. We shall note that the European Commission (EC) has formulated a list of objectives for National Regulatory Authorities (NRA) to be taken into consideration [12]. Within the regulatory framework of electronic communications networks and services, these directives cover aspects such as competition on the market, efficiency of the spectrum usage and management, protection of customer benefits, limitation of radio interference, promotion of infrastructure investments.

Starting from a fixed assignment of the spectrum, there are several ways in which portions of the spectrum available to one or more operators can be used concurrently by all of them, Fig. 1.2. One possible solution is to open the spectrum usage of a particular channel to all operators, still constraining the actual allocation of the channel to only one user of a specific operator at a time. This kind of sharing, referred to as orthogonal spectrum sharing (OSS), can increase the multi-user diversity of the system, thereby improving the resource utilization efficiency [13]. In [14], this very approach is used to minimize the cell blocking probability by using the shared frequencies to enlarge the available bandwidth. Orthogonal sharing is relatively simple to implement, but provides performance gains only in asymmetric scenarios, i.e., whenever the amounts of traffic in the operators buffers are unbalanced. In fully loaded scenarios, the gain is given only by the increased multi-user diversity, and is marginal if the number of users is large [15]. A further improvement can be obtained by exploiting non-orthogonal spectrum sharing (NOSS) that allows multiple operators to use the shared spectrum resources at the same time. This configuration allocates multiple

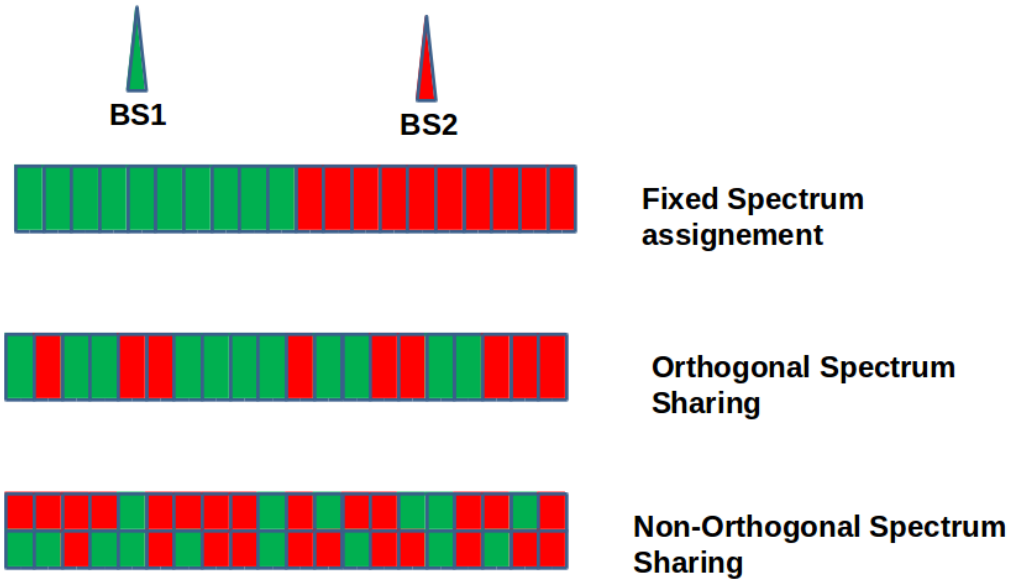

Figure 1.2. *Spectrum sharing configurations.*

users to the same frequency simultaneously, thereby causing a degradation of the Signal-to-Interference-plus-Noise-Ratio (SINR) at the intended receivers. The interference has to be controlled through the use of multiple antennas at the BS and proper mitigation techniques, such as beamforming [16].

Moreover, the sharing paradigm can be extended to the infrastructure through the use by the operators of the same communication point (IS-NOSS) with further improvement in terms of capital and operational expense (CAPEX, OPEX) costs [17]. In both cases the performance can be improved with the combined use of scheduling algorithms that consider the users related to the different operators as one pool, so as to exploit their channel characteristics.

A possible extension of the spectrum sharing concept can be the cooperation between BSs often referred to as coordinated multipoint transmission (CoMP) [18]. This technique encodes (for downlink; for uplink, it decodes) messages for multiple users, exploiting a distributed multiple-input multiple-output (MIMO) system [19]. Multiple BSs are grouped to form a CoMP cluster, which is the elementary coordination unit. Interference among BSs belonging to the same cluster is then cancelled to achieve a multiplexing gain [20]. Two transmission schemes are considered for downlink CoMP transmission: joint transmission

(JT) and coordinated scheduling/beamforming (CS/CB). In JT, the transmission to a single user is performed coherently by the BSs of the same CoMP cluster. Thus, interference is mitigated and the signal-to-interference-plus-noise ratio (SINR) is improved. As a special case, it may even be that only one BS of the cluster, e.g., the one with the best channel to the user, is allowed to transmit at a time, while the others are inactive [21]. Differently from JT, in CS/CB multiple users are allocated simultaneously in the same resource unit. In this case, the CoMP cluster forms a distributed MIMO system, where cooperative beamforming is adopted. By exchanging channel state information (CSI) among the BSs, linear precoding beamforming can be applied to mitigate the interference perceived by the users.

The tools exploited for the management of spectrum sharing can be applied also to study the coexistence among different wireless networks and, in particular, to analyze the feasibility of the deployment of the next cellular communications standard within novel spectrum bands. According to the vision of the major mobile cellular companies [22], the NGMNs will exploit the use of broad bands in millimeter wave (mmWave) frequency ranges. In particular, cellular allocations today are largely constrained under 6 GHz but it will be possible to obtain a spectrum 200 times greater by exploiting the frequencies between 20 and 300 GHz [23]. One of the candidate bands for the deployment of mmWave cellular mobile networks is the portion of spectrum between 17 and 30 GHz. Currently, part of this band is allocated on a co- primary basis to fixed services (FSs), cellular network back-haul, and fixed satellite services (FSSs) [24]. Therefore, it is important to study the possible coexistence between FSSs and mmWave mobile base stations (BSs) in order to preserve the functionalities of the satellite services.

Another challenge for the NGMNs and in particular for the HetNets is the management of the users mobility that, differently from the classical cellular networks, has to deal with cells of widely varying coverage areas. The current static setting of the handover (HO) process standardized by 3GPP is no longer effective for HetNet systems, because of the large variety in cell characteristics [25]. In particular, the number of handovers has a strong impact on the users Quality of Experience (QoE) due to the losses generated by the HO procedure and the signalling among the cells. Therefore, it will be crucial to regulate the users mobility considering the context parameters, such as the channel conditions, cell users loads, user position and speed.

In this thesis we study all these aspects from analytical and simulative points of view proposing novel algorithm for the resource scheduling and mobility management in a mobile cellular network. Firstly, we extend the well know open-source network simulator ns3 [26] with new functionalities to study the resource sharing among operators and the use of multi antenna systems. In particular, for the non-orthogonal spectrum sharing case we developed an extension of the ns3 LTE module able to support such scenarios and flexible enough to permit the validation of many new user-defined spectrum sharing algorithms. We consider the use of a 2×2 and a 2×1 MIMO systems in order to regulate the operator coexistence exploiting several linear precoding beamforming techniques. After an initial performance evaluation of the NOSS and OSS potentials, we study analytically the simultaneous usage of the spectrum resources to define the main system parameters and to provide a mathematical framework for the resource management. Starting from this analysis, we develop different resource scheduling algorithms that exploit in various ways the channel characteristics and the way the resources are shared, considering the total throughput and the fairness among the operators as performance metrics.

In the second part of this thesis, we apply the tools exploited in the NOSS scenario to the CoMP and to the coexistence between cellular networks and FSS. In the first case, we present a novel distributed clustering algorithm that adapts the cluster configuration according to the users distribution and the average cluster size. In the second case, we study the impact of the deployment of the NGMNs (5G) on the FSSs considering the metrics and the parameters provided by the standard. Moreover, we present a novel cooperative scheduling algorithm based on a game theoretic framework that, exploiting the use of analog beamforming at the BSs, meets the regulatory recommendation concerning the interference level at the FSS and at the same time provides a good user spectral efficiency. Finally, we develop a framework for the HetNets handover optimization, we compute the average Shannon capacity as a function of the handover parameters and we propose a optimization policy for the handover procedure based on the context informations.

The remainder of this thesis is organized as follows. Chapter 2 describes the implementation of the simulative framework that was exploited to provide the main results of this work. In particular, we focus on the implementation of a multi-antenna system and a spectrum sharing scenario within the ns3 simulator. Therefore, the NOSS and OSS scenarios are

analyzed statistically in Chapter 3 considering the use of MISO systems. Chapter 4 extends the analysis to more advanced spectrum sharing techniques as CoMP and the use of the mmWave spectrum for the NGMNs. A framework for the analysis and the optimization of the handover procedure in HetNets is provided in Chapter 5. Conclusions are given in Chapter 6.

The chapters were written by exploiting the material published in the papers reported in the section "List of publication", inserted at the end of this thesis. More specifically, the mapping is as follow:

- Chapter 2 is based on C1, C2 and C7.
- Chapter 3 is based on C3, C4 and J2.
- Chapter 4 is based on J1, C8 and C9.
- Chapter 5 is based on C5, C6 and J3.

Chapter 2

NS3 MIMO NOSS Extension

Starting in the mid-1990s [27], MIMO wireless communication has emerged as one of the most fertile areas of research in information and communication theory. The fundamental results of this research show that MIMO techniques have enormous potential to improve the spectral efficiency of wireless links and systems. These techniques have already attracted considerable attention in the cellular world, where simple MIMO techniques are already appearing in commercial products and standards, and more sophisticated ones are actively being pursued. Since the early 2000s, MIMO techniques have been adopted in cellular standards in parallel with the development of the MIMO theory. The earliest MIMO standardization focused on downlink single-user spatial multiplexing to address the demand for data downloading and higher peak data rates. Recently, there has been more interest in uplink MIMO, multiuser MIMO, and coordinated base techniques [28]. In this chapter we focus on the analysis of the performance provided by the MIMO techniques in a LTE scenario.

The main problem in the evaluation of MIMO systems is that, due to their mathematical complexity, their analytical assessment is often limited to simplified scenarios with a limited number of nodes. A way to address this problem may be to use simulation tools. Simulation platforms are used in the scientific community to test protocols and systems whenever the analytical tools are inadequate, because either the system is too complex or it cannot return a closed-form solution. In this chapter we describe our development of the ns3 simulator in order to provide a reliable framework for the analysis of the use of MIMO in a spectrum sharing context.

In the first part of this chapter we follow the approach of building an accurate repre-

sentation of a 2 $\times$ 2 MIMO system and integrating it with a simulator of an LTE network. It is worth noting that, while simulators can overcome some burdens of the mathematical analysis, they also have complexity issues. However, we found that implementing a 2 $\times$ 2 MIMO system represents a good compromise solution that meets all the requirements of manageability and realism. Provided that the simulator is modular enough, such a solution can be conceptually easy to extend to larger antenna arrays. We consider the ns3 network simulator [26], a well known open source tool that offers a modular and accurate representation of the whole protocol stack. We extend an existing LTE module of ns3, exploiting the post-processing SINR formulas for a MIMO system, which are investigated analytically in [29], [30]. The resulting software is not affected by the mathematical complications that plague the analytical evaluations. While computational complexity may be still an issue (however, for a 2 $\times$ 2 system it is fairly manageable), the simulator does not need to derive any closed-form solution. On the other hand, while the analytical approaches necessarily have to consider an abstract version of the upper layers, the simulator with our added modules is able to give a comprehensive system view. Thus, the degree of realism of the results is highly improved.

In the second part of this chapter the contribution is extended with a performance evaluation of a tunable representation of beamforming based on game theory [31]. Under this framework, we exploit the fact that efficient beamforming strategies achieve Pareto optimal (PO) operation points for the achievable data rates of the users, meaning that no user can be provided with a higher rate without another being worse off. In this context, we extend to a system-level perspective and for a realistic LTE scenario the analysis of [32]. Our work enables a comparison of different approaches and between theory and practically achievable performance.

Finally, we exploit the same simulative framework to demonstrate the advantages of non orthogonal spectrum sharing when compared to exclusive resource usage. In paticular, we decided to keep a general and modular approach, which can be used in a network simulator. Therefore, we abstract all the physical layer effects by considering the SINR to be regulated by a parameter that we call Interference Suppression Ratio (ISR). This parameter depends on the mutual interference among the operators and their capability of reducing it by proper interference suppression techniques, such as efficient beamforming. The quantification of

the ISR influences overall metrics such as capacity, throughput, and overall QoS of the system. Thus, by giving an estimation of this parameter, the performance of non orthogonal spectrum sharing can be characterized. In particular, we will show that for scenarios where the value of the ISR parameter can be considered realistic, non orthogonal sharing leads to significant gains compared to the exclusive bandwidth allocation.

2.1 State of the Art

The importance of developing an accurate simulation platform for complex communication systems such as an LTE network is self-evident, given that several details of the LTE standard cannot be adequately captured analytically. We focus here only on those solutions that meet generality and reproducibility requirements for scientific purposes, and aim at modeling the entire system, not just certain parts of it. In this spirit, there exist some system level simulators for LTE cellular systems that have been developed by equipment vendors, universities and research centers to realistically evaluate the performance of LTE. However, many of them do not make the source code publicly available. For example, a commercial physical layer simulation Toolbox implementation can be found in [33] or an LTE Specialized Model able to design LTE networks and devices is proposed in [34]. An open-source system level simulator developed in MATLAB is also presented in [35]; this work includes issues such as cell planning, scheduling and inter-cell interference but does not consider the upper layers of the protocol stack. We focus on extending an already available LTE module [36] of the open-source network simulator ns3 [26]. The code of the simulator is publicly available and several developers from the worldwide research community are free to contribute to it. The whole protocol stack is implemented; most of the modules involve the layers from datalink up, and this is true also for the models of LTE cellular networks. At the PHY layer, there is still room for many extensions, which should be produced in a modular fashion to be integrated with the rest of the existing implementations. Presently, the simulator is able to model a SISO channel and every aspect of multiple user medium access. Within this framework, the developers can test resource allocation algorithms for a plain network with single- antenna terminals. Our contribution extends this framework to MIMO, and does so in a separable manner from the rest of the simulator. We base our characterization of the MIMO system on existing analytical models and different practical implementations

of the MIMO rationale [29], [30], [37] [38] [39]. The ns3 simulator operates by deriving SINR metrics and evaluating the resulting performance indicators from them. This may involve the estimation of the Channel Quality Indicator (CQI) according to the LTE standard, or the evaluation of theoretical capacity metrics, e.g., according to Shannon's theorem. To keep the simulator approach modular, the overall idea is to exploit post-processing SINR formulas [29], so as to replace the plain evaluation of the ratio where interference is treated as noise with more advanced formulas, that depend on the applied policy for interference management. Similar formulas are used, e.g., to select an optimal subset of transmit antennas in a spatial multiplexing system in [40]. Our implementation includes several MIMO transmission schemes. LTE supports rank-1 transmit diversity and multi- rank transmission to select the optimal MIMO scheme that suits the channel conditions of the mobile. In rank-1 transmit diversity, the Alamouti space-time block code [37] is used, which improves the SINR at the receiver's side in case of high interference or weak signal. In multi-rank transmission multiplexing [38], [39] multiple information streams are sent to the receiver to increase throughput, but this solution is appropriate in high SINR regions with rich scattering environments.

2.2 Implementation of 2 $\times$ 2 MIMO for the ns3 Simulator

Our developed module implements two different MIMO transmission modes: Trasmission Diversity and Open Loop Spatial Multiplexing. The former has been implemented by closely following Alamouti's precoding scheme [37], while the latter makes use of several models proposed in [30] based on different receiver designs: zero forcing (ZF) [41], minimum mean-squared error (MMSE) and ordered successive interference cancellation based on MMSE (OSIC-MMSE) [42].

Although we modeled two transmit and two receive antennas, the traces used for the channel can be modified for other channel models or configurations and the SINR expressions can be extended to systems with a different number of antennas, precoding schemes or receiver implementations. The module creates three new classes that are inserted within the LTE module of ns3, *MimoRxSignal*, *ScmMimoChannel* and *TransmissionMode*, described in the following subsections.

2.2.1 MimoRxSignal

SISO systems require the knowledge of a single channel coefficient. For MIMO systems we need a matrix **H**, modeling the channels between all possible antenna pairs. The elements of **H** are complex coefficients h_{ij} representing the instantaneous gain due to fast fading from transmit antenna j to receive antenna i.

Class *MimoRxSignal* manages these parameters. It provides a flexible structure that includes a *MimoRx* object for every combination of a transmit and a receive antenna. *MimoRx* objects consist of four *SpectrumValue* [26] instances describing the power spectral density of the signal, the real part of the coefficient h_{ij}, the imaginary part of the coefficient h_{ij}, and the magnitude of the coefficient h_{ij}, respectively, in the domain of the whole LTE bandwidth. All the instances are populated by the class *ScmMimoChannel*.

2.2.2 *ScmMimoChannel*

For the channel model, we used several traces representing the complex coefficients h_{ij} for every LTE subframe, based on 3GPP SCM model [43]. The traces are generated offline by a two-step process. In the first step, a MATLAB script available at [44] is used to generate the time-domain coefficients $\eta_{ij}[n]$ with n as a time index. In the second step, we obtain the equivalent frequency-domain channel coefficients for every LTE resource block by Fast Fourier Transform. The downlink of LTE uses an Orthogonal Frequency Division Multiple Access (OFDMA) scheme, where the allocation atom is a time/frequency unit element referred to as Resource Block (RB), which consists of a subchannel in frequency for a subframe in time.

Thus, for every RB r we get a matrix of coefficients

$$\mathbf{H}[r] = \begin{pmatrix} h_{11}[r] & h_{12}[r] & \dots & h_{1S}[r] \\ h_{21}[r] & h_{22}[r] & \dots & h_{2S}[r] \\ \dots & \dots & \dots & \dots \\ h_{U1}[r] & h_{U2}[r] & \dots & h_{US}[r] \end{pmatrix} \tag{2.1}$$

where S is the number of transmit antennas, U the number of receive antennas and $r = 1, ..., N_{RB}$, with N_{RB} being the number of resource blocks. Coefficients $h_{us}[r]$ are derived through FFT from the multipath components $\eta_{ij}[n]$, so that the variability of the gains throughout the subchannels depends on the FFT, while over time it depends on the correlation of

Number of antennas at the transmitter	2
Number of antennas at the receiver	2
Distance between elements at transmitter in wavelenghts	6
Distance between elements at receiver in wavelenghts	0.4
Transmitter per path Angle Spread in degrees	2
Receiver per path Angle Spread in degrees	35
Number of paths — subpaths	6 — 20
Path power in dB	[-3,...,-16]
Path delays in μs	[10,...,60]
Receiver velocity in km/h	2

Table 2.1. *Channel parameters*

the $\eta_{ij}[n]$'s. Such a structure realistically generalizes to a $U \times S$ matrix the current model of a SISO channel with just one coefficient.

The channel parameters used to generate the trace inserted currently in the module are given in Table 2.1, while Fig. 2.1 shows the fast fading gain graphs obtained for two different antenna pairs in the resource-block/time domain.

2.2.3 TransmissionMode

The class *TransmissionMode* computes the post-processing SINR for the different MIMO systems implemented. The SINR formulas are based on [30] for a 2×2 MIMO system, with slight modifications for interference terms. for which we consider the possibility of multiple transmitters. Thus, we denote with h_{ijk} the term h_{ij} related to the kth transmitter. Also, the RB index r is omitted for notational simplicity, as the procedures are simply repeated for every RB.

For the **transmission diversity** case, which corresponds to transmission mode 2 of the downlink of the LTE standard [43], we considered the Alamouti scheme [37]. The SINR expression for the zth receiver, under the assumption that noise plus co-channel interference

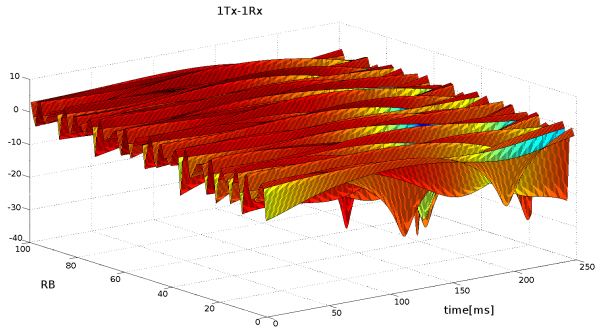

(a) Channel gain between antenna pair Tx = 1, Rx = 1

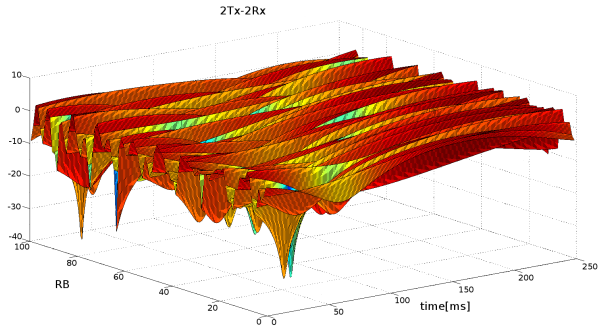

(b) Channel gain between antenna pair Tx = 2, Rx = 2

Figure 2.1. *Fast fading gain matrix for different antenna pairs*

can be treated as complex Gaussian [45], is

$$SINR_z = \frac{\sum_{i=1}^{N_{rx}} \sum_{j=1}^{N_{tx}} P_{zjk} \mid h_{ijk} \mid^2}{\sigma^2 + \sum_{m \neq k} \sum_{i=1}^{N_{rx}} \sum_{j=1}^{N_{tx}} P_{zjm} \mid h_{ijm} \mid^2} \tag{2.2}$$

where N_{rx} is the number of antennas at the receiver, N_{tx} is the number of transmit antennas, k is the index of the intended transmitter, $P_{zj\ell}$ is the power received at receiver z from the jth antenna of transmitter ℓ after path and shadow fading losses, and σ^2 is a noise term. Note that the SINR formula refers to the whole receiver z.

Conversely, in **spatial multiplexing** we need to know the SINR value for every antenna at the receiver's side. For the ZF receiver the SINR post-processing expression for the ith

antenna of receiver z is derived as [40]

$$SINR_{z,i} = \frac{P_{zik}}{\sigma^2 \left[H_k^* H_k\right]_{ii}^{-1} + \sum_{m \neq k} \sum_{j=1}^{N_{tx}} P_{zjm} |h_{ijm}|^2 [H_k^* H_k]_{ii}^{-1}} \tag{2.3}$$

where $N_{rx} \times N_{tx}$ matrix $\mathbf{H}_k$ refers to the intended transmitter.

In the case of an **MMSE receiver**, the SINR is [30]

$$SINR_{z,i} = \underline{h_{ik}^*} R_{ik}^{-1} \underline{h_{ik}}, \quad \text{where:}$$

$$R_{ik} = \underline{h_{\ell k}} \underline{h_{\ell k}^*} + \frac{\sigma^2 + \sum_{m \neq k} \sum_{j=1}^{N_{tx}} P_{zjm} |h_{ijm}|^2}{P_{zik}} \mathbf{I}_2, \; i \neq \ell \tag{2.4}$$

where ℓ is the other antenna than i, $\mathbf{I}_2$ the 2×2 identity matrix, $\underline{h_{ik}}$ the ith column of $\mathbf{H}_k$, and $*$ denotes conjugate transpose.

The **OSIC-MMSE** case is an improvement of MMSE, where ordered successive interference cancellation is performed [27]. The related SINR post processing expression is obtained differently for the two antennas; first, SINR MMSE post-processing is applied for both antennas, then the substream with the highest SINR is detected and cancelled. If we denote it with i then its SINR is still according to (2.4). Instead the other substream, labeled l is computed as:

$$SINR_{z,\ell} = \frac{\underline{h_{jk}^*} \underline{h_{jk}} P_{z\ell k}}{\sigma^2 + \sum_{m \neq k} \sum_{j=1}^{N_{tx}} P_{zjm} |h_{\ell jm}|^2}. \tag{2.5}$$

In all the MIMO schemes described above, perfect knowledge of the channel at the receiver is assumed.

The UML sequence diagrams reported in Figs. 2.2 and 2.3 describe the interactions between the new classes and the existing LTE modules of ns3. Fig. 2.2 represents the transmission of a signal, and shows that the new classes *ScmMimoChannel* and *MimoRxSignal* are connected to the class *SingleModelSpectrumChannel* belonging to the Spectrum Framework of ns3 through the methods of the *SpectrumPropagationLossModel* class and the *LtePropagationLossModel* class [36]. Fig. 2.3 shows instead the receiver's operation. The class *LteSpectrumPhy* separates the useful signal from interference to compute the SINR from the *LteInterference* class. Within the instance transmission mode the programmer can set, directly from the

simulation script, a variable *t-mode* in order to redirect the method *ComputeSinr(..)* into the MIMO scheme of choice.

In terms of computation complexity, using MIMO schemes with the proposed approach increases the load by a factor of $N_{rx} \times N_{tx}$. Interestingly, the new classes proposed can be applied with relatively minor modifications to any other air-interfaces using OFDMA for multiple access.

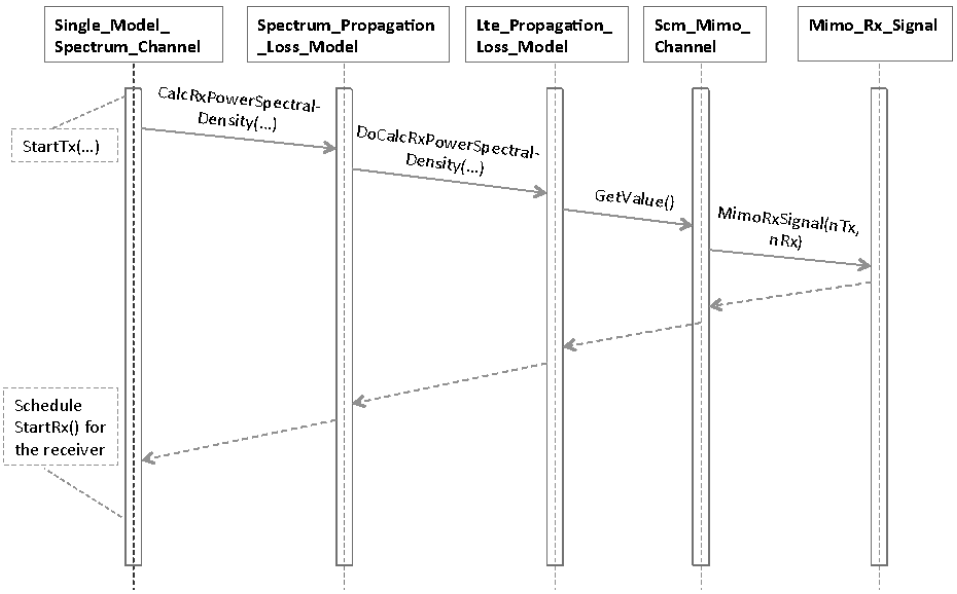

Figure 2.2. *StartTx method for the transmitter*

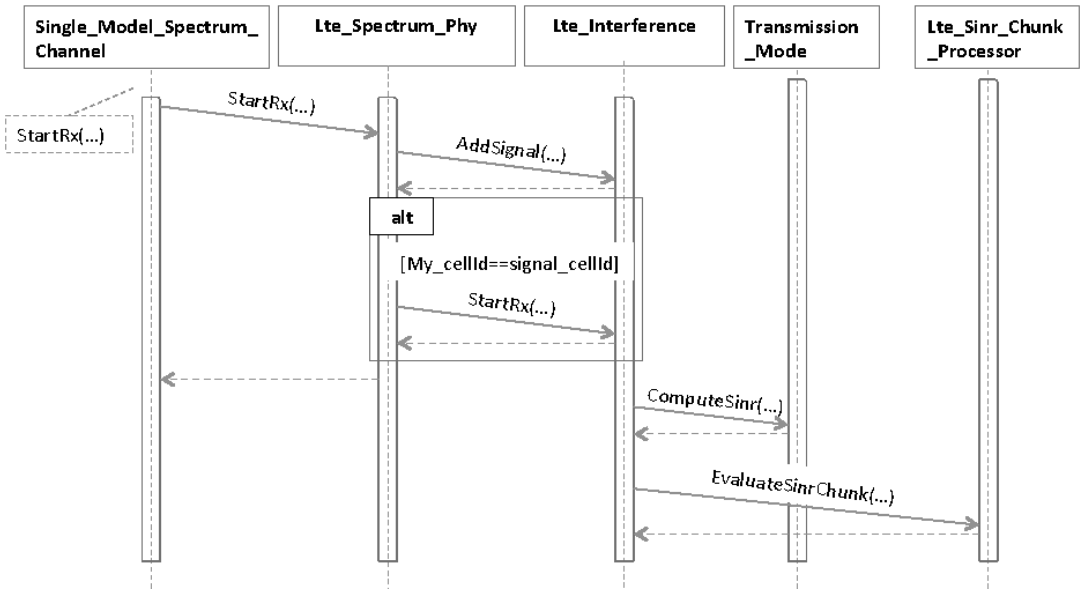

Figure 2.3. *StartRx method for the receiver*

2.2.4 Simulation Results

We ran two simulation campaigns using the approach implemented in ns3 that computes the Transport Block size considering the modulation and coding as per the standard specification.

In the former, we compare the simulation results with the approaches proposed in the literature to test the accuracy of our implementation. The analytical results may have limited validity in practical cases, as they necessarily neglect certain implementation aspects of the LTE standard (e.g., that the data rate is upper bounded by the highest order modulation scheme). Our simulation framework closely matches the analytical results where they are meaningful, while it generalizes them when they are no longer consistent with the system at hand (e.g., in high SINR regions).

In the latter campaign, we compare different MIMO schemes in terms of their spectral efficiency in the downlink. The purpose is to show that, even though some schemes cannot be evaluated through exact mathematical formulas, the simulator is still able to offer a quantitative comparison.

Center frequency	2.1 GHz
Channel Bandwidth	5 MHz
Subcarrier Bandwidth	15 kHz
$RB_{bandwidth}$	180 kHz
$RB_{subcarriers}$	12
Noise figure	5 dB
Noise Spectral Density	-174 dBm/Hz
Path loss model	COST Hata model (suburban areas)
BS antenna height	32 m
MS antenna height	1.5 m
Frame duration	10 ms
TTI	1 ms
Simulated interval	25 s

Table 2.2. *Simulation parameters*

The main system parameters used in the numerical evaluations are reported in Table 2.2. Both campaigns consider a single cell scenario, therefore intercell interference is absent and SINR simply becomes SNR (Signal-to-Noise Ratio). This choice is not due to a limitation of the simulator, but rather to make a meaningful comparison with the analysis. We remark that the extension to multiple cells would be straightforward in the simulator (but not in the analytical framework).

Fig. 2.4 shows the results obtained by the first simulation. The theoretical curves are given by the formula provided in [29], whose parameters have been also fitted to our scenario and the LTE standard. The value of the SNR is given by the ratio between the power at the receiver after macro and shadow fading losses and the noise value. Note that the channel model is slightly different from that considered in [29]; in spite of that, simulated and theoretical curves are similar below 35 dB, after which we obtain a saturation of the simulated curves. As argued above, this effect is due to the configuration of the LTE system which reaches at high SNRs, the most efficient modulation and coding scheme in transmission. Moreover, Fig. 2.4 shows that the performance of the ZF system is better than that of the SISO system for high SNR, and this behavior matches what expected from the theoretical analysis.

The theoretical approach used in [29] provides the performance analysis only in the cases of SISO and ZF systems. However, thanks to our module we can extend the same analysis to the transmit diversity case and to other spatial multiplexing cases. Our second simulation campaign, whose results are reported in Fig. 4.1, investigates the performance of the different MIMO schemes implemented in the module in terms of spectral efficiency. As in Fig. 2.4, the SNR considered is the ratio between the power at the receiver after macro and shadow fading losses and the noise value. An analysis of the curves related to the MIMO spatial multiplexing schemes (ZF, MMSE, OSIC-MMSE) highlights that the OSIC-MMSE receiver, thanks to the iterative signal detection, achieves the best performance. Comparing the MIMO-MMSE curve with the MIMO-ZF curve, we notice that the MIMO-MMSE receiver provides better performance than MIMO-ZF below an SNR of 20 dB. This behavior is due to the improvement given by MMSE over ZF to reduce the impact of noise, and it is more pronounced in the region of low SNR.

Alamouti MIMO is the only diversity-based scheme included in our framework. This

kind of system aims at improving the post-processing SNR at the receiver. In Fig. 4.1, we see how the Alamouti system achieves the best performance in the low SNR region. This result confirms that spatial multiplexing MIMO solutions are optimal only for high SNR (or SINR).

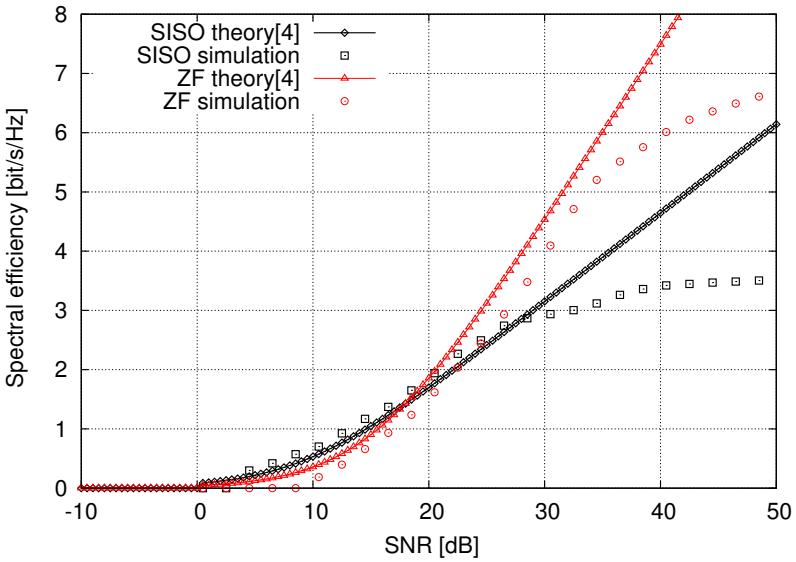

Figure 2.4. *Theoretical versus simulated spectral efficiency*

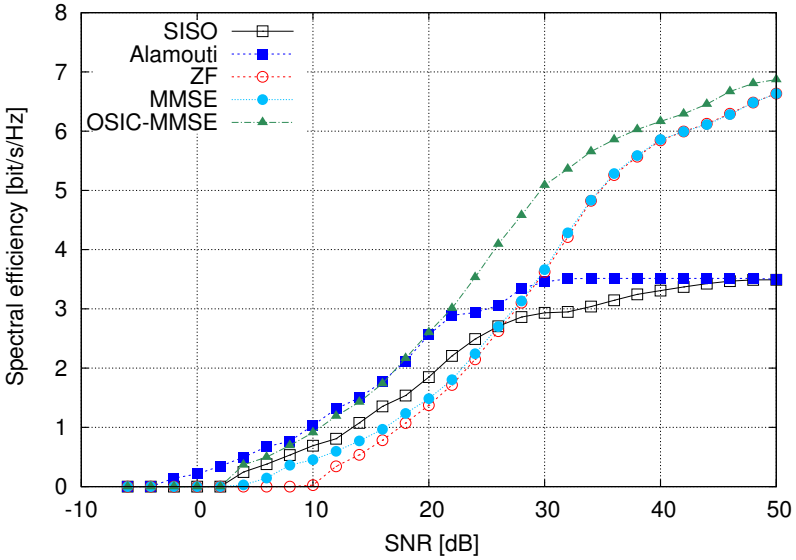

Figure 2.5. *Comparison among the implemented MIMO schemes*

2.3 Extension to a MISO beamforming system

In this extension of the ns3 framework, we will focus on the scenarios of Fig. 2.6, i.e., a multiple-input single-output (MISO) downlink where the BS and the UE have two and one antennas, respectively.

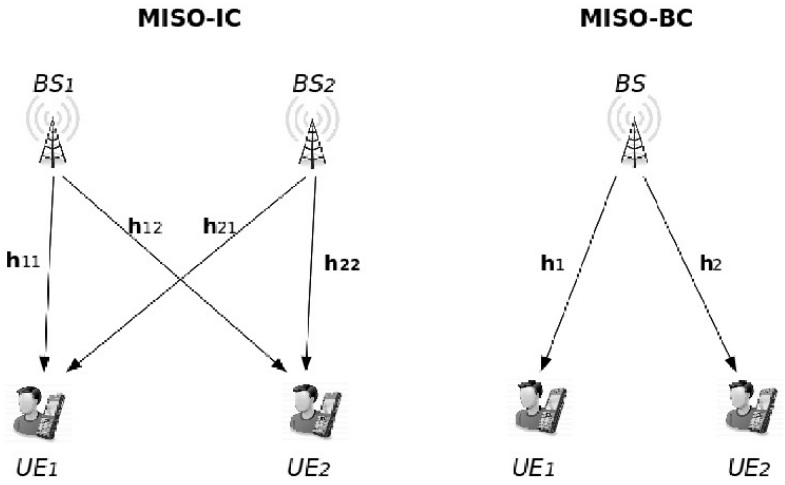

Figure 2.6. *MISO-IC and MISO-BC scenarios*

We consider the two applications of MIMO [46] shown in Fig. 2.6: (i) two neighboring BS-UE pairs that operate simultaneously on the same band, a scenario known as MISO interference channel (IC); (ii) a BS that serves two UEs in a MU mode, realizing a MISO broadcast channel (BC). From the network point of view, MISO-IC corresponds to two operators coexisting in the same geographical area and coordinating their operation, whereas MISO-BC can be realized by either a single operator or even two operators sharing the infrastructure (so that one transmitter can serve users of different operators). In particular, we analyze the performance of different transmit beamforming vectors that, applied to the users streams, achieve several PO operation points. The linear transmit beamforming vectors are computed using the points of the Pareto boundary curve provided by the closed-form parameterization developed in [31]. As examples, we select three PO beamforming configurations, corresponding to three different points of the Pareto boundary, which pursue three different global objectives: sum rate (SR), proportional fairness (PF) and max-min fairness (MMF) [32]. That is, SR selects the point that maximizes the sum of the individual rates, PF maximizes the product of the rates of the two users, while MMF maximizes

the minimum of the two rates. These techniques are compared with ZF and maximum rate (MR) beamforming vectors. The former entirely cancels the interference created by the other link, while MR maximizes the transmission rate on each link assuming that interference is absent. All these techniques are studied specifically focusing on an LTE system; thus, we also include a heuristic re-scaling of LTE capacity to obtain realistic performance, which is performed with a fully independent approach.

For a fair comparison, the total amount of power available for the downlink is equal to P in both cases, and is equally distributed among the users. That is, both BSs in MISO-IC have a power budget of $P/2$, and the BS of MISO-BC can be seen as a superposition of the BSs from the MISO-IC case. In both cases, the network operators controlling the BSs are willing to cooperate by sharing channel information, so that a (nearly) perfect global knowledge of the channels at the transmitters can be assumed. This makes it possible to counteract mutual interference and improve channel usage.

2.3.1 Pareto optimal beamforming models

We assume perfect collaboration among the operators of the BSs; every resource allocation is performed with full knowledge of the (conjugated) complex coefficients (denoted as $\mathbf{h}_i$ or $\mathbf{h}_{ij}$) of the channels between the antennas of each BS and UE. The channel vectors incorporate the effects of path loss, shadowing, and fast fading.

We use the implementation of a 2×2 MIMO system depicted in the previous section, on top of which we consider beamforming techniques and the MU approach. We take the linear transmit beamforming from the LTE module of ns3, with methods providing the post-processing SINR values for SR, PF, MMF, ZF and MR, in the MISO-IC and MISO-BC scenarios.

For MISO-BC, the SINR at UE$_i$, $i, j \in \{1, 2\},\ j \neq i$, is

$$\text{SINR}_i = \frac{p_i |\mathbf{h}_i^H \mathbf{w}_i|^2}{p_j |\mathbf{h}_i^H \mathbf{w}_j|^2 + \sigma_i^2} \tag{2.6}$$

where p_i is the transmit power and $\mathbf{w}_i$ is the linear transmit beamforming vector applied to the signal intended for UE$_i$ and σ_i^2 is the receiver noise variance.

For MISO-IC, the SINR at UE$_i$, $i, j \in \{1, 2\},\ j \neq i$, is

$$\text{SINR}_i = \frac{p_i |\mathbf{h}_{ii}^H \mathbf{w}_i|^2}{p_j |\mathbf{h}_{ji}^H \mathbf{w}_j|^2 + \sigma_i^2} \tag{2.7}$$

with the same meaning of the variables as before.

To compute the SINR at each receiver we need the beamforming vectors $\mathbf{w}_1$ and $\mathbf{w}_2$, which are a combination of the channel coefficients related to the intended signal and the interfering signal [32]. Thus, we expand the *LteSpectrumPhy* class to keep track of the *MimoRxSignal*, and the channel gains between the receivers and their respective intended and interfering transmitters. These matrices are then used by the methods of *TransmissionMode* to compute the beamforming vectors, and then the receiver SINR.

For MISO-BC and MISO-IC, ZF beamforming is given by

$$\mathbf{w}_i^{ZF} = \frac{\mathbf{P}_{\mathbf{h}_j}^{\perp}\mathbf{h}_i}{\|\mathbf{P}_{\mathbf{h}_j}^{\perp}\mathbf{h}_i\|} \quad \text{and} \quad \mathbf{w}_i^{ZF} = \frac{\mathbf{P}_{\mathbf{h}_{ij}}^{\perp}\mathbf{h}_{ii}}{\|\mathbf{P}_{\mathbf{h}_{ij}}^{\perp}\mathbf{h}_{ii}\|} \tag{2.8}$$

respectively, where $\mathbf{P}_{\mathbf{h}_j}^{\perp} \triangleq \mathbf{I} - \mathbf{h}_j(\mathbf{h}_j^H\mathbf{h}_j)^{-1}\mathbf{h}_j^H$ and $\mathbf{P}_{\mathbf{h}_{ij}}^{\perp} \triangleq \mathbf{I} - \mathbf{h}_{ij}(\mathbf{h}_{ij}^H\mathbf{h}_{ij})^{-1}\mathbf{h}_{ij}^H$.

The MR beamforming matrix $\mathbf{w}_i^{MR}$ is

$$\mathbf{w}_i^{MR} = \frac{\mathbf{h}_i}{\|\mathbf{h}_i\|} \quad \text{and} \quad \mathbf{w}_i^{MR} = \frac{\mathbf{h}_{ii}}{\|\mathbf{h}_{ii}\|} \tag{2.9}$$

for MISO-BC and MISO-IC, respectively.

The beamforming vectors that achieve different points on the Pareto boundary are represented [32] as linear combinations of $\mathbf{w}_i^{ZF}$ and $\mathbf{w}_i^{MR}$ for real λ_i, with $0 \leqslant \lambda_i \leqslant 1$:

$$\mathbf{w}_i(\lambda_i) = \frac{\lambda_i\mathbf{w}_i^{MR} + (1-\lambda_i)\mathbf{w}_i^{ZF}}{\|\lambda_i\mathbf{w}_i^{MR} + (1-\lambda_i)\mathbf{w}_i^{ZF}\|} \tag{2.10}$$

This parameterization holds for both MISO-IC and MISO-BC. By choosing particular values for λ_1 and λ_2, as per [32], it is possible to obtain the vectors corresponding to the SR, PF, MMF points and then compute the respective SINRs.

2.3.2 Numerical Results

We simulate with ns3 the configurations described above, obtaining the achievable rate region and the Pareto curve in an LTE context fixing the distance between the BSs and between the UEs and the serving BS to 1.5 Km. Table 2.2 reports the system parameters. The wireless channel model exactly follows propagation and fading models of the LTE standard [1].

First, we aim at comparing the theoretically achievable rate of the channel with the actual *spectral efficiency* of the LTE network, denoted with ν and computed as the ratio between

the throughput and the channel bandwidth used. The throughput, in turn, depends on the transport block (TB) size of LTE, determined by the modulation and coding scheme, also computed according to LTE specifications, see [1]. Since we expect the actual spectral efficiency to be significantly lower than the theoretical rate, these results are further compared with a heuristic estimate of the actual throughput of LTE, taken from [47], which takes into account the signaling overhead. The idea is to weigh the theoretical achievable rate of the system with a coefficient lower than 1, derived as follows: first, a scaling coefficient that adjusts the system bandwidth efficiency of LTE is set depending on the TB size, for which we took the same values reported by [47] as their SISO system has the same TB as ours. Moreover, a scaling coefficient for the SNR is also considered depending on the target BER. The result is a rescaling of the theoretical value, which is therefore totally independent of our simulation experiments. Note that, while the analytical model is manageable only for a 2×1 MISO, the simulator can operate with larger systems as well.

Figs. 2.7 and 2.8 show the achievable rate region of one specific channel realization for MISO-BC and MISO-IC, respectively. These curves are shown just as sample results, to confirm the validity of the analytical framework; actually, any other channel realization performs in a qualitatively similar way, hence Figs. 2.7 and 2.8 are representative of a general behavior. While the achievable rate curve and the actual spectral efficiency are qualitatively similar, the simulated results closely match the heuristic evaluations of [47] also from a quantitative standpoint. However, there is a significant gap between the theoretical Pareto boundary and the actual LTE throughput. Also, the simulated values have coarser granularity (i.e., the LTE spectral efficiency curve has fewer points), due to the quantization in mapping the SINR values to a finite number of TB choices, as opposed to a continuous rate value. The figures also show the SR, PF, and MMF points along the Pareto boundary curve, their projections on the theoretical LTE rate curve, and the simulation results.

Our evaluations are not limited to a single channel trace, as the simulator is also able to show dynamic evolution over time-varying channels. Figs. 2.9 and 2.10 consider multiple channel realizations and compare different beamforming techniques, for both MISO-BC and MISO-IC in terms of the cumulative probability distribution of the spectral efficiency. The results show that MISO-IC outperforms MISO-BC, i.e., beamforming is more efficient for inter-cell interference cancellation than spatial multiplexing, due to the distance among the

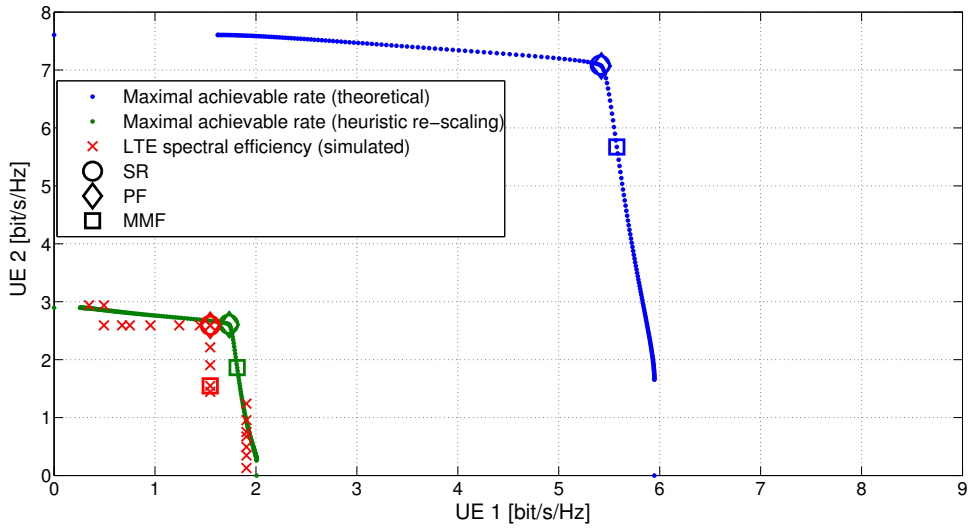

Figure 2.7. *Theoretical vs. simulated rate regions for MISO-BC*

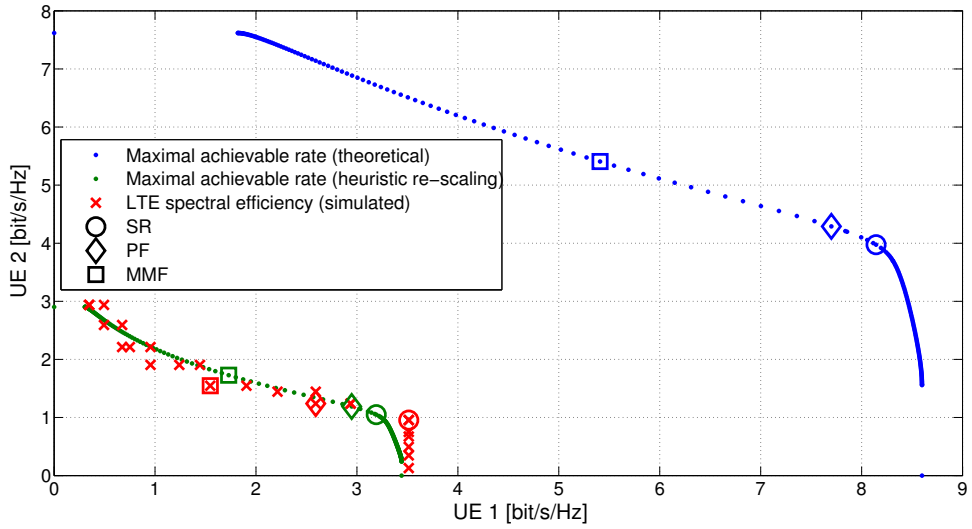

Figure 2.8. *Theoretical vs. simulated rate regions for MISO-IC*

BSs that decreases the interference at the receivers. This conclusion actually depends on the interference management technique, e.g., there is no improvement for ZF, which cancels the interference anyway. MR gets the worst spectral efficiency, thereby confirming that an uncoordinated interference management is not recommended for efficient communication. The linear beamforming for SR achieves the best total spectral efficiency on the Pareto boundary, but the difference with other techniques may be limited due to the quantization of the TBs. We remark that these results incorporate many details of the LTE standard, and therefore

represent more realistic evaluations than those generally available in the literature.

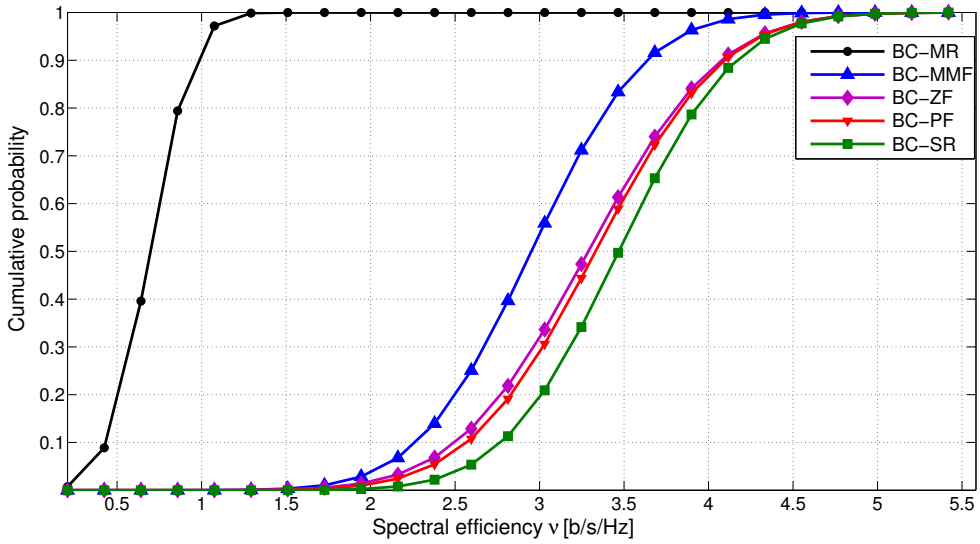

Figure 2.9. *Spectral efficiency comparison for a MISO-BC scenario*

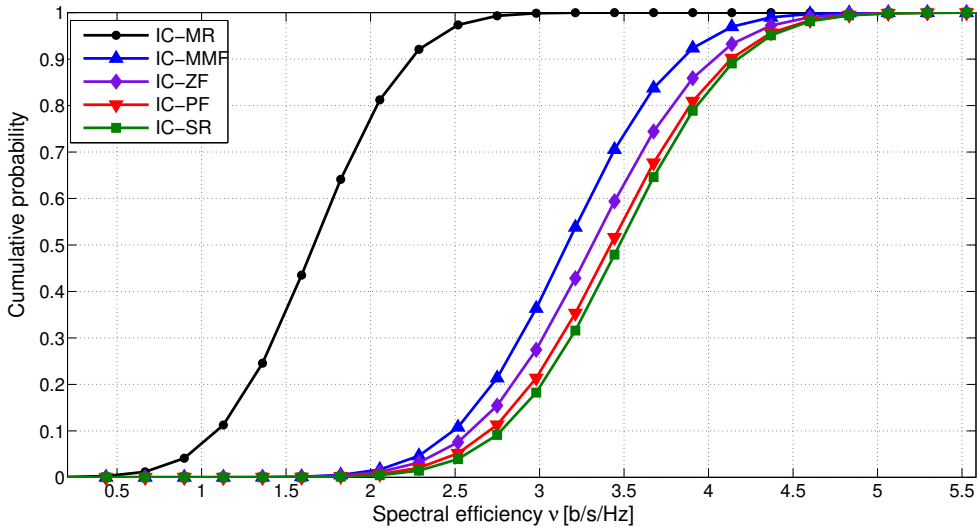

Figure 2.10. *Spectral efficiency comparison for a MISO-IC scenario*

We also compare the techniques in terms of *fairness* of rate allocations. Fig. 2.11 reports an index of fairness IF equal to:

$$IF = \frac{\min(\nu_1, \nu_2)}{\max(\nu_1, \nu_2)} \in (0, 1] \tag{2.11}$$

where ν_i is the spectral efficiency of user i. We exclude the MR approach that does not

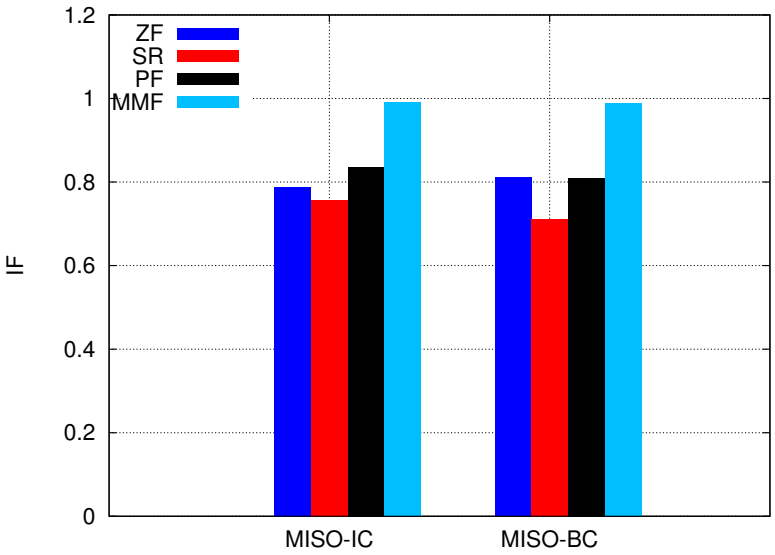

Figure 2.11. *Fairness of the schemes implemented*

involve cooperative transmission and would give meaningless results. The highest IF is reached by MMF that aims at $\nu_1 = \nu_2$. In MISO-BC, this technique gains 18% over PF and 27% over the SR approach. Comparing the results of MISO-BC and MISO-IC, we notice how the latter corresponds to a gain of 6.3% for SR. This is due to lower interference at the receivers, which implies a weaker influence of the used beamforming technique on the SINR perceived by the users. In the ZF case, IF reaches an intermediate value; indeed, while the interferers are entirely suppressed, fairness is not a primary objective.

2.4 A framework for spectrum sharing evaluation in LTE networks

The exact characterization of spectrum sharing in a network-wide scenario may be extremely challenging, especially when evaluating the performance of a beamforming system involving dozens of users. In this section, we present a general and modular approach, which can be used in a LTE network simulator. Therefore, we abstract all the physical layer effects by considering the SINR to be regulated by the ISR parameter. Moreover, we exploit this definition into the spectrum sharing framework [48] of ns3 and we evaluate the system performance to demonstrate the advantages of non orthogonal spectrum sharing when compared to exclusive resource usage.

2.4.1 System model

Our reference scenario involves two adjacent LTE BSs managed by different operators that are serving two groups of users in the same geographical region. The operators have the opportunity to share, partially or totally, their spectra, as shown in Fig. 2.12, here $\mathcal{Q}$ is the set of all sub-channels for the downlink, equally divided between the two BSs, and $s \in (0, 1)$ represents the sharing percentage. The spectrum is divided into groups of adja-

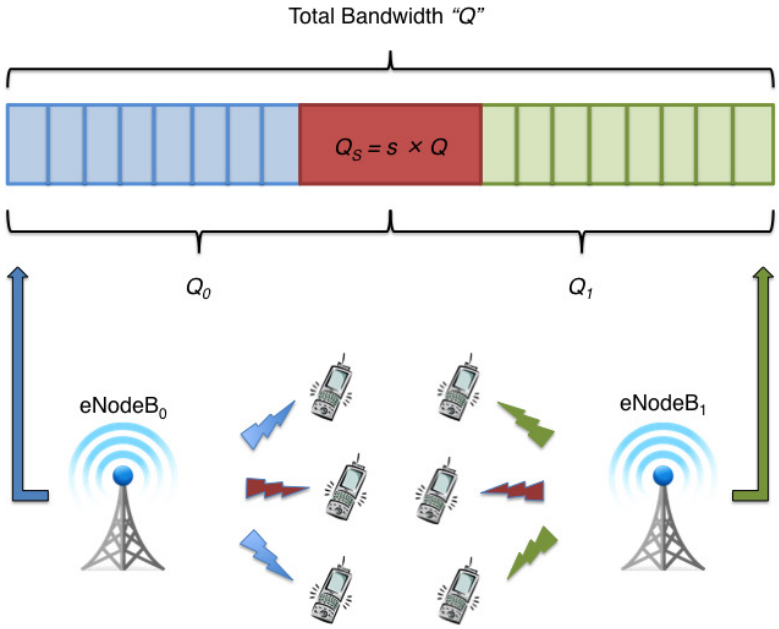

Figure 2.12. *Adopted scenario*

cent sub-carriers, called sub-channels; a private subchannel can be accessed by a single user whereas a shared one can be accessed by one users *per operator*, depending on the scheduling algorithm used.

Non orthogonal sharing introduces the problem of inter-operator interference. The signal received by each UE is affected by the transmission toward other users that are sharing the same time-frequency resource. The SINR perceived by the users is degraded with respect to the no-sharing case, where access to the resource is mutually exclusive and the inter-operator interference is zero. This effect can be reduced, or entirely cancelled, by using linear precoding beamforming techniques that are able to reduce the interference but that at the same time decrease the useful power level received by the UEs. If SNR_{nsh} is the SINR in the no-sharing case and $SINR_{sh}$ is the SINR in the non orthogonal sharing case, we can

re-evaluate the performance of spectrum sharing by considering the same indicators of the case without sharing and doing the following replacement

$$SNR_{nsh} = \frac{P_S}{\sigma^2} \implies SINR_{sh} = \frac{P_Q}{\sigma^2 + P_I} \tag{2.12}$$

where P_S is the useful power in the no-sharing case, P_Q is the useful power in the non orthogonal sharing case, P_I the inter-operator interference and σ^2 is the noise power.

To summarize the SINR user degradation experienced in the no-sharing case, we introduce the parameter ISR $\in (0, 1)$, defined as:

$$ISR = \frac{SINR_{sh}}{SNR_{nsh}} \, . \tag{2.13}$$

As will be shown next, the definition of the ISR enables a compact, low-complex representation of all PHY layer effects to be considered in the network performance evaluation. Actually, the evaluation becomes quite flexible, as the impact of beamforming procedures and user selection mechanisms can be translated into the proper ISR value.

2.5 Numerical Results

To assess the performance of the ISR parameter we run a simulation campaign extending the version presented in [49] of ns3. In our version, the resource allocation scheduling depends on the type of channel, namely private or shared. For private channels, a "max throughput" policy is implemented, i.e., all the resources are allocated to these users with the highest Channel Quality Indicator (CQI). Users without a resource assignment are allocated in the shared pool. Here the pairwise allocation that maximizes the throughput sum is made. The SNR perceived by the users in the shared resource pool are then perturbed according with to ISR.

The scenario consists of two eNBs spaced by 50 m and 40 UEs for each eNB, uniformly distributed within the associated eNB coverage area. The other main system parameters are reported in Table 2.3.

The results obtained are expressed in terms of throughput, which represents the average sum data rates delivered to all UEs. For non orthogonal sharing, throughput increases with respect to the no-sharing case when a certain ISR threshold has been exceeded and when noise power is sufficiently low. Clearly, if the system is noise limited, rather than interference

Parameter	**Value**
1-st sub-channel frequency	2110 MHz
Downlink Channel Bandwidth	5 MHz
Sub-Carrier Bandwidth	15 kHz
Doppler Frequency	60 Hz
Resource block bandwidth	180 kHz
Resource block carriers	12
Resource block OFDM symbols	7
BS downlink TX power	43 dBm
Noise spectral density	-174 dBm/Hz
Macroscopic Pathloss (distance R)	$128.1 + (37.6 \cdot \log(R))dB$
Shadow fading	log-normal
Multipath fading	Jakes (6-12 scatterers)
Wall penetration loss	10 dB
Frame duration	10 ms
TTI (sub-frame duration)	1 ms
Cell coverage	5 km
Cell distance	50 m
Number of UEs per BS	40

Table 2.3. *Main system parameter*

limited, there is no improvement in coordinating interference. Fig. 2.13 shows that the asymptotic case when the ISR is equal to 1, i.e., perfect interference cancellation, and the BSs share all of their spectra, is the best case, the gain is even higher than 100% due to increased multi-user diversity. However, it is worth noting that the curves are sufficiently flat so that significant gains are achieved even when these conditions are not met.

Moreover, the results show that it is always better to have a full, i.e., 100% sharing of the available frequencies. This may not be possible due to internal policy requirements of the operators; nevertheless, the larger the fraction of shared spectrum, the better.

Then, we compare the previous results with the performance obtained by applying fea-

sible beamforming techniques in a MISO 2×1 full sharing LTE system. The main system parameters used in the simulation are reported in Table 2.3 but in this case only two UEs, positioned at 1.5 km from the BS, are involved in the communication. We considered two different linear precoding beamforming techniques: the Maximum Ratio Transmission technique (MRT) and the Sum Rate technique (SR).

The first approach, MRT, uses linear preconding beamforming matrices that maximize the transmission rate when no interference is perceived by the users. Since this technique does not include any kind of collaboration, it achieves a Nash Equilibrium, i.e. the best result for each user individually, from a selfish standpoint. However, its global performance, i.e., considering the two users jointly, is inefficient due to the high mutual interference. Conversely, in SR, the linear precoding beamforming matrices are computed to achieve the PO operation point that achieves the best sum rate. This operation point is one point of the upper-right boundary (Pareto Boundary) of the region that collects all ratetuples that can be achievable simultaneously by the users under a certain set of transmit-power constraints. So a point on the Pareto Boundary consists of rate tuples at which it is impossible to increase the rates of some users without decreasing the rate of at least one of the other users [16].

Fig. 2.14 compares the performance of the no-sharing approach with that provided by full sharing, where the multi-user mode is obtained by using the beamforming techniques described previously. As expected, the MRT system performs poorly in terms of spectral efficiency with a significant loss respect to the no-sharing setting. On the other hand, the SR system outperforms the MRT system and provides some improvement compared to the no-sharing scenario.

Comparing the gains achieved in the sharing cases, it can be seen how the MRT technique corresponds to a value of ISR around 0.002, while the SR technique corresponds to a value of ISR between 0.02 and 0.05. We expect that a higher value of ISR can be achieved using a smart selection of the users that consider the conditions of the channel and the beamforming technique used. In any event, this confirms our assumption that suppression ratios of 5% or higher are feasible for practical systems, thus implying that the gains achievable by non orthogonal sharing are realistic.

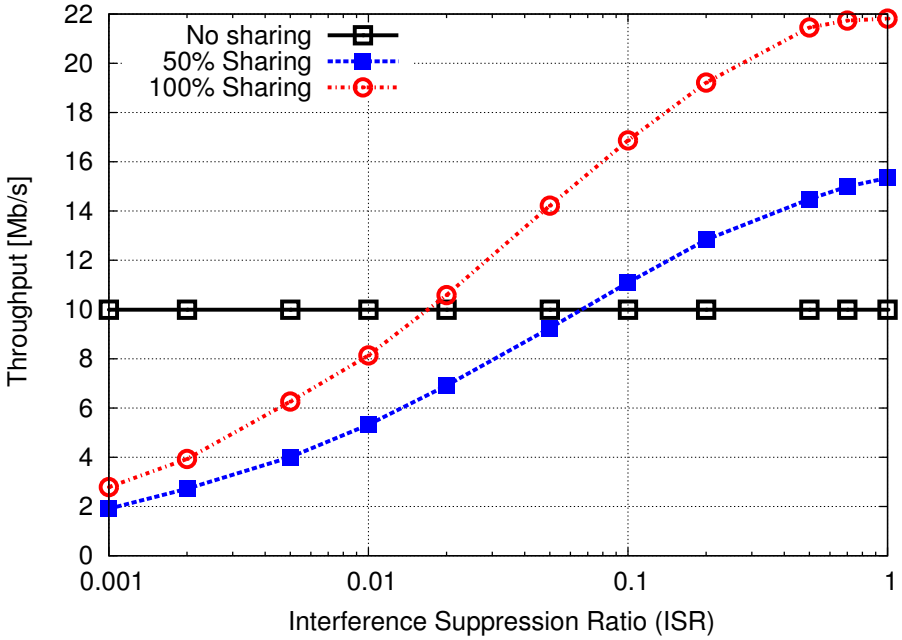

Figure 2.13. *Total sum throughput varying ISR parameter.*

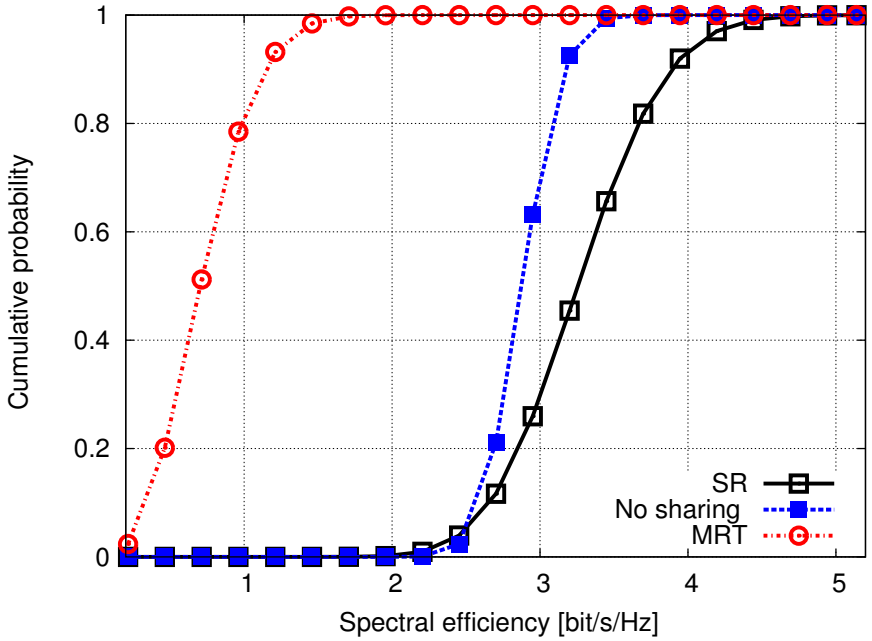

Figure 2.14. *Spectrum sharing gain for different beamforming techniques*

Chapter 3

Spectrum Sharing Management

In the context of dynamic spectrum access, spectrum sharing among multiple operators has recently emerged as a promising paradigm to improve the efficiency of resource usage. Several theoretical evaluations have proven the benefits offered by pooling the available frequencies so as to tune the capacity offered by the operators according to their different needs, especially the service demands from their users. However, practical aspects concerning the application of sharing techniques are rarely studied, and deserve more detailed investigations. Exploiting the features of LTE, which implies a careful design of the PHY layer, may allow different operators to jointly use the spectrum resources. However, while the PHY layer is the subject of several investigations, so far little attention has been paid to the impact of these techniques on upper layers, from medium access control (MAC) up to application, which are those that mostly determine the quality experienced by the users [50]. As we will discuss, there are several challenges in this approach, including the definition of a synthetic mathematical representation of the beamforming, that abstracts from the specific technological features. Even though the related signal processing techniques are well understood, they are too complex to scale in a network-wide environment, and some simplifications are needed. Conversely, when multiple users are present, it is not obvious how they should be coordinated so that maximum efficiency results from physical resource sharing.

NOSS allows the operators to use the same shared spectrum resource simultaneously. This configuration allocates multiple users to the same frequency at the same time, thereby causing a degradation of the SINR at the intended receivers. The interference has to be con-

trolled through the use of multiple antennas at the BSs and proper mitigation techniques, such as beamforming [16]. Moreover, the sharing paradigm can be extended to the infrastructure if the operators use the same communication point. This case, denoted as IS-NOSS, brings further improvements in terms of capital and operational expense (CAPEX, OPEX) costs [17].

In the first part of this chapter we consider the two NOSS scenarios are graphically represented in Fig. 5.1. For both NOSS and IS-NOSS, a careful allocation of the users is required. If the users are just assigned based on individual performance metrics, OSS can achieve some benefits since it increases multi-user diversity. However, non-orthogonal sharing aims at allocating more than one user on the same resource, and therefore should also consider the mutual interaction among the selected users. Thus, it is not necessarily optimal (on the contrary, it may actually be a poor choice) to select the best users, i.e., those with the most favorable channel conditions when considered individually, to be allocated on the same channel. Rather, it is a choice that relates to the channel characteristics of the users, considered not only individually, but paired with each other. Thus, we must define a proper scheduling strategy for user selection in each resource block, whose outcome can be to allocate only one user from either operator, or even two at the same time, one per operator.

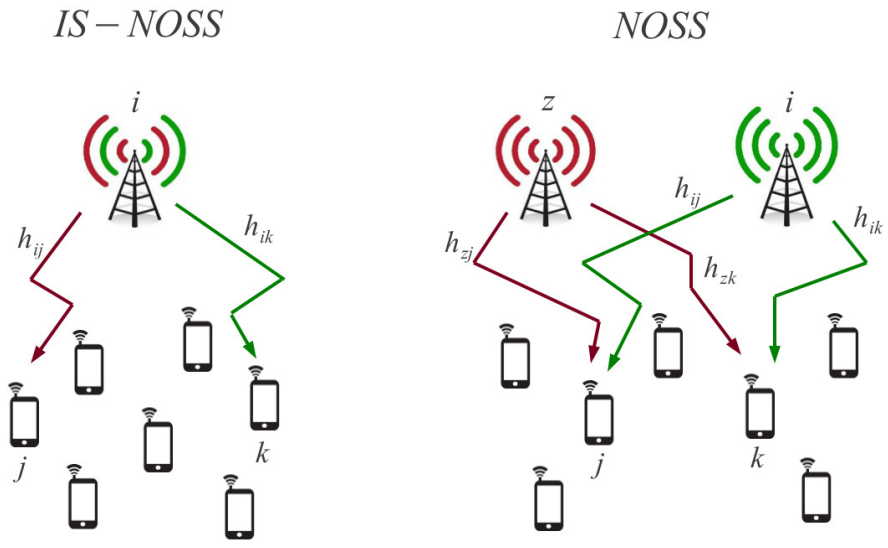

Figure 3.1. *IS-NOSS and NOSS scenarios*

If the channel coefficients are shared among the operators, the two cases of NOSS and

IS-NOSS can be treated within the same mathematical framework, as co-location of the BSs just causes a different arrangement of the channel coefficients.

Differently from many contributions where the analysis is limited to the physical layer and therefore these scenarios are just seen with two or three transmitters/receivers, the goal of our work is to study these scenarios as cellular *networks*, where the number of users is very large and therefore several beamforming options are available, also including higher layers in the analysis. Even though, for concreteness, we will focus on zero forcing beamforming, our approach abstracts from the specific beamforming technique used, and thus offers the advantage of being flexible and especially scalable to a large number of users, as is expected for LTE networks. Also, several scheduling strategies can be considered, to exploit the channel characteristics and the relationships among the operators.

We emphasize that the problem is different from just controlling intercell interference, since in this case mutual interference of the users allocated on the same resource is intentional. Indeed, if users are properly scheduled according to the beamforming configuration and to the channel conditions, NOSS may offer additional gains. Conversely, one simple way to avoid mutual interference would be to apply OSS, which fully avoids interference.

In the OSS case frequency resources owned by the operators are simply put in common, but their usage is still exclusive by one operator at a time. This can be realized by letting one operator "borrow channels" from another, e.g., when the traffic loads in two neighboring cells are highly asymmetric [51]. Alternatively, this can be originated by the operators pooling all or part of their resources together and defining some sharing policy, for example through a virtual market [49]. When the traffic loads of the operators are known to be asymmetric, there surely is an interest and an immediate gain if both operators share their resources. However, in practice such asymmetries are not precisely known in advance to the operators, and only average values of user demands on a given time-of-day may be known, but not their actual value, which must be estimated in real-time. In this case, it becomes interesting to understand whether the theoretical gain found by spectrum sharing investigations also translates to practical policies that can be implemented in NGMNs. In the second part of this chapter, we will discuss how resources should be shared among the operators according to the traffic load, which may be known either precisely or through a statistical characterization only. We will analyse whether an approximate division of the

bandwidth is still beneficial to achieve spectrum sharing gains, or the number of connected users to each cell should be closely monitored and tracked. To evaluate this, we consider an LTE network where user arrivals and departures in and from the system are regulated according to memoryless processes with known rates. Moreover, besides the throughput improvement brought by spectrum sharing, we also investigate fairness among the users. According to our evaluations, getting a precise knowledge of the traffic load asymmetries at a given time instant (as opposed to knowing it only on average) is important to reach a satisfactory fairness among the served users. Thus, each operator should apply spectrum sharing between one of its cells and a neighboring cell belonging to another operator with accurate information about the traffic load of both cells, and even more so if fairness is a key objective for this operator. These techniques are also discussed in terms of flexibility and computational complexity. It is also shown that a sufficiently precise knowledge of the traffic asymmetries, which can be exploited for spectrum sharing, can be achieved by updating the reported cell loads just every few seconds (or more, depending on the user mobility and call service rate). Therefore, a practical implementation of such techniques can definitely be envisioned as realistic and viable.

3.1 Statistical Analysis of NOSS and Scheduling Strategies

We consider a downlink MISO system where the BSs use multiple antennas in transmission while the users are equipped with a single antenna in reception. Moreover, we assume a perfect knowledge at the BSs of the channel coefficients as a column vector $\mathbf{h}_{ij}$, where indices *i* and *j* refer to the BS and the user, respectively. The use of multiple antennas in transmission makes it possible to spatially steer the power to the receiver according to linear precoding vectors $\mathbf{w}_{ij}$ determined through the channel coefficients.

In OSS, each spectrum resource is exclusively assigned to one user; thus, the linear precoding vector $\mathbf{w}_{ij}$ can be computed to maximize the intended signal level received by the user in the absence of interference through the maximum transmission ratio technique (MRT) [52]:

$$\mathbf{w}_{ij}^{(MRT)} = \frac{\mathbf{h}_{ij}}{\|\mathbf{h}_{ij}\|} \tag{3.1}$$

If a spectrum resource is instead shared non-orthogonally (either NOSS or IS-NOSS) between the operators, note first that there may be two users using the resource at the same

time. Thus, if user j is sharing the resource with another user k, the beamforming vector for user j will in general also depend on k. Moreover, with non-orthogonal sharing, the MRT technique is inefficient due to the large amount of interference created by the BSs to the users. Thus, it is more convenient to exploit cooperation between the two operators. For instance, the ZF approach [53] makes it possible to cancel the interference generated by the other link computing the unit-norm beamforming vector that is orthogonal to the channel of the second user, and which at the same time maximizes the product $\mid \mathbf{w}_{ij}^H \mathbf{h}_{ij} \mid$. Hence, we can determine the vector $\mathbf{w}_{ij}$ for ZF beamforming as

$$\mathbf{w}_{ij}^{(ZF)}(k) = \frac{\mathbf{P}_{\mathbf{h}_{ik}} \mathbf{h}_{ij}}{\|\mathbf{P}_{\mathbf{h}_{ik}} \mathbf{h}_{ij}\|} \tag{3.2}$$

where $\mathbf{P}_{\mathbf{h}_{ik}}$ is defined as:

$$\mathbf{P}_{\mathbf{h}_{ik}} \triangleq \mathbf{I} - \mathbf{h}_{ik}(\mathbf{h}_{ik}^H \mathbf{h}_{ik})^{-1} \mathbf{h}_{ik}^H$$

and as discussed above, the beamforming vector depends on k. However, in order to keep the notation simple, in the following we omit this dependence on k.

Without sharing, there is no interference term in the SINR, which is therefore just a signal-to-noise ratio (SNR). The SNR of user j in the non sharing (NSH) case is then

$$SNR_j^{(NSH)} = \frac{p_{ij} |\mathbf{w}_{ij}^{(MRT)H} \mathbf{h}_{ij}|^2}{\sigma^2} \tag{3.3}$$

where p_{ij} is the power transmitted to user j and σ^2 is the noise power.

In the NOSS and IS-NOSS cases, ZF can be employed to simultaneously allocate another user k on the same resource of user j, and the SINR values of user j, denoted as $SINR_j^{(NOSS)}(k)$, $SINR_j^{(ISNOSS)}(k)$, respectively, are

$$SINR_j^{(NOSS)}(k) = \frac{p_{ij} |\mathbf{w}_{ij}^{(ZF)H} \mathbf{h}_{ij}|^2}{\sigma^2 + p_{zj} |\mathbf{w}_{zk}^{(ZF)H} \mathbf{h}_{zj}|^2} \tag{3.4}$$

$$SINR_j^{(ISNOSS)}(k) = \frac{p_{ij} |\mathbf{w}_{ij}^{(ZF)H} \mathbf{h}_{ij}|^2}{\sigma^2 + p_{zj} |\mathbf{w}_{zk}^{(ZF)H} \mathbf{h}_{ij}|^2} \tag{3.5}$$

where z is the index of the other BS that is sharing the same spectrum resource, i.e., serving k (possibly z is the same as i, e.g., in IS-NOSS) and $p_{zj} |\mathbf{w}_{zk}^{(ZF)H} \mathbf{h}_{zj}|^2 = p_{zj} |\mathbf{w}_{zk}^{(ZF)H} \mathbf{h}_{ij}|^2 = 0$. The denominators of (3.5) and (3.4) are then reduced to the noise components since the ZF precoding matrix cancels the interference at the receiver. At the same time, unlike in the MRT case, the use of ZF beamforming also leads to a power degradation for the intended

signal in general.This degradation is due to the non-perfect orthogonality among the channel matrices used for the construction of the beamforming matrices.

This gives the idea for our proposed analytical framework. The exact development of formulas (3.3), (3.4), and (3.5), could in principle be extended to an exact derivation of the capacity (and, for higher network layers, of throughput and data rate achieved by the mobile users); however, this would be infeasible in a network with several users. Moreover, it would be unclear how the users from either operator should be selected and coordinated, as the computational complexity of considering all the possible pairs of users and evaluating their achieved SINR would be overwhelming. For these reasons, we just focus on the *degradation* of the SINR induced by resource sharing, simply meant as a ratio between the SNR value in the non-sharing case and the SINR (with added interference) in the sharing case. Also, such a degradation may be compensated by the higher availability of resources for both operators, also due to sharing. This will be investigated through statistical reasoning related to the wireless channel distribution. In other words, we will determine how the statistics of the radio channel affects the statistics of the ratio between SINR and SNR for the sharing and no sharing cases, respectively. This also poses the following challenges: (i) how to model the process of user selection, i.e., the scheduling strategies according to which users j and k are determined, and (ii) what is the resulting performance in terms of network capacity.

3.1.1 Analytical Evaluation

In this section we discuss the analytical framework to evaluate the impact of resource sharing on the network performance. First of all, we define some parameters to investigate the impact of spectrum sharing and beamforming on higher layers. Then, we introduce a number of scheduling strategies, starting from simple centralized algorithms, and later extend them to a decentralized case where different operators schedule their users in a distributed way.

3.1.1.1 Parameters of the representation

To study the degradation of the SINR of a user in the NOSS case in relation with the SNR obtained in the OSS scheme we define the parameter ISR of user j when sharing the

resources with another user k as

$$ISR_j(k) = \frac{SINR_j(k)}{SNR_j^{(NSH)}} \tag{3.6}$$

where $SINR_j(k)$ can be considered as $SINR_j^{(NOSS)}(k)$, see (3.4), or $SINR_j^{(ISNOSS)}(k)$, see (3.5).

Also we introduce the orthogonality ρ_{jk} of users j and k as

$$\rho_{jk} = \frac{|\mathbf{h}_{ik}^H \mathbf{h}_{ij}|}{\|\mathbf{h}_{ik}\| \|\mathbf{h}_{ij}\|}\,, \tag{3.7}$$

which describes the degree of compatibility of the users that can be selected to share the same spectrum resource assigned by BS i, related to their channel coefficients. A value of ρ_{jk} close to 1 represents an inefficient coupling of these two users, which would cause them high mutual interference. Conversely, as $\rho_{jk} \to 0$ the losses due to the simultaneous usage of the frequency resource are reduced.

It is possible to express (3.6) as a function of the coefficients ρ_{jk}. The detailed derivation is shown in Appendix A.1. The result is

$$ISR_j(k) = 1 - \rho_{jk}^2 \tag{3.8}$$

Through (3.8) it is possible to obtain the statistical behavior of ISR from the probability distribution of ρ, which in turn depends on the choice of the scheduler. Therefore, we need to consider which scheduling policies can be adopted to select the users that share the allocation.

3.1.1.2 Scheduling strategies

Having defined an abstract and parametric representation of beamforming through ISR, we can now investigate several scheduling strategies, which are classified according to how they select the users based on their channel gain and SNR and also how they interfere with the allocation of the other operators, which is mapped through the ISR.

We call Max SNR (M-SNR) the scheduling policy where the allocation is based on the SNR of the users in the case of no-sharing without considering the ρ parameter. In particular, for every spectrum resource the operators select from the overall pool of users those with the best SNR, exploiting the multi-user diversity derived from a larger number of users.

Assume a unit-variance Rayleigh fading, i.e., $\mathbf{h}_{ij} \sim CN(\mathbf{0}, \mathbf{I})$, where $\mathbf{0}$ is the all-zero vector and $\mathbf{I}$ is the identity matrix; thus, the CDF of ρ, $F_\rho(x)$, is given by the regularized incomplete beta function $I_x(\alpha, \beta)$:

$$I_x(\alpha, \beta) = \frac{B_x(\alpha, \beta)}{B(\alpha, \beta)} = \frac{\int_0^x t^{\alpha-1} (1-t)^{\beta-1} \, \mathrm{d}t}{\int_0^1 t^{\alpha-1} (1-t)^{\beta-1} \, \mathrm{d}t} \tag{3.9}$$

where $B_x(\alpha, \beta)$ is the incomplete beta function and $B(\alpha, \beta)$ is the (complete) beta function [54]. The shape parameters α and β are obtained by simulation; we found that $\alpha = 1, \beta = 2$ are suitable values for a MISO configuration with two antennas in transmission and one antenna in reception. This analysis can be extended to the case of a NOSS or IS-NOSS network for different scheduling policies.

We consider two other different schedulers in addition to the M-SNR scheduler: a Max ISR scheduler (M-ISR) and a priority scheduler (PS). The former uses, as the M-SNR scheduler, a single metric as the criterion for a greedy selection, and considers the users of both operators as belonging to a common pool; that is, it always selects two users, but not necessarily one for each operator. However, differently from M-SNR that aims at maximizing the SNR, the M-ISR uses the ISR parameter instead. Thus, for every spectrum resource, the two users that mutually achieve the highest ISR are chosen without considering the SNRs.

In the PS case, the two operators allocate their users separately, but their allocations are prioritized. More specifically, this policy accounts for the fact that either of them is the original licensed "owner" (O) of the resource, i.e., the operator that would exploit the spectrum resource in case of no sharing. The other operator (S) is just exploiting the same channel, but with lower priority. Basically, we aim at establishing a prioritization akin to the typical primary-secondary relationship of cognitive networks [13]. The rationale behind this motivation is that the licensed owner O should be able to assign the resource first, and the secondary operator S should act by avoiding disturbance to the primary. Thus, O assigns its user with the best no-sharing SNR, then S chooses the user achieving the best ρ, with the aim to preserve the utility of the selection performed by O. In a game theoretic context, this framework would be akin to that of a Stackelberg game [55].

In the IS-NOSS case, since the operators are sharing the same infrastructure, the channel coefficients and the ρ are identical for both. Thus, the pdf $f_\rho(x)$ for the r.v. ρ having value x is given, as explained in Appendix A.2, by the pdf of the maximum of n standard beta

variables. This leads to

$$f_{\rho}^{(ISNOSS)}(x) = n\left(\frac{B_x(\alpha,\beta)}{B(\alpha,\beta)}\right)^{n-1}\frac{x^{\alpha-1}(1-x)^{\beta-1}}{B(\alpha,\beta)} \tag{3.10}$$

where n is equal to the number of possible pairs in the network, i.e.:

- $\binom{N_i+N_z}{2}$ for M-ISR;
- N_i if the owner operator is i or N_z if the owner operator is z for PS.

where N_i and N_z are the number of users for the operators i and z.

In the NOSS case, the BSs are not colocated and the value of ρ for each operator is different. Then the objective of the scheduler is not to maximize a single value of ρ but rather the sum of the two values obtained. According to the results presented in [56], the pdf of the sum of the ρ values achieved for the two schedulers in the NOSS case is (see Appendix A.2)

$$f_{\rho}^{(NOSS)}(x) = n\left(\frac{B_x(\alpha,\beta,a,b)}{B(\alpha,\beta)}\right)^{n-1}\frac{(x-a)^{\alpha-1}(b-x)^{\beta-1}}{B(\alpha,\beta)(b-a)^{\alpha+\beta-1}} \tag{3.11}$$

where n is the number of possible pairs available in the network as per (3.10) and $\frac{B_x(\alpha,\beta,a,b)}{B(\alpha,\beta)}$ is a general beta variable with parameters $\alpha = \frac{7}{3}, \beta = \frac{14}{3}, a = 0, b = 2$. These numerical values are computed considering the beta distribution with $\alpha = 1$ and $\beta = 2$ assumed for the IS-NOSS case and following the approach in [56] that provides the exact distribution of the sum of two independent beta variables.

Figs. 3.2 and 3.3 depict the CDF of the ISR based on the ρ statistics described above when 5 users per operator are active in the network. In the NOSS case, the value of the sum of ρ that is computed statistically is divided using a uniform distribution among the users. As expected, since the ISR of the selected users is the same, the IS-NOSS configuration obtains better results than the NOSS configuration. Moreover, Figs. 3.2 and 3.3 compare the CDFs obtained by simulation and by statistical analysis for a MISO 2x1 scenario. In the IS-NOSS case the analytical curve shows a very good fit with the simulation results, while in the NOSS case the fit is slightly degraded (but still acceptable) due to the assumption of uniform distribution of the ρ among the users. We emphasize that these are statistical results, plotted versus the ISR parameter that depends on the orthogonality of the users. Therefore, they do not depend on a particular configuration of the users, but are instead general.

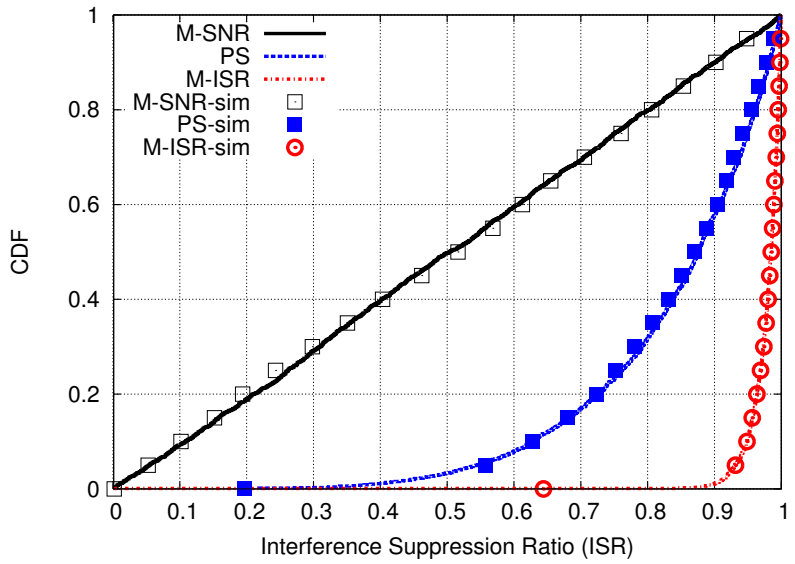

Figure 3.2. *ISR CDF and validation curves for the IS-NOSS case*

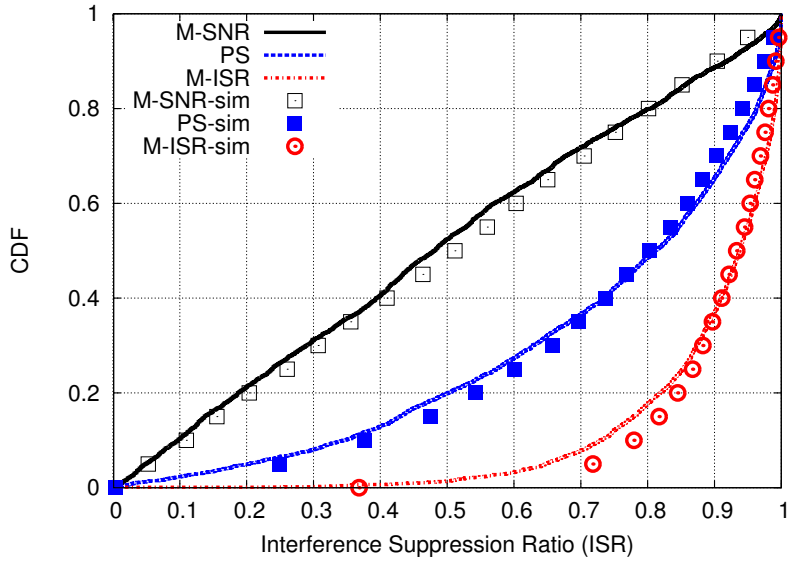

Figure 3.3. *ISR CDF and validation curves for the NOSS case*

3.1.1.3 Hybrid resource allocation schemes

The resource allocation algorithms described above assume that the allocation is performed entirely by a central authority that selects for each RB both users to optimize certain metrics, or one of them in the case of the PS scheduler. Moreover, it is assumed that for every resource a non-orthogonal policy is adopted although this solution leads to a substan-

tial degradation of the performance. In this section, we proposed two additional algorithms that offer an independent selection of the users for all the RBs. The allocation is then optimized to perform non-orthogonal or orthogonal spectrum sharing in the different resources, using respectively ZF or MRT linear transmit beamforming. The first algorithm is designed to maximize the throughput of the network selecting the configuration of users and beamformer that optimizes the spectral efficiency. Conversely, the second algorithm is based on a game theoretical framework in order to add a fairness component to the users scheduling.

In general, in the first step of all the algorithms, the operators propose an allocation map of their users on the resources of the shared bandwidth without considering the possible coupling with the users of the other operator. We assume that the scheduling is based on the assignment of each RB to the user that experiences the best SNR level. Then, these maps are managed by a central authority that performs the final resource allocation according to the different policies.

The first scheduler, called Maximum Rate (MR), tries to maximize the total spectral efficiency in the network. Given the allocation maps over the entire set of RBs $\mathcal{N} = \{1, 2, ..., N\}$, the RBs are assigned to the operators a, b as follows:

$$\begin{cases} a & \text{if} \quad C_i(a) > C_i(b), C_i(a,b) \\ b & \text{if} \quad C_i(b) > C_i(a), C_i(a,b) \\ (a,b) & \text{if} \quad C_i(a,b) > C_i(b), C_i(a) \end{cases} \tag{3.12}$$

where $i \in 1, ..., N$ corresponds to the RB index, $C_i(x) = \log(1 + SNR_i(x))$ is the channel capacity related to the user scheduled by operator x in RB i, $C_i(x, y)$ is the sum-capacity obtained when both operators x and y share the same RB, and (x, y) means that the RB is shared non-orthogonally by both operators. If different configurations achieve the same channel capacity the RB is assigned randomly selecting one of the alternatives. In this way, if the users selected to share the same spectral resource achieve a low value of ISR the use of NOSS is avoided. A weak aspect of this approach is the lack of fairness from the operators' point of view in the selection of the users. In particular, the exclusive assignment of a resource to an operator does not consider any priority, as for example in the PS scheduler, and so the spectrum usage can be unbalanced among the operators.

To improve fairness, we propose a new scheduling algorithm able to manage the use of the NOSS scheme over the spectrum resource as a function of the operators utilities. We

based this algorithm on a Nash bargaining solution. This approach has been used, for example, to regulate access control in a heterogeneous QoS scenario [57].

The Nash bargaining solution is used to model situations in which two players can cooperate by negotiating an outcome or payoff from a set of feasible payoffs. There are two important elements in this framework: the set of feasible payoffs $\mathcal{F}$ and the disagreement vector (v_a, v_b). The role of the disagreement vector is to reflect the situation when negotiation breaks down. $v_i, i \in \{a, b\}$ is the payoff or utility for user i when users cannot agree on a mutually acceptable operating point.

Considering the utility of each operator as the Shannon capacity achieved, we assume that the operators negotiate for a specific ISR level (ISR_{thr}), that defines the schedule as:

$$\begin{cases} (a,b) & \text{if } ISR_i(a) > ISR_{thr} \wedge ISR_i(b) > ISR_{thr} \\ a & \text{if } ISR_i(a) < ISR_{thr} \vee ISR_i(b) < ISR_{thr}, i \in a \\ b & \text{if } ISR_i(a) < ISR_{thr} \vee ISR_i(b) < ISR_{thr}, i \in b \end{cases} \tag{3.13}$$

where $ISR_i(x)$ is the value of ISR at RB i for operator x, and $i \in x$ means that x is the owner operator of the resource i. We can choose the disagreement vector to be the payoff when the operators do not agree to any ISR level, i.e. $ISR_{thr} = 1$, and the resources are assigned as in the case of no-sharing. Considering that the operators a, b are owners respectively of the orthogonal resource sets $\mathcal{A} = \{a_1, a_2, ..., a_A\}$ and $\mathcal{B} = \{b_1, b_2, ..., b_B\}$, where $A + B = N$, we obtain that the disagreement vector $\mathbf{v} = (v_a, v_b)$ is

$$v_a = \sum_{i \in \mathcal{A}} \log(1 + SNR_i(a))$$
$$v_b = \sum_{i \in \mathcal{B}} \log(1 + SNR_i(b))$$

where $SNR_i(x)$ is the SNR of operator x in RB i.

The set of payoffs F achievable by the operators $\{(U_a(ISR_{thr}), U_b(ISR_{thr})) : 0 \leq ISR_{thr} \leq 1\}$ is determined by the parameter ISR_{thr}. We define the indicator functions $\mathbb{1}_{ISR_{thr}}(ISR)$ and $\not\mathbb{1}_{ISR_{thr}}(ISR)$ as:

$$\mathbb{1}_{ISR_{thr}}(ISR_i) = \begin{cases} 1 & \text{if } ISR_i(a) > ISR_{thr} \wedge \quad ISR_i(b) > ISR_{thr} \\ 0 & \text{if } ISR_i(a) < ISR_{thr} \vee \quad ISR_i(b) < ISR_{thr} \end{cases}$$
$$\not\mathbb{1}_{ISR_{thr}}(ISR_i) = 1 - \mathbb{1}_{ISR_{thr}}(ISR_i)$$

The payoffs achievable by the two operators are then

$$x_a = \sum_{i \in \mathcal{N}} \log(1 + ISR_i(a) \cdot SNR_i(a)) \cdot \mathbb{1}_{ISR_{thr}}(ISR_i) + \sum_{i \in \mathcal{A}} \log(1 + SNR_i(a)) \cdot \not{\mathbb{1}}_{ISR_{thr}}(ISR_i) \tag{3.14}$$

$$x_b = \sum_{i \in \mathcal{N}} \log(1 + ISR_i(b) \cdot SNR_i(b)) \cdot \mathbb{1}_{ISR_{thr}}(ISR_i) + \sum_{i \in \mathcal{B}} \log(1 + SNR_i(b)) \cdot \not{\mathbb{1}}_{ISR_{thr}}(ISR_i) \tag{3.15}$$

where, for the sake of simplicity, $x_a = U_a(ISR_{thr})$, $x_b = U_b(ISR_{thr})$.

The Nash bargaining solution is unique if the set F is compact and convex, and there exists at least one vector $\mathbf{x} \in F$ such that $\mathbf{x} \succ \mathbf{v}$, i.e., $\mathbf{x}$ is strictly greater than $\mathbf{v}$ element-wise, [57]. The unique solution is found to be:

$$s = \arg\max_{\mathbf{x} \in F} (x_a - v_a)(x_b - v_b) \tag{3.16}$$

Using the first part of (3.16) we obtain that:

$$\begin{aligned}
&x_a - v_a \\
&= \sum_{i \in \mathcal{N}} \log(1 + ISR_i(a) \cdot SNR_i(a)) \cdot \mathbb{1}_{ISR_{thr}}(ISR_i(a)) \\
&+ \sum_{i \in \mathcal{A}} \log(1 + SNR_i(a)) \cdot \not{\mathbb{1}}_{ISR_{thr}}(ISR_i(a)) - \sum_{i \in A} \log(1 + SNR_i(a)) \\
&= \sum_{i \in \mathcal{N}} \log(1 + ISR_i(a) \cdot SNR_i(a)) \cdot \mathbb{1}_{ISR_{thr}}(ISR_i(a)) - \\
&\sum_{i \in \mathcal{A}} \log(1 + SNR_i(a)) \cdot \mathbb{1}_{ISR_{thr}}(ISR_i(a)) \\
&= \sum_{i \in \mathcal{A}} \log\left(\frac{1 + ISR_i(a) \cdot SNR_i(a)}{1 + SNR_i^{(1)}}\right) \cdot \mathbb{1}_{ISR_{thr}}(ISR_i(a)) \\
&+ \sum_{i \in \mathcal{B}} \log(1 + ISR_i(a) \cdot SNR_i(a)) \cdot \mathbb{1}_{ISR_{thr}}(ISR_i(a))
\end{aligned}$$

A similar expression holds for the second part of (3.16). So the optimization problem is:

$$
\begin{aligned}
s = \arg \max_{ISR_{thr} \in (0,1)} & \\
& \left(\sum_{i \in \mathcal{A}} \log \left(\frac{1 + ISR_i(a) \cdot SNR_i(a)}{1 + SNR_i(a)} \right) \cdot \mathbb{1}_{ISR_{thr}}(ISR_i(a)) \right. \\
& \left. + \sum_{i \in \mathcal{B}} \log(1 + ISR_i(a) \cdot SNR_i(a)) \cdot \mathbb{1}_{ISR_{thr}}(ISR_i(a)) \right) \\
& \cdot \left(\sum_{i \in \mathcal{B}} \log \left(\frac{1 + ISR_i(b) \cdot SNR_i(b)}{1 + SNR_i(b)} \right) \cdot \mathbb{1}_{ISR_{thr}}(ISR_i(b)) \right. \\
& \left. + \sum_{i \in \mathcal{A}} \log(1 + ISR_i(b) \cdot SNR_i(b)) \cdot \mathbb{1}_{ISR_{thr}}(ISR_i(b)) \right)
\end{aligned}
$$

Analyzing the optimization problem we notice that the first terms of the product describe the capacity loss due to the fact that the resource is shared with another operator, while the second terms describe the capacity gain because of the increased availability of resources since now each operator has also access to the resources of the other. The problem can be solved through discrete optimization over the domain of the ISR values obtained for a particular user allocation. To bound the computational complexity of the algorithm, the sums of the capacities over the RBs can be performed only for $ISR_{thr} = 0$, whereas for other ISR_{thr} values the utility can be computed as the difference between the total sum and the contribution of the RBs where $ISR_i(a) < ISR_{thr} \vee ISR_i(b) < ISR_{thr}$. We emphasize that in the IS-NOSS case we obtain that $ISR_i(a) = ISR_i(b)$.

In order to exploit the multiuser diversity due to the usage of an extended spectrum, a further RB rearrangement is applied where the RBs ownership is not given a priori but is adjusted according to the SNR values achieved by the users. In particular, for fairness reasons the same number of RBs is assigned to the operators as before, but the frequency diversity is exploited allocating the RBs to the operator that schedules the user with the best SNR. After this first RBs allocation, the value of ISR_{thr} is computed with the bargaining optimization problem reported above.

3.1.2 Simulation Results

In the first part of this section we validate the analytical results obtained in Section 3.1.1 by simulating the proposed scheduling algorithms. In particular, we simulate a 2×1 MISO

system with 5 users per operator and a unit-variance Rayleigh fading, i.e., $\mathbf{h}_{ij} \sim CN(\mathbf{0}, \mathbf{I})$. Thus, we compute the ρ for each possible pair of users and select one pair according to the different scheduling policies; finally, the ISR of the scheduled users is computed. To evaluate the performance of the proposed scheduling algorithms in an LTE system we exploit the framework described in the previous chapter. In particular, we extend the simulator implementing the ISR statistical framework by generating users in the LTE cell and randomly assigning to each pair of them a degree of orthogonality ρ that is generated according to the distributions given in (3.10) and (3.11). The degree of orthogonality is independent and identically distributed among the users. Through this approach it is possible to evaluate the impact of the ISR parameter together with the SNR level of the users on the downlink spectral efficiency. We compare the results also with: (i) an optimal OSS scheduler that for every RB chooses in the overall pool a single user, i.e., the one with the best SNR, and (ii) the optimal NOSS scheduler that selects a pair of users, namely the two users achieving the best spectral efficiency in every RB.

The scenario consists of two BSs, which may either be colocated (IS-NOSS scenario) or non-colocated (NOSS scenario), and are equipped with two antennas. A variable number of mobile users equipped with one antenna are randomly positioned (with uniform distribution) in the cell of their operator. Cells have a radius of 1.5 km. The downlink bandwidth available per operator, equal to 5 MHz, is divided into 25 RBs. Moreover, we assume a fully loaded scenario, i.e., the downlink traffic saturates each BS buffer, so all the RBs are used during each frame. Each operator has a total downlink power of 43 dBm that is equally divided among the RBs used. The detailed system parameters are reported in Table 3.1.

Figs. 3.4 and 3.5 show the results obtained in the IS-NOSS case and in the NOSS case, respectively. We notice that in the user selection it is important to have both high SNR and high ISR for spectrum sharing to be efficient. In particular, using the M-ISR scheduler the performance is degraded due to the high probability of selecting two users with low SNRs, while in the M-SNR case the higher probability of selecting users with low orthogonality causes a performance loss. By comparing these schedulers with the OSS scheduler, we notice that selecting the users without considering the orthogonality among their channel coefficients is inefficient. Only in the case of a large number of users (50 per operator) is the optimal OSS scheduler outperformed by the M-SNR scheduler, due to the many degrees

Parameter	Value
1-st sub-channel frequency	2110 MHz
Downlink Bandwidth per operator	5 MHz
Sub-Carrier Bandwidth	15 kHz
Doppler Frequency	60 Hz
Resource block bandwidth	180 kHz
Resource block carriers	12
Resource block OFDM symbols	7
BS downlink TX power	43 dBm
Noise spectral density	-174 dBm/Hz
Macrosopic Pathloss (distance R)	$128.1 + (37.6 \cdot \log(R))dB$
Shadow fading	log-normal, ϑ = 8 dB
Wall penetration loss	10 dB
Frame duration	10 ms
TTI (sub-frame duration)	1 ms
Target Bit Error Rate	5×10^{-5}
Cell coverage	1.5 km
BS distance (NOSS case)	50 m
Number of UEs per BS	1, 2, 5, 10, 20, 50

Table 3.1. *Main system parameters*

of freedom in choosing the users. We emphasize also that the bandwidth exploited by each operator in the NOSS case is larger than in the OSS case. Then, since the scenario is fully loaded, the power in the NOSS case is divided among all the RBs while in the OSS case it is divided only among the RBs used by the operators and the power spectral density is higher in the OSS case than in the NOSS case.

Thus, for a low number of users, the NOSS configuration is less efficient than the OSS configurations, and this behavior is more acute when the BSs are not colocated due to a worse coupling among the users scheduled in the same spectrum resource.

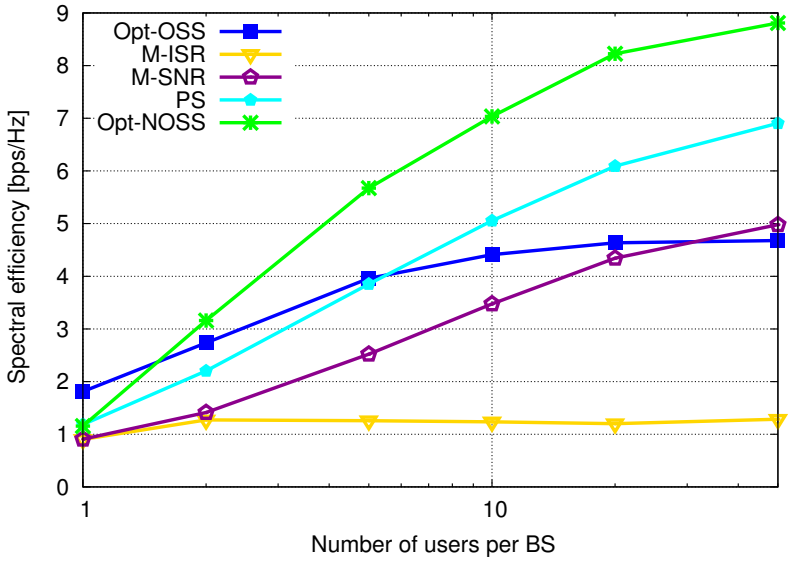

Figure 3.4. *Scheduler comparison for the IS-NOSS case*

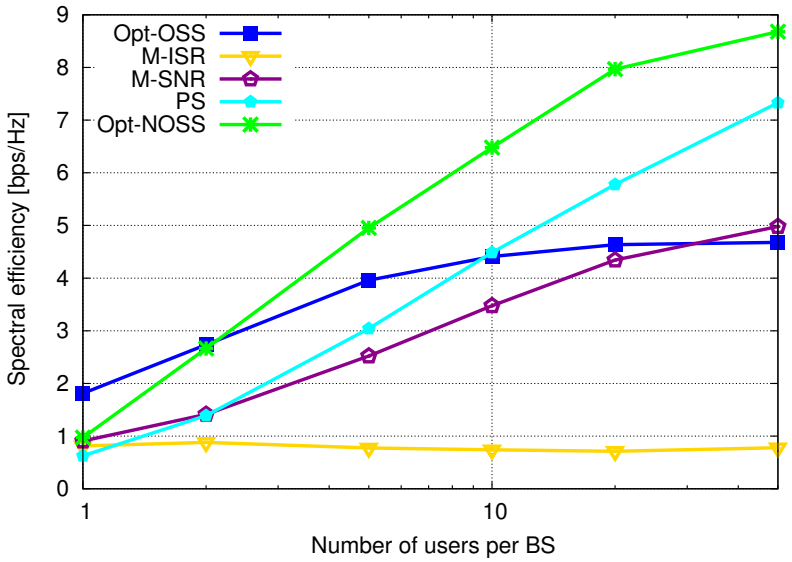

Figure 3.5. *Scheduler comparison for the NOSS case*

Besides, this observation is confirmed by the results obtained when one user is available per operator, in particular, user selection is mandatory for the NOSS scheduler, whereas in the OSS case, multi-user diversity can be exploited so as to achieve a more efficient power allocation. Differently, the PS scheduler results in a good trade-off between the two metrics considered. Moreover, the performance obtained by the optimal NOSS algorithm is

better than what obtained with the PS algorithm, but at the cost of a higher computational complexity. In particular, the complexity of the three allocation algorithms proposed in the choice of the two users for every resource is $o(N)$ while for the optimal NOSS algorithm it is $o\left(N^2\right)$, where N is the number of users in the cell. If we compare the IS-NOSS and the NOSS cases, we notice that the former achieves slightly better results; thus, sharing the infrastructure can give the operators a further improvement in terms of spectral efficiency for the scheduling algorithms that we investigated.

In the second part of this section, we compare the two hybrid resource allocation algorithms proposed in terms of spectral efficiency and throughput. We compare the performance obtained with the Opt-OSS algorithm considered in the previous simulation and with a modified M-SNR algorithm where one user per operator is selected for every RB to achieve the best non-orthogonal spectral efficiency. The last algorithm is considered to compare the solutions proposed with a simple fair approach where both operators can exploit all the RBs. In Fig. 3.6 the spectral efficiencies obtained for the hybrid resource allocation algorithms in the IS-NOSS case are compared. As expected the best performance is achieved by the MR algorithm that maximizes the total throughput of the network. We emphasize how for a low number of users there is a high probability that two users with very different values of SNR are selected, so the allocation of one user in each RB turns out to be the optimum strategy in terms of total spectral efficiency while, increasing the number of users, the NOSS strategy becomes optimal. This fact explains the behavior of the MR algorithm in relation with the Opt-OSS curve. The Nash bargaining solution algorithm (NBS) achieves better performance than the M-SNR approach but lower than the MR algorithm since the NBS also considers fairness among operators. Fig. 3.7 shows the average spectral efficiency achieved by the worst operator. We note that the NBS algorithm outperforms the other solutions thanks to a fairness aware scheduling. On the contrary, Opt-OSS achieves the worst results since the operators with the users located in the best positions may exploit all the RBs orthogonally. Increasing the number of users the performance improves for all the non-orthogonal algorithms because the probability that both operators have users placed close to the base station is higher. We notice also that the MR approach, which was the one achieving the best performance in terms of aggregate spectral efficiency, obtains the worst results among the non-orthogonal algorithms when fairness is considered.

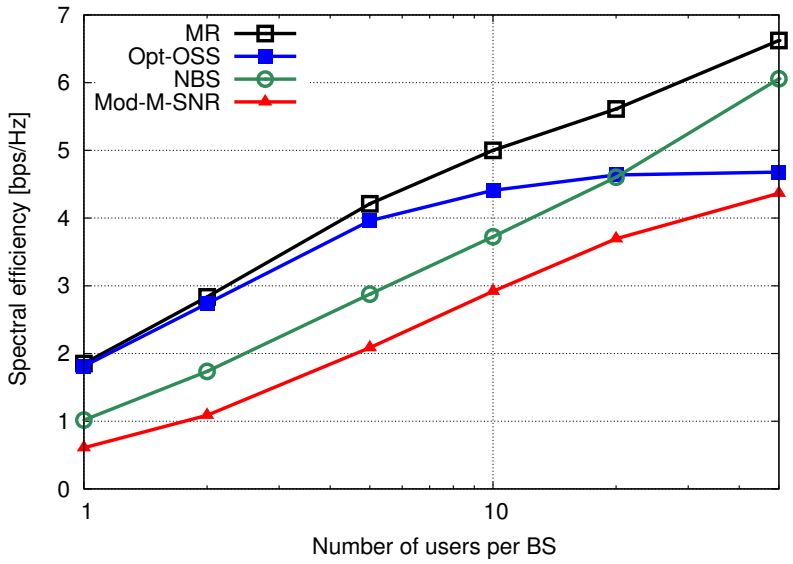

Figure 3.6. *Spectral efficiency of the different algorithm proposed for the IS-NOSS case*

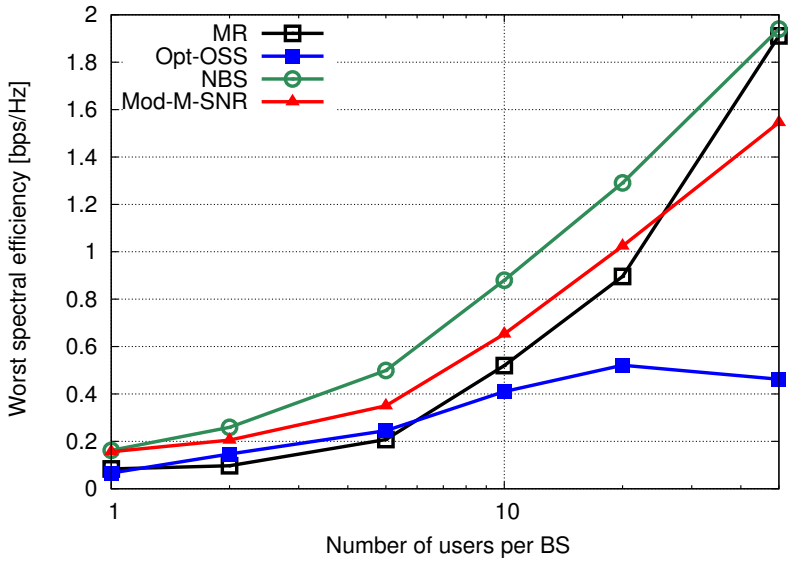

Figure 3.7. *Fairness of the different algorithm proposed for the IS-NOSS case*

Similar considerations for the NOSS case can be obtained analyzing Figs. 3.8 and 3.9 that describe the aggregate spectral efficiency and the worst operator's spectral efficiency, respectively. In conclusion, we can affirm that the MR solution maximizes the performance of the entire system without considering the effects on the single operator. On the contrary, the NBS solution provides a trade-off between the total achievable throughput and the fair-

ness among the operators to provide connectivity also to the cell edge users.

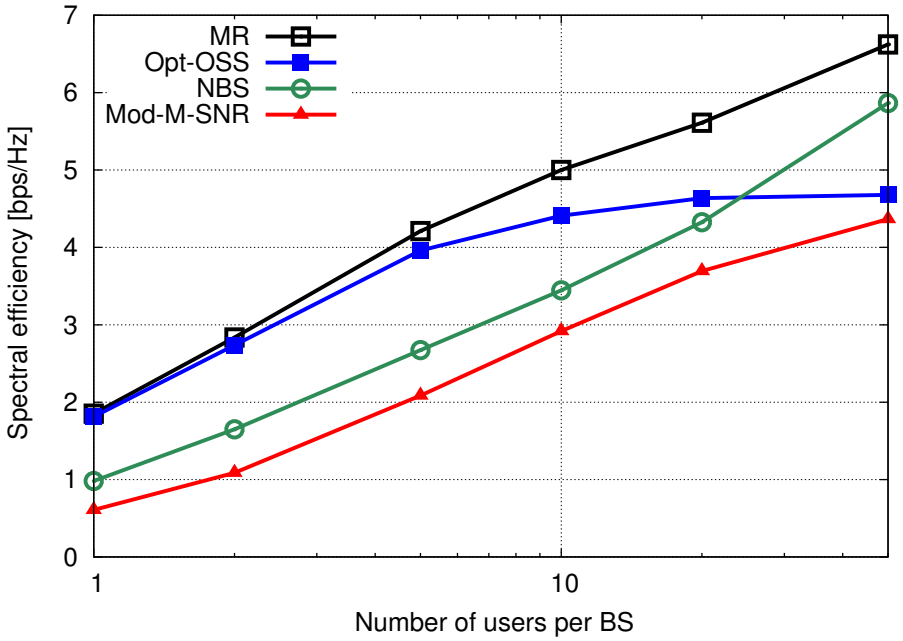

Figure 3.8. *Spectral efficiency of the different algorithm proposed for the NOSS case*

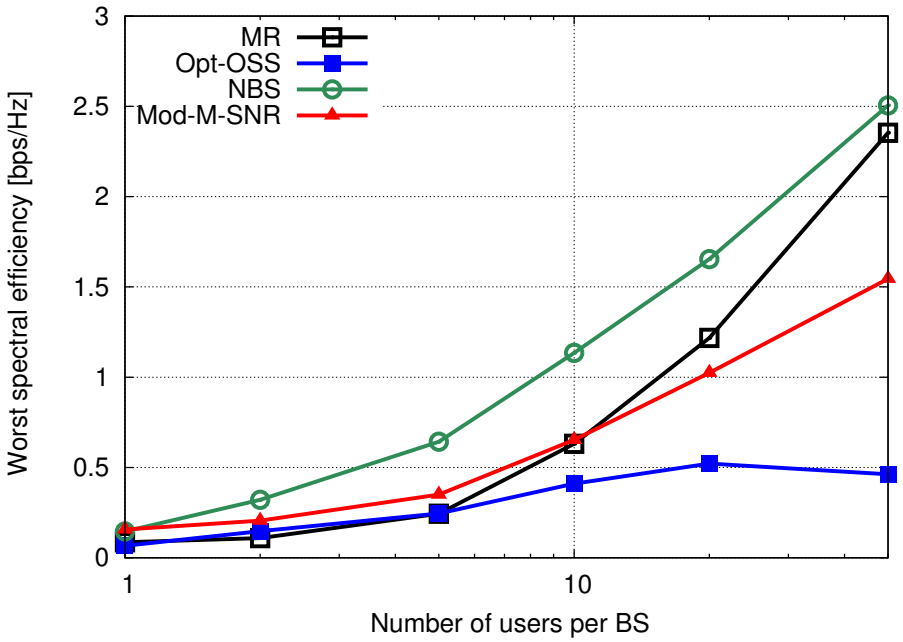

Figure 3.9. *Fairness of the different algorithm proposed for the NOSS case*

3.1.3 Orthogonal Spectrum Sharing Techniques for LTE networks

Differently from the previous analysis, in this section we consider an OSS scenario. A possible reference scenario is represented in Fig. 3.10. Here, two neighboring cells are considered, which coexist in the same geographical area but are managed by different operators. The BSs of both cells transmit over *orthogonal* (i.e., disjoint) frequency bands. Therefore, it does not matter whether the cell borders are just adjacent to each other or even overlapping (in principle, the two BSs could even cover the exact same area). Also for the sake of simplicity, in the following we will discuss of resources just seen as "frequencies;" however, in LTE jargon, the resource units to be allocated to the users are RBs.

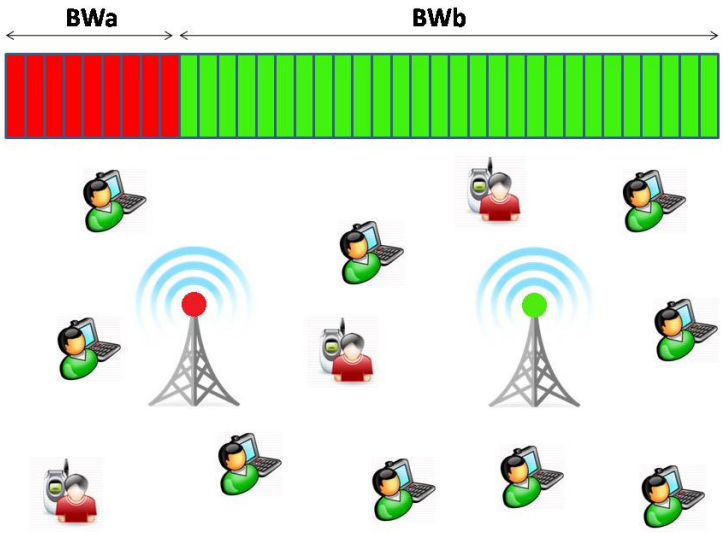

Figure 3.10. *Two operators managing neighboring cells, with spectrum sharing*

Users are spread over the region and are subscribers of either of the operators. Service to each user is uniquely provided by its serving base station (note that also this assumption is just made for the sake of discussion, but in reality nothing would prevent us from considering a similar setup with BSs possibly handing over users to each other). Spectrum sharing intervenes by determining some of the frequency resources to be re-assigned from their initial owner to the other one, upon necessity. As a result, the number of users served by each operator varies. This clearly works better whenever asymmetry is present among the traffic loads of the operators; for example, in the figure, the green BS to the right should

serve more users than the red BS to the left, thus it makes sense to allocate a larger share of the spectrum to the green operator than to the red one.

The question we address in this section is however, how do we quantify that either BS has a "larger" demand than the other? How is "larger" defined, by average values or the actual instantaneous value monitored on a close-knit time scale? And most importantly, what is the resulting performance of each of these approaches?

3.1.4 System Model

To answer these questions, we consider users entering the system, requesting service, and leaving upon service completion according to Markov processes. In particular, the users in service for each operator are taken Poisson distributed; the arrivals of users in each cell are modeled with independent and identically distributed (iid) inter-arrival times $\tau_1, \tau_2, \ldots, \tau_n$, following an exponential distribution with parameter $\lambda = 1/m_\tau$, where $m_\tau = \mathbb{E}[\tau_j]$, with $\mathbb{E}[\cdot]$ being the expectation operator. The service is also a Markov process, i.e., service times $y_1, y_2, \ldots, y_n$ are iid exponential random variables with parameter $\mu = 1/m_y$, where $m_y = \mathbb{E}[y_j]$. We denote the two operators as a and b, and therefore all the parameters above (i.e., average interarrival and service time, or their reciprocals) have in general different values for the two operators, which are written as $m_{\tau a}$ and $m_{\tau b}$, m_{ya} and m_{yb}, and so on. We remark that the choice of a Poisson distribution has been made only for the sake of simplicity in discussing the subsequent numerical results. Indeed, tuning the average inter-arrival and service times it is possible to describe asymmetric traffic loads and to simplify the representation of the numerical results. However, we also tried other arrival distributions of the users; in a network simulator, such a choice would be actually fully modular. Therefore, we remark that the evaluations we will show in the following have been qualitatively confirmed also for other kinds of distributions

Assuming that the bandwidth of each operator is divided in m RBs and that each operator adopts a Round Robin scheduler, the model can be considered as an $M/M/m$ queue where a user is served immediately if the number of users in service is less than the number of RBs. We consider that this condition is always satisfied, so that the system can be seen as an $M/M/\infty$ queue, thus the number of users in service is equal to the number of the users in the system, which is Poisson distributed with mean $m_x = \lambda/\mu$ [58]. The Poisson distribu-

tion permits to represent synthetically the scenario considered, a more realistic and complex model would be feasible but it leads to similar results.

Considering the statistical parameters defined above, we define three different modes for the adaptation of the division of the spectrum among the operators, distinguished as follows.

No Sharing: the total available bandwidth is equally divided among the operators without considering the traffic load; this is actually the result of the absence of spectrum sharing, i.e., each operator just uses the licensed frequencies without "borrowing" anything. This mode is used as a comparison term describing the baseline performance without spectrum sharing. Thus, if BW_{tot} is the total bandwidth of the system, we have $BW_a = BW_b = BW_{tot}/2$, where BW_a and BW_b are the portions assigned respectively to the operators a and b.

Static mode: the bandwidth is divided proportionally to the average number of users in service. Given that operator a has an average of m_{xa} users in service and operator b has an average of m_{xb} users in service, we obtain

$$BW_a = \left\lfloor BW_{tot} \frac{m_{xa}}{m_{xa} + m_{xb}} \right\rfloor . \tag{3.17}$$
$$BW_b = BW_{tot} - BW_a$$

Dynamic mode: the bandwidth is distributed dynamically in each Transmission Time Interval (TTI) proportionally to the number of users in service. If n_a and n_b are the number of users in service during a TTI for operator a and b, respectively, we obtain

$$BW_a = \left\lfloor BW_{tot} \frac{n_a}{n_a + n_{nb}} \right\rfloor \tag{3.18}$$
$$BW_b = BW_{tot} - BW_a$$

The aim of this work is to evaluate the performance achievable by the different modes in relation with the statistical parameters described above. We evaluate two metrics of interest: throughput and fairness among the users. The former can be simply quantified through the total transmission rate achieved by the operators. The latter can be evaluated by using Jain's fairness index (denoted as J) [59]:

$$J = \frac{\left(\sum_{i=1}^{n} \eta_i\right)^2}{n \sum_{i=1}^{n} \eta_i^2} \tag{3.19}$$

where η_i is the throughput of user i and n is the total number of users in the system. We emphasize that $J \in \left[\frac{1}{n}, 1\right]$, where $\frac{1}{n}$ is the value that corresponds to a minimum fairness, while 1 indicates perfect fairness among the users.

The last approach presented, i.e., the Dynamic mode, introduces an increase in the implementation complexity by allowing the adaptation of the parameters of the system in real time. Then, in the last part of this work, we study a pseudo-dynamic approach where the bandwidth is distributed among the operators as in Dynamic mode but the update of the spectrum topology is performed every regular intervals of T seconds starting from an equal division of the spectrum. In particular, we analyze the performance of this algorithm for different values of T for scenarios with different degrees of dynamics.

3.1.5 Performance Evaluation

To evaluate the performance of the proposed spectrum sharing algorithms in an LTE system, we exploit the simulative framework presented in the previous chapter. Thanks to its modular structure, it has been possible to implement the previously discussed spectrum sharing techniques within an LTE-compliant system. The dynamic spectrum sharing allocation (Dynamic mode) is realized with an instantaneous and genie-like knowledge of the traffic of each operator; this assumption will be relaxed later on in this very section.

The scenario characteristics follow those reported in Fig. 3.10 with two BSs, one per operator, positioned at 2 km of distance. Note that the distance between the BSs does not actually influence the performance, as previously discussed. The mobile users try to receive the same kind of traffic and are uniformly distributed at random in a circular cell with a radius of 1.5 km centered at the BSs. The total downlink bandwidth available that is distributed between the operators is 20 MHz and is divided into 100 RBs. Moreover, we assume a fully loaded scenario, i.e., the downlink traffic saturates each BS buffer, so all the RBs are used during each frame. Each operator has a total downlink power of 30 dBm that is equally divided among the used RBs. The number of users per BS is variable according to the Markov process explained in Section 3.1.4. A comprehensive list of system parameters is reported in Table 3.1.

In the first simulation, we analyze the evolution of downlink throughput for the two operators in a specific scenario with the following parameters: $m_{\tau a} = 10$, $m_{ya} = 80$, $m_{\tau b} =$

15, $m_{yb} = 40$. The number of users in service is then unbalanced, since $m_{xa} = 8$ and $m_{xb} = 2.667$. The results are reported in Figs. 3.11 and 3.12.

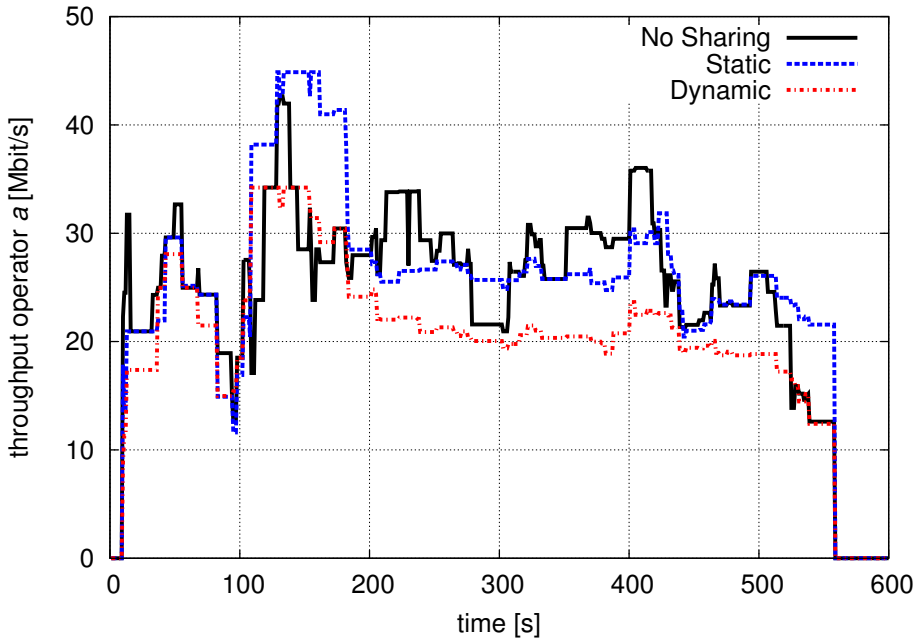

Figure 3.11. *Throughput of operator a.*

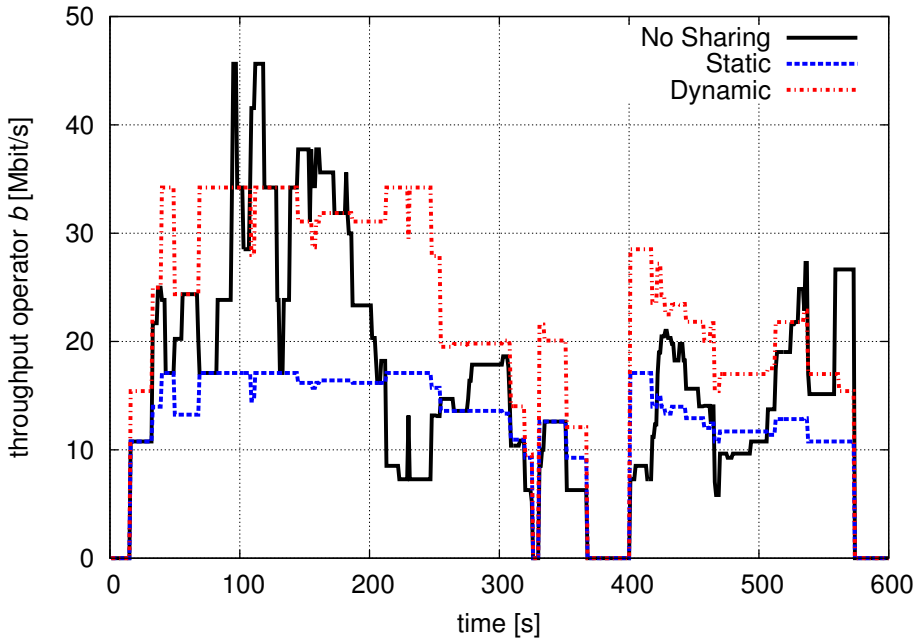

Figure 3.12. *Throughput of operator b.*

We notice that, as expected, both allocation policies with spectrum sharing (either Static or Dynamic) achieve a higher total throughput, since the operator with more users also gets more resources. However, since the scenario is fully loaded, the throughput improvement is marginal, as it is not related to serving more users, that in any case saturate the available bandwidth, but to a better exploitation of frequency diversity. Operator a can assign resources to a wider set of users and therefore better exploit multi-user diversity by selecting those with better SINR. The graphs shown above refer to a single scenario, run with the same simulation seeds in the ns3 simulator. Nevertheless, the trend is exactly the same for any individual scenario. The general conclusion is that, even though spectrum sharing seems to be better suitable to track load asymmetries of the operators, resulting in some local throughput enhancements, overall the *aggregate* throughput gain is limited. After all, if the network is properly dimensioned, the entire channel capacity is used.

However, the results also suggest that the usage of resources is significantly improved by spectrum sharing in terms of how they are distributed among the operators, and consequently among the users. For this reason, in the graphs shown in the following, we analyze how the proposed algorithms impact on *system fairness*, which is in our scenario a more significant metric and is rarely investigated when discussing allocation algorithms for cellular networks, despite being an important characterization of the perceived quality of service. Also note that the graphs shown next are the results on averaging on a large number of simulation runs (and all the users in the same simulation run) to obtain a statistical confidence close to 99%.

Firstly, we define a variable that represents the balance degree of the average traffic loads of the operators.

$$\gamma = \frac{\max\left(m_{xa}, m_{xb}\right)}{\min\left(m_{xa}, m_{xb}\right)} \tag{3.20}$$

If $\gamma = 1$ the operators are perfectly balanced, while the higher γ, the lower the balance between the operators.

Fig. 3.13 describes the CDF of Jain's index. Here, the curves clearly show that the use of the adaptive spectrum sharing algorithms results in improved fairness, since the resources are more evenly partitioned among the users. Moreover, the flexibility of the Dynamic mode permits a further improvement, even though at the cost of a slightly higher implementation complexity.

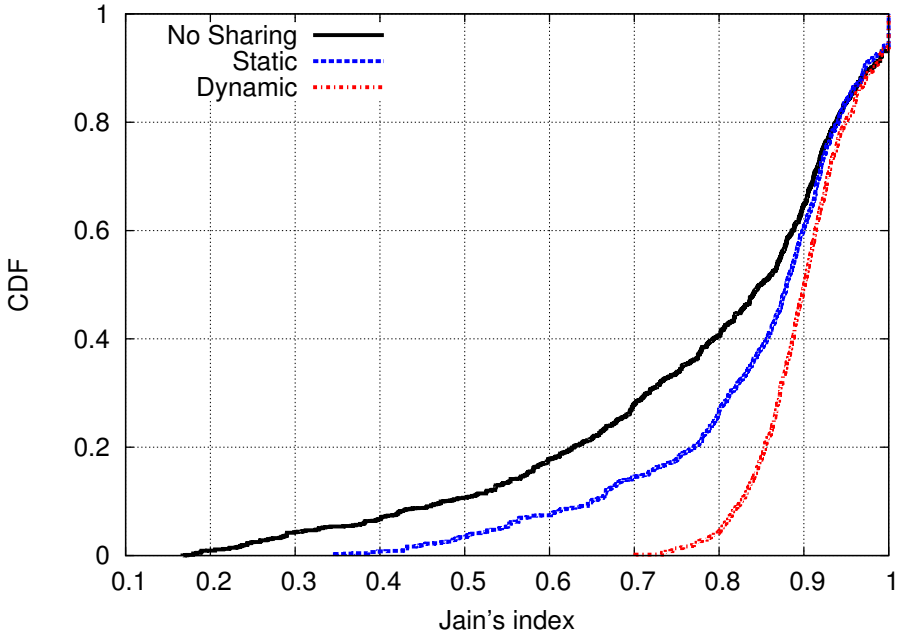

Figure 3.13. *Jain's index CDF for an unbalanced scenario (γ=3).*

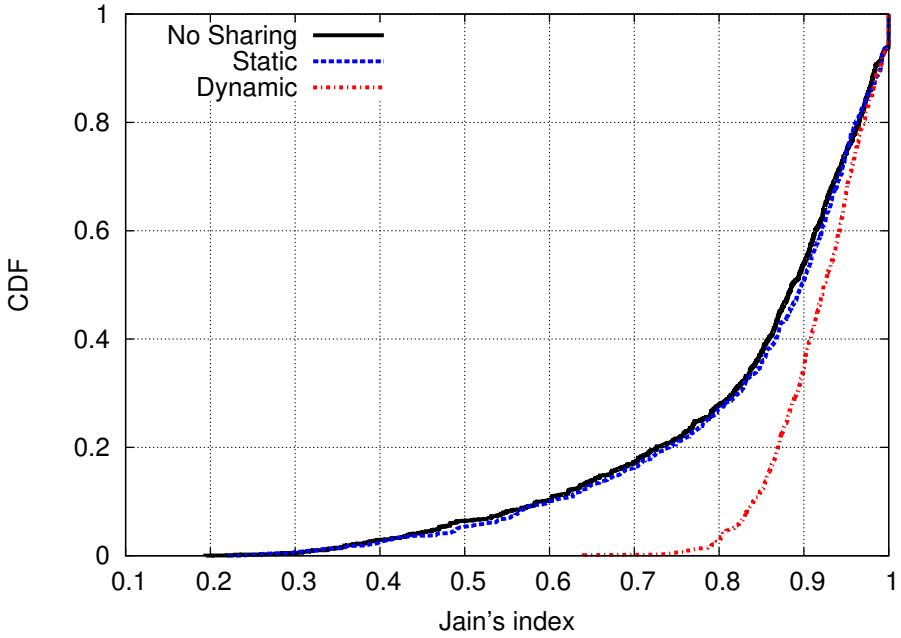

Figure 3.14. *Jain's index CDF for a more balanced case ($\gamma = 1.5$).*

In the second simulation, we evaluate fairness for a scenario with parameters: $m_{\tau a} = 10$, $m_{ya} = 40$, $m_{\tau b} = 15$, $m_{yb} = 40$. The number of users in service is more balanced than

before, since we obtain $m_{xa} = 4$ and $m_{xb} = 2.667$. Fig. 3.14 reports the results. Differently from the previous case, no gain is obtained with the use of a static spectrum sharing policy, which is due to the relatively small difference between the average number of served users. Conversely, a dynamic allocation achieves a better fairness level. The previous results show how the improvement obtained with the use of the different spectrum sharing algorithms is related to characteristics of the traffic load at the operators.

Fig. 3.15 describes the value of the average Jain's index versus the γ parameter. By increasing γ, the fairness performance rapidly decreases for the non-cooperative allocation; when spectrum sharing is employed (Static mode and Dynamic mode), Jain's index remains almost constant. However, a sufficiently high level of fairness (around $J = 0.9$) is reached only when dynamically adapted spectrum sharing is used. Compared to a static spectrum sharing, there is a consistent fairness gain; notably, this is true for all values of γs, which means that a dynamic spectrum sharing is able to track also local unbalances of traffic, even when the operators have the same average load.

We can conclude that, in general, spectrum sharing is able to offer a better allocation fairness, which translates in a higher quality of service for the users, even when the system is heavily unbalanced. On the other hand, this fairness gain is fully available only if a dynamic spectrum sharing strategy is employed.

Finally, we investigate the flexibility of the Dynamic mode, and the relaxation of the assumption of perfect traffic monitoring of the BSs. In other words, we check how the dynamically updated spectrum sharing allocation, which is shown to achieve the best performance, can deal with the update complexity. Indeed, gaining full knowledge of the user demands at both operators at every time instant would require a considerable overhead burden for the spectrum manager and is likely not feasible in practice.

Thus, we relax the assumption that a dynamic spectrum sharing is realized with genie-like knowledge of the traffic patterns, and instead we consider a possibly outdated information about each operator's traffic, which is periodically updated with a given frequency. This also enables us to evaluate the most proper frequency of update that offers the correct tradeoff between performance and overhead/complexity. We define three different scenarios for what concerns the speed of users' traffic evolution, where the difference is in the parameters of the inter-arrival and service times of the users. The parameters of these sce-

narios, which are labeled as “almost stationary,” “slowly variable,” and “rapidly variable” scenario, are defined in Table 3.2.

Scenario	$m_{\tau a}$	m_{ya}	$m_{\tau b}$	m_{yb}
Almost stationary	20	80	20	60
Slowly variable	10	80	15	40
Rapidly variable	2	6	2	4

Table 3.2. *Scenario parameters*

We also evaluate the average Jain’s index obtained for different update frequencies, i.e., every 1, 2, 5, 10, 20, 50, or 100 s. The results obtained are reported in Fig. 3.16. We notice that the fairness performance of the different scenarios is almost optimal for update frequencies between 1 and 0.5 Hz. Below 0.5 Hz we obtain a rapid degradation of the performance in the high dynamics scenario, while for the low dynamics scenario the performance decreases significantly only below 0.05 Hz. Thus, the knowledge of the statistical parameters of the system is important to properly set the update frequency of the spectrum configuration used. In particular, by adopting a frequency update value equal to $1/\min(m_{\tau a}, m_{\tau b})$ it is possible to reach an average Jain’s index value corresponding to 0.98 and therefore a good tradeoff between complexity and performance. We emphasize that, since the scenario is fully loaded, the total throughput is not affected by the update frequency.

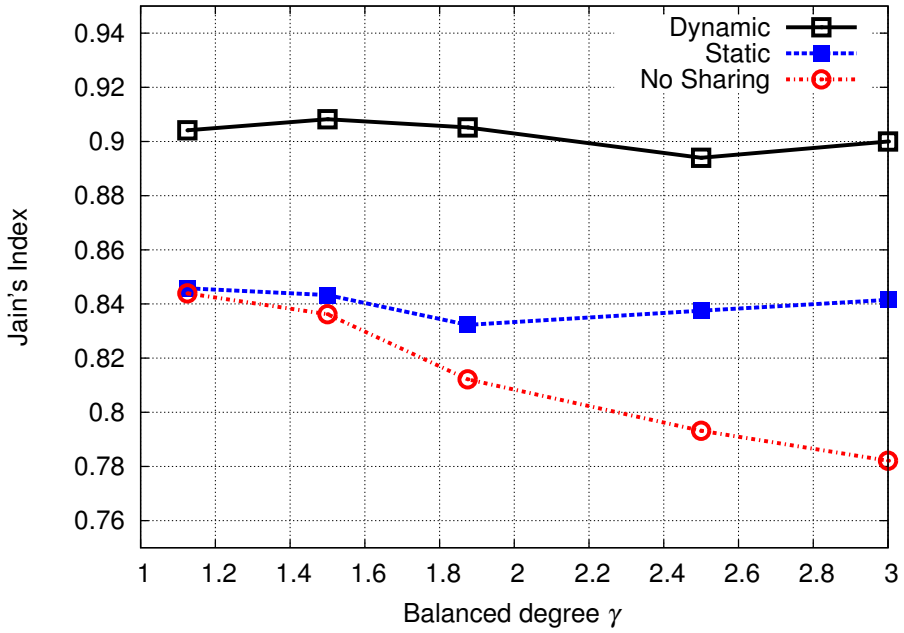

Figure 3.15. *Average Jain's index as a function of the balance degree of the system.*

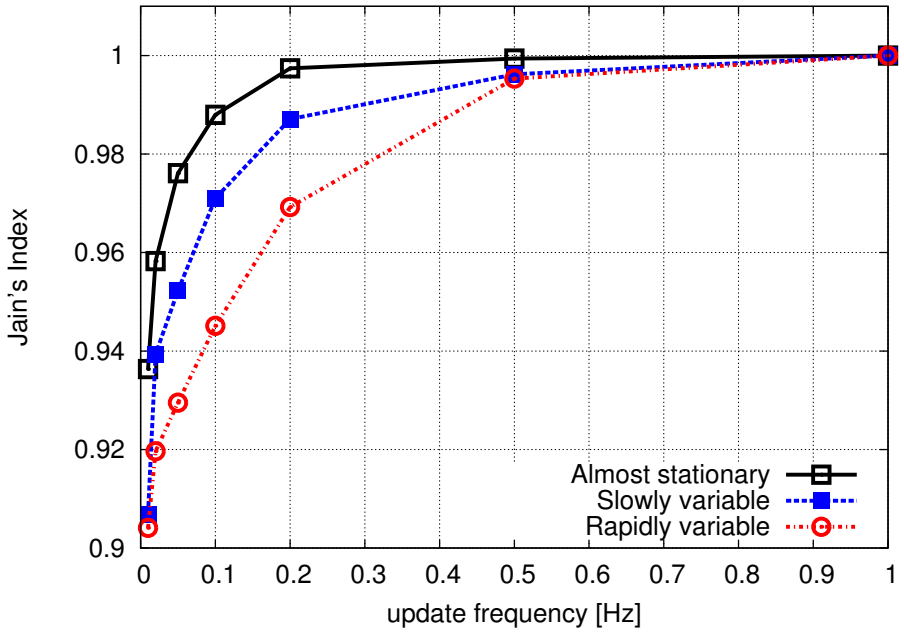

Figure 3.16. *Average Jain's index as a function of the update frequency for different scenarios.*

Chapter 4

Advanced Cellular Resource Management

Coordination and cooperation among transmitters are fundamental paradigms to improve the performance of the next generation of mobile networks (5G). In this chapter we extend the concept of interference management and spectrum sharing to two aspects of the NGMNs: cooperation among transmitters and coexistence between different communication technologies to allow the usage of the millimeter wave (mmWave) frequency spectrum. In the first case, by grouping multiple transmitters into clusters and exploiting multi antenna and beamforming techniques, interference can be managed to improve the performance at the end user's side. In particular, we present a novel distributed clustering algorithm that adapts the cluster configuration according to the users distribution and the average cluster size. In the second part, we analyze the use of a larger bandwith in mmWave spectrum for the NGMNs. Currently, part of this band is allocated on a co-primary basis to a number of other applications such as the fixed satellite services (FSSs). we investigate the coexistence between a cellular network and FSSs in a mmWave scenario. In light of the parameters recommended by the standard and the recent results presented in the literature on the mmWave channel model, we analyze different BSs deployments and different antenna configurations at the transmitters. Finally, we show how, exploiting the features of a mmWave scenario, the coexistence among cellular and satellite services is feasible and the interference at the FSS antenna can be kept below recommended levels.

4.1 An LTE Distributed Clustering Algorithm for CoMP

A very promising concept to achieve high spectral efficiency for interference-limited cellular networks is the cooperative communication between BSs, often referred to as CoMP. In particular, we focus on a particular CoMP technique named coordinated scheduling / beamforming (CS/CB). In CS/CB the BSs are grouped in clusters of cooperative transmitters forming MIMO distributed systems. In each cluster, users are allocated simultaneously in the same resource unit and the interference generated to the users of the same cluster is mitigated exploiting linear precoding beamforming. Therefore, the higher the number of cooperating BSs, the higher the mitigation of the interference. However, in realistic systems the number of cooperating BSs is limited by coordination signaling [60]; thus, it is important to partition the transmitters of the whole network into clusters of proper size.

The problem of network clustering has been treated in the literature especially following a *centralized* approach. In [61], a centralized clustering technique is proposed, where the users report the SINR gain expected when merging neighboring clusters and a central unit uses these data to optimize the network coordination. In [62] and [63], dynamic joint clustering and scheduling are studied by assuming limited CSI at the BSs, and adopting a greedy algorithm, respectively. The use of a centralized approach leads to an increase of traffic signaling (CSI estimation, CSI feedback, synchronization) and infrastructure overhead [64] that may turn the network clustering procedure into a bottleneck. To reduce this overhead, a cooperative distributed approach may be adopted. In [65] a decentralized framework is presented in a simplified scenario, where BSs negotiate the composition of fixed size clusters. In [66], a dynamic coalition formation game is modeled for cooperative spectrum sharing. In this case, the BSs are serving one user and the spectrum is orthogonally divided among the BSs of the same cluster. Coalitions are formed by joining the BSs according to a utility value based on channel capacity and coalition size. Network topology is taken to be fixed, so rearrangements of the clusters are not considered. In [67], coalition game theory is used to develop a merge-and-split algorithm. A utility function is computed by each cluster, seen as a coalition, considering the signaling cost among the BSs and the gain obtained through cooperation. According to this computation, existing coalitions may be joined or split. Thus, this algorithm offers the additional advantage that cluster sizes are not fixed, yet a goal size can be set, which works well on average. However, this algorithm is only

partially distributed. Being based on game theory, it computes distributed utilities for each BS, but requires their coordinated exchange within each cluster, which may be expensive.

We present a novel *fully distributed* algorithm for the LTE downlink, based on the utility perceived by each BS. Our proposal can be seen as a further improvement over the game-theory based algorithm. Similarly to it, we use a (different) utility function based on the SINR, and also the cluster size is specified only on average. However, the important advantage over all existing algorithms (including the game theoretic ones) is that all the computations made by the BSs within our approach are fully distributed, and there is no need for additional signaling exchange.

We implemented our algorithm and evaluated its performance for a large LTE network through the open-source network simulator ns3. We compared it with static clustering, a greedy algorithm based on [60] and the coalition game theoretic algorithm inspired by [67], also originally implemented in the simulator. These benchmarks are fully representative of the existing clustering techniques. Our distributed approach, where each BS decides about its participation to a coalition without negotiating it with the entire cluster, still achieves good performance, while being able to significantly decrease signaling. Also, it is even able to improve the performance for the worst users of the scenario; in particular, we observe a significant improvement for the low-SNR users, since the BSs are able to manage them more promptly, without the need to coordinate with the entire cluster it belongs to.

4.1.1 System Model

We consider a scenario with a set $\mathcal{S} = \{1, 2, ..., S\}$ of pico LTE BSs, each equipped with one omnidirectional antenna. A set $\mathcal{I} = \{1, 2, ..., I\}$ of users are placed according to a Poisson point process (PPP) with intensity λ, and associated with the BS with the strongest signal. In LTE, the downlink channel is organized according to time division and orthogonal frequency division multiplexing. Time is divided into frames of 10 ms, each consisting of 10 sub-frames of 1 ms, while the downlink spectrum is divided into groups of adjacent sub-carriers, called sub-channels. We consider that each BS adopts a proportionally fair scheduler and allocates a single user in each RB. Assuming uniform power allocation over the entire bandwidth, if no coordination is adopted among the BSs, user i assigned to BS j

is affected by interference received from the neighboring BSs and its SINR value is

$$SINR_i = \frac{|h_{ji}|^2 P_j}{\sigma^2 + \sum_{s \neq j, s \in \mathcal{S}} |h_{si}|^2 P_s} \tag{4.1}$$

where h_{mn} is the channel coefficient from BS m to user n, P_m is the power transmitted by base station m and σ^2 is a noise term. When coordination among a subset $\mathcal{K} = \{S_1, S_2, ..., S_K\}$ of the BSs is allowed, a BS cluster can be seen as a MIMO distributed system so as to exploit the use of linear precoding beamforming matrices to mitigate the mutual interference. If $\mathbf{H}(\mathcal{K}, \mathcal{Q}) \in \mathbb{C}^{K \times Q}$ denotes the matrix of channel coefficients, where $\mathcal{Q}$ is the subset of the Q users scheduled within the cluster, ZF can be obtained by selecting the Moore-Penrose pseudoinverse of the channel as the precoding matrix $\mathbf{W}(\mathcal{K}, \mathcal{Q})$, with

$$\mathbf{W}(\mathcal{K}, \mathcal{Q}) = \left[\mathbf{H}^H(\mathcal{K}, \mathcal{Q})\, \mathbf{H}(\mathcal{K}, \mathcal{Q})\right]^{-1} \mathbf{H}^H(\mathcal{K}, \mathcal{Q}) \tag{4.2}$$

so that $\mathbf{W}(\mathcal{K}, \mathcal{Q})\, \mathbf{H}(\mathcal{K}, \mathcal{Q}) = \mathbf{I}_Q$ (identity matrix of size Q).

If a cluster $\mathcal{K}$ of BSs, where internal interference is cancelled, manages user i, the resulting SINR is

$$SINR_i = \frac{P_j}{|w_i|^2 \sigma^2 + \sum_{s \in \mathcal{S} \setminus \mathcal{K}} |h_{si}|^2 P_s} \tag{4.3}$$

where w_i is the beamforming coefficient for user i.

The benefits of CoMP depend on the size of the clusters and the distribution of the BSs within the clusters. Especially, the larger the clusters, the higher the amount of interference cancelled through ZF beamforming. Selecting an efficient clustering is then key to exploit CoMP techniques. We consider a realistic cluster size of about 4 BSs.

We compare the performance of our algorithm with three different feasible algorithms. We emphasize that we have not considered the exhaustive search among all the possible cluster combinations because it is infeasible from a practical point of view due to the high computational complexity.

Static Clustering. A simple clustering procedure defines static groups of neighboring BSs, without rearranging them over time. Signaling among the BSs is limited to the coherent combining signal coordination within the cluster and no central control unit (C-CU) is needed for dynamic updates. Even though this scheme has the least amount of signaling exchange, it is inefficient for what concerns interference management, since it does not consider the distribution of the users. Moreover, the cluster size is fixed and cannot be adapted to the actual amount of interference to be cancelled.

Greedy Clustering [60]. In this case, a BS is randomly chosen and a cluster is formed iteratively with the BSs maximizing the joint capacity, until a predefined cluster size is reached. The scheme increases network fairness and cluster efficiency, even though the CoMP benefits are higher for the clusters formed in the earlier stages that can exploit more degrees of freedom. Moreover, a C-CU is needed to get CSI from the BS and run the clustering algorithm. As in static clustering, the cluster size is fixed. Even though we refer to the implementation of [60], other algorithms [63,65] are also based on greedy clustering and obtain similar performance.

Game Theoretic Clustering, inspired by [67] and based on a coalitional merge-and-split. Consider cluster C_i comprising a subset $\mathcal{K} = \{S_1, S_2, ..., S_K\}$ of BSs, where the set of users assigned to BS k is $\mathcal{M}_k = \left\{m_1^k, m_2^k, ..., m_n^k\right\}$. Given that user m is assigned to BS k within cluster $\mathcal{K}$ and scheduled in RB r, its SNR and SINR are

$$SNR_{r,m,k} = \frac{P_k}{|w_{r,m}|^2 \sigma^2} \tag{4.4}$$

$$SINR_{r,m,k}(\mathcal{K}) = \frac{|h_{r,km}|^2 P_k}{\sigma^2 + \sum_{s \in \mathcal{K} \setminus \{k\}} |h_{r,sm}|^2 P_s} \tag{4.5}$$

where $h_{r,mn}$ is the channel coefficient from BS m to user n in RB r. Thus, we define the cluster utility as

$$u(\mathcal{K}, \mathcal{M}_k, \mathcal{R}_m) = \sum_{\substack{k \in \mathcal{K} \\ m \in \mathcal{M}_k \\ r \in \mathcal{R}_m}} \frac{\log_2(1 + SNR_{r,m,k})}{\log_2(1 + SINR_{r,m,k}(\mathcal{K}))} - \beta\, \xi(z - z_0)$$

where $\mathcal{R}_m$ is the subset of RBs where user m is scheduled, $\xi(z - z_0) = 1/(1 + e^{-(z-z_0)})$ is a sigmoid function where z is the cluster size, z_0 is equal to the reference cluster size, and β is an adjusting parameter. The utility function has two terms. The first one is proportional to the capacity gain obtained by canceling the interference within the cluster. The second is the cost due to the coalition size, which serves to obtain a non super-additive game and drive the average coalition size towards a predefined value (z_0=4 in our setup).

Given an initial set $\mathcal{C} = \{1, 2, ..., C\}$ of clusters, a coalition is randomly chosen; the C-CU computes the utilities for all possible merges among clusters and/or when clusters are split. The following rules are adopted.

- **Merge Rule:** Two coalitions $\mathcal{C}_j$ and $\mathcal{C}_i$ can be merged if $u(\mathcal{C}_j) + u(\mathcal{C}_i) < u(\mathcal{C}_i \bigcup \mathcal{C}_j)$.

- **Split Rule:** A coalition $\mathcal{C}_j = \bigcup_{i=1}^{k} \mathcal{C}_{ji}$ can be split into $\mathcal{C}_{j1}, \mathcal{C}_{j2}, ..., \mathcal{C}_{jk}$ if $\sum_{i=1}^{k} u(\mathcal{C}_{ji}) > u(\mathcal{C}_j)$.

The configuration that provides the best utility value according to split and merge rules is formed and added to the set of clusters. The external cluster interference is neglected.

As in the previous case this scheme needs the use of a C-CU to manage all the CSI from the BSs and to apply split-and-merge and rearrange the network clustering. In this specific algorithm, the cluster size is not fixed and can be tuned through β. Thus, cluster configurations are adaptive, i.e., clusters are larger where the user density is higher.

The proposed Dynamic and Distributed Clustering. We avoid using a C-CU and, at the same time, provide a dynamic network clustering able to follow the evolution of the network. The re-configuration of the clusters is shifted from the C-CU to the BSs that we assume to be capable of collecting CSI from all the users. We consider that the clustering configuration is known at each BS and all BSs synchronously exchange data and CSI over a logical X2 interface, see [68].

Each BS has a counter initially set to a random value that decreases by 1 every TTI. Given a cluster configuration $\mathcal{C}$, when the timer expires, the BS computes the value of its utility for each coalition in $\mathcal{C}$:

$$u_k(\mathcal{C}_i) = \sum_{m \in \mathcal{M}_k, r \in \mathcal{R}_m} \frac{\log_2(1 + SNR_{r,m,k})}{\log_2(1 + SINR_{r,m,k}(\mathcal{C}_i))} - \sum_{\substack{s \in \mathcal{C}_i \setminus \{k\} \\ m \in \mathcal{M}_s \\ r \in \mathcal{R}_m}} \frac{\log_2(1 + SNR_{avg})}{\log_2(1 + SINR_{r,m,s}(\{s,k\}))} \frac{1}{z} - \beta\xi(z - z_0) \tag{4.6}$$

where SNR_{avg} is a reference SNR for all the users, and $SINR_{r,m,s}(\{s,k\})$ is given by (4.5) with a reference fixed power in the numerator.

The first term of the utility represents the gain achieved by BS k within cluster $\mathcal{C}_i$, while the second term gives the contribution to interference mitigation of BS k in the cluster. In particular, the latter makes the cluster stable, and considers not only the improvement of BS k but also the effects on the other BSs. To keep the terms comparable, the latter is divided by the number of BSs in cluster $\mathcal{C}_i$. As in the game theoretic approach, the third term regulates the average size of the clusters through the choice of β. After computing the utilities for all

the clusters, the BS joins the cluster providing the highest utility, or stay within the current cluster if no improvement is achievable.

4.1.2 Performance Evaluation

First of all, we compare the complexity of the considered algorithms. The greedy strategy requires the evaluation of $\mathcal{O}(S)$ steps. The game theoretic clustering requires $\mathcal{O}(C)$ steps, where $C = \mathcal{O}(S/z_0)$. For each step, $\mathcal{O}(M + D)$ operations are required, where M is the number of possible merges and D is the number of splits; note that $M = \mathcal{O}(C)$ and $D = \mathcal{O}(2^{z_0})$. Finally, our proposed algorithm requires $\mathcal{O}(S)$ step, each with $\mathcal{O}(C)$ operations. This means that the complexity of our approach is comparable with the game theoretic clustering (actually, it is slightly lower, since the term D is missing). The greedy algorithm obviously has lower computational complexity (linear vs. quadratic in S) but in our algorithm the quadratic term is scaled down by z_0, thus they are comparable in practical setup. Besides, as shown next, the slight increase in complexity is more than justified by the performance enhancement. More in general, our proposed algorithm offers the additional advantage of better reconfigurability and highly reduced signaling exchange, since all the decisions are made by the BSs in a fully distributed manner. To evaluate the performance quantitatively, with reference to a realistic LTE system, we used the open-source network simulator ns3 [26].

The scenario consists of 40 pico base stations with transmission power equal to 30 dBm placed on a rectangular lattice structure, and a user distribution modeled using a PPP with $\lambda = 100$ users/(entire area). Neighboring BSs are positioned at distance 1.3 km from each other and equipped with one antenna. The total downlink power of 30 dBm is equally divided among the used RBs. The total downlink bandwidth is 5 MHz and is divided into 25 RBs with a frequency reuse factor equal to 1. Moreover, we assume a fully loaded scenario, i.e., the downlink traffic saturates each BS buffer, so all the RBs are used during each frame. The detailed system parameters are reported in Table 4.1; in short, the simulator includes realistic propagation and interference models and fully LTE-compliant specifications.

We evaluate the per-user downlink throughput. To test the adaptivity of the algorithms, we initially set all the clusters to size 1 and we re-distribute the user positions as an independent PPP every 1 s. To improve the readability of the results, we call "low-SNR users" and

Parameter	Value
1-st sub-channel frequency	2110 MHz
Total Downlink Bandwidth	5 MHz
Sub-Carrier Bandwidth	15 kHz
Resource block bandwidth	180 kHz
Resource block carriers	12
Resource block OFDM symbols	7
BS downlink TX power	30 dBm
Noise power spectral density	-174 dBm/Hz
Pathloss at d meters, in dB	$128.1 + 37.6 \log_{10} d$
Shadow fading	log-normal with $\sigma = 8$ dB
Frame duration	10 ms
TTI (sub-frame duration)	1 ms
Target Bit Error Rate	5×10^{-5}
BS distance	1.3 km
User distribution	PPP with $\lambda = 100$

Table 4.1. *Main system parameters*

'high-SNR users" those users obtaining a throughput lower and higher than the average, respectively. We set β to obtain the same average cluster size for each clustering scheme.

Fig. 4.1 depicts the throughput CDF for all users. As expected, the static scheme achieves the worst performance due to its lack of adaptation. An improvement is obtained by the greedy and game-theoretic schemes. In these cases, the clusters are re-arranged according to the user distribution and, in the game theoretic case, larger clusters can be employed if needed. However, since this latter scheme uses a cluster-wise computation of utility, its improvements come at a higher complexity and signaling cost. Moreover, we see that the proposed dynamic algorithm obtains further performance improvements, in spite of the lower required signaling.

To better emphasize the benefits of our scheme, Fig. 4.2 shows the throughput CDF of the low-SNR users. Notice that low-SNR users are more significantly affected by interference, thus the performance improvement becomes more significant. Our proposal brings an

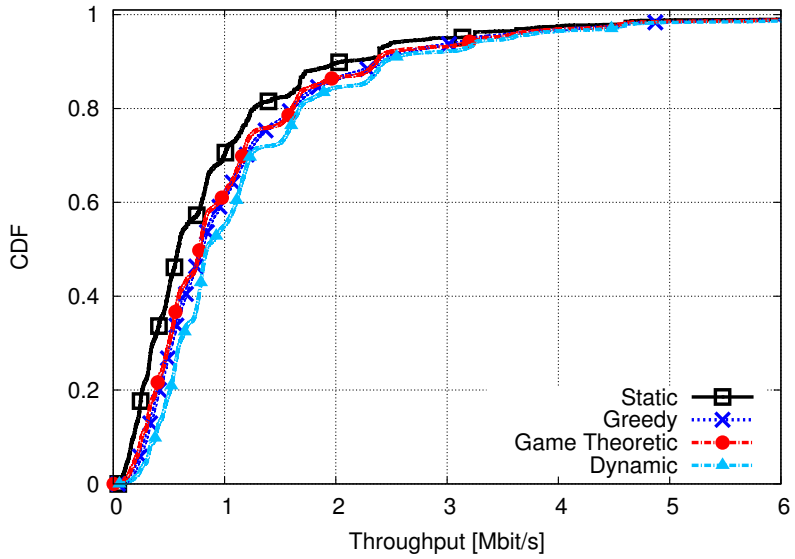

Figure 4.1. *Total Throughput CDF*

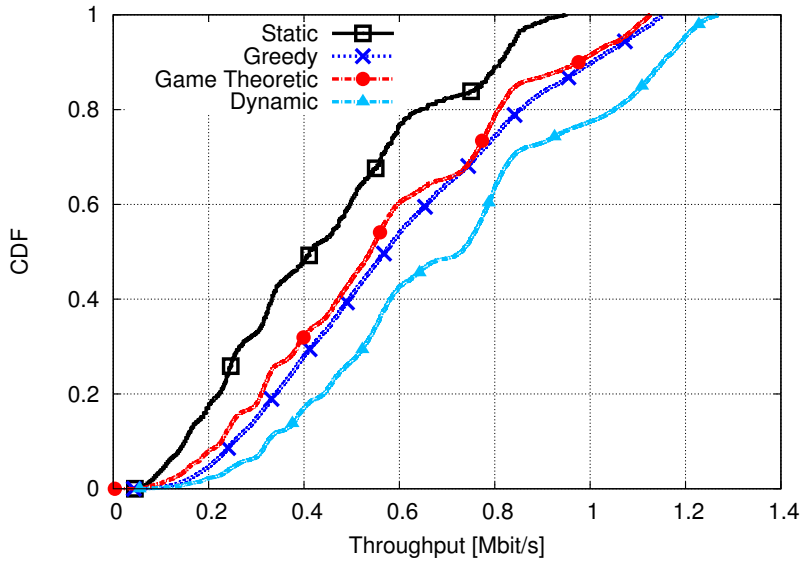

Figure 4.2. *Throughput CDF of the low-SNR users*

improvement to the top-90% throughput of the low-SNR users by at least 15% versus all the competitors, and by 43% versus the static approach. For the worst-case low-SNR users that are in the bottom-10% of the throughput, a higher improvement is present, about 26% (and 53% versus the static approach). The improvement provided by the scheme proposed is then twofold. On the one hand, it avoids the need for a C-CU through a distributed approach;

on the other hand, it increases the throughput achieved by the low-SNR users adapting the clusters to the user distribution.

4.2 Analysis of the Coexistence between FSS and Cellular Networks in the mmWave spectrum

One of the most promising technologies to support the fast growing demand of high rate connectivity in the next generation mobile cellular networks is the use of broad bands in millimeter wave (mmWave) frequency ranges. In particular, cellular allocations today are largely constrained under 6 GHz but it will be possible to obtain a spectrum 200 times greater by exploiting the frequencies between 20 and 300 GHz.

Recent studies demonstrate the feasibility of mmWave mobile communications using multiple antenna arrays in conjunction with adaptive beamforming in order to compensate far propagation losses at high frequencies [69]. Some experimental results obtained using a prototype developed by Samsung are reported in [70]. The small wavelengths of these frequencies (in fact, of the order of 10^{-3} m) allow to use large arrays of antennas to support directional beams to the users. A hybrid analog-digital beamforming scheme that exploits the mmWave channel and an antenna array with a low implementation complexity is presented in [71] and several measurements and capacity studies recently performed in New York City at 28 and 73 GHz are presented in [72]. These studies are used in [73] [74] to develop statistical channel models including pathloss, number of spatial clusters, angular dispersion and outage probability. In general, even in non-line-of-sight scenarios, strong signals can be detected 100 to 200 m from the BS and spatial multiplexing can be supported. Similar channel models based on indoor and outdoor measurements are presented in [75]. One of the candidate bands for the deployment of mmWave cellular mobile networks is the portion of spectrum between 17 and 30 GHz. Currently, part of this band is allocated on a co-primary basis to fixed services (FSs), cellular network backhaul, and FSSs [24]. FSS is the official classification for geostationary communications satellites that provide, for instance, broadcast feeds to television stations, radio stations and broadcast networks. The FSS uplink (from FSS to satellite) is allocated in the band from 27.5 to 30 GHz and the downlink (from satellite to FSS) is allocated from 17.3 to 21 GHz [76]. Fig. 4.3 shows the spectrum allocations

of the FSSs and high density FSSs (HDFSS) designated by the International Telecommunication Union (ITU). Therefore, it is important to study the possible coexistence between FSSs and mmWave mobile BSs in order to preserve the functionalities of the satellite services.

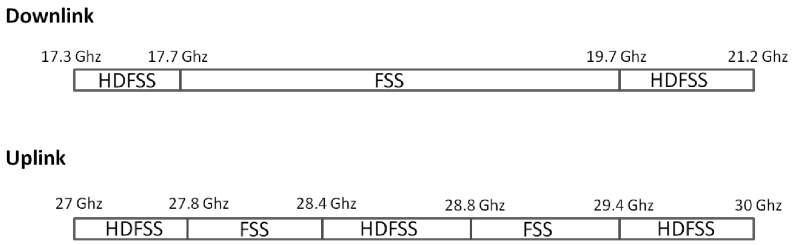

Figure 4.3. *FSSs and HDFSSs spectrum allocation*

ITU investigated the spectrum sharing between FSSs and IMT-advanced systems in the frequency band from 3.4 to 6.4 GHz considering the devices as primary and secondary users respectively [77] [78]. The aim of these works is to evaluate the interference at the FSS and to design possible interference mitigation techniques able to guarantee a minimum signal to interference ratio (SIR) at the primary user. Several techniques can be applied to mitigate the interference towards the FSS and improve the BS-FSS coexistence. Some cognitive SatComs underlay, interweave and database related techniques to manage the BS-FSS interference are presented in [79]. An interference mitigation technique based on a nullsteering MU-MIMO spatial division access scheme for frequency sharing between an IMT-advanced system and FSSs is proposed in L [80]. A study on the separation distance between geostationary satellite communications (GSO) and terrestrial network in Ka band that guarantees a fixed interference to noise level (I/N) at the primary receiver is presented in [81]. A transmit beamforming technique at the BS to maximize the SINR towards the desired secondary user and to mitigate the interference towards the primary satellite terminals is proposed in [82].

Differently from this literature, in our work we study the coexistence between FSSs and mobile cellular BSs in the mmWave bands. In particular, we consider the parameters and the FSSs radiation pattern provided by the ITU standards and the channel models provided by the literature in these frequency bands. We analyze the level of I/N at the FSS considering various multiple antenna configurations at the BS and different deployments of the mobile transmitters when no cooperation is allowed between the BSs. We show that exploiting a large number of antennas at the BSs and properly setting the protection distance between FSS and mobile BS, coexistence between the two systems is feasible. Moreover, we

design a cooperative scheduling algorithm where each BS schedules one user considering the achievable spectral efficiency and the impact on the FSS interference over noise (I/N) level. We present a novel cooperative scheduling algorithm for mobile BSs that, exploiting a game theoretic framework, regulates the FSS-mobile BSs coexistence maintaining the I/N at the FSS below the threshold indicated by the regulatory recommendations. In particular, we model the scenario as a potential game [83]. This technique has been applied recently in the literature to design several wireless network problems. For instance, a game theoretic solution based on potential games for joint channel selection and power allocation in cognitive radio networks is presented in [84]. Exploiting the potential game framework, a resource allocation scheme in a multicell OFDMA uplink scenario for energy-efficient power control is proposed in [85]. Moreover, a distributed potential game-based algorithm that addresses the minimum transmission broadcast problem in wireless networks is presented in [86]. Our potential game formulation ensures equilibrium of user scheduling and we present three different versions of the algorithm. The first is based on the throughout maximization, the second is based on the FSS interference minimization and the third considers both aspects. Finally, we show how applying the algorithm proposed it is possible to meet the regulatory recommendations and at the same time to reach a high level of spectral efficiency.

4.2.1 System Model

We consider the frequency allocation at 18 GHz that corresponds to the downlink band of the FSS system. The scenario is depicted in Fig. 5.1. We define as *primary link* the transmission from the satellite to the FSS while as *secondary link* the connection from a cellular BS to a mobile UE. An additional *interfering link* is present from the BS to the FSS.

We can compute the interference (on a log scale) generated on such a link by BS n to the FSS as

$$I_n = P_{BS} + G_{FSS}(\phi) + G_{BS} - L(d) \tag{4.7}$$

where P_{BS} is the BS transmission power, $G_{FSS}(\phi)$ is the FSS antenna gain in the direction ϕ, G_{BS} is the BS antenna gain, ϕ is the angle between the main FSS antenna lobe and BS n, $L(d)$ is the pathloss component at distance d, which in turn is the FSS-BS distance.

The FSS antenna gain is computed as a function of the off-boresight angles, which can be calculated using the model in [87]. Considering ϑ as the azimuth of the BS w.r.t. the FSS

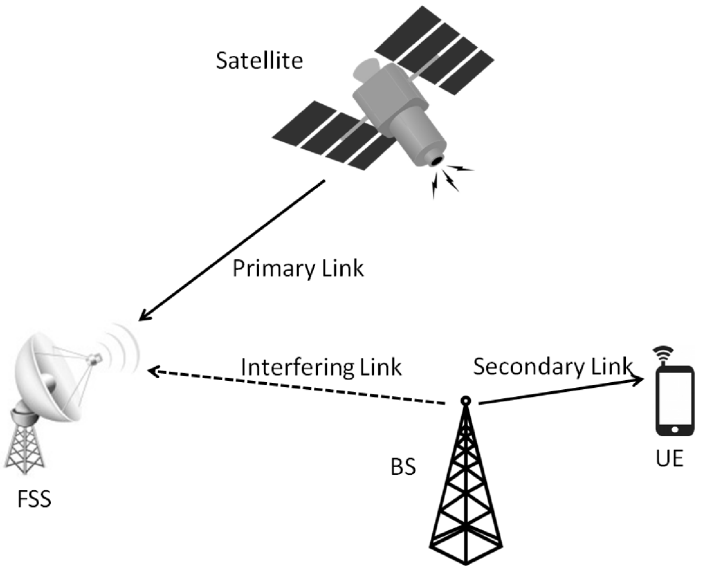

Figure 4.4. *FSS-BS coexistence scenario*

Rx main lobe, the off-boresight angles ϕ of the BS towards the FSS can be calculated as

$$\phi = \arccos(\cos(\alpha)\cos(\epsilon)\cos(\vartheta) + \sin(\alpha)\sin(\epsilon)) \tag{4.8}$$

where α is the FSS elevation angle and ϵ is computed as:

$$\epsilon = \frac{h_t - h_s}{d} - \frac{d}{2r} \tag{4.9}$$

where h_s and h_t are the heights of the BS and the FSS in meters, respectively, while r is the effective Earth radius ($\approx 8.5 \cdot 10^6$ m). The FSS off-boresight antenna gain pattern in dB can be computed as [88]:

$$G_{FSS}(\phi) = \begin{cases} G_{max} & if\ 0° < \phi < 1° \\ 32 - 25\log\phi & if\ 1° \leq \phi < 48° \\ -10 & if\ 48° \leq \phi \leq 180° \end{cases}$$

where G_{max} is the main beam axis FSS antenna gain.

Since mmWave channels are expected to have limited scattering, we adopt a double-directional geometry based stochastic model with L scatterers [89]. Assuming N_{UE} antennas at the UE and N_{BS} antennas at the BS the $N_{UE} \times N_{BS}$ channel matrix $\mathbf{H}$ can be computed as

$$\mathbf{H} = \sqrt{\frac{N_{BS}N_{UE}}{L}} \sum_{\ell=1}^{L} \alpha_\ell \mathbf{a}_{UE}(\gamma_\ell^{UE})\mathbf{a}_{BS}^*(\gamma_\ell^{BS}) \tag{4.10}$$

where α_ℓ is the complex gain of the ℓ^{th} path and $\gamma_\ell^{UE}, \gamma_\ell^{BS} \in [0, 2\pi]$ are uniformly distributed random variables that represent the angles of arrival and departure, respectively. Finally, $\mathbf{a}_{UE}$ and $\mathbf{a}_{BS}$ are the antenna array responses at the UEs and BSs respectively. Assuming uniform linear arrays, $\mathbf{a}_{BS}$ can be written as

$$\mathbf{a}_{BS} = \frac{1}{\sqrt{N_{BS}}} \left[1, e^{j\frac{2\pi}{\lambda} d \sin(\gamma_l^{BS})}, ..., e^{j(N_{BS}-1)\frac{2\pi}{\lambda} d \sin(\gamma_l^{BS})}\right] \tag{4.11}$$

where d is the distance between antennas. Similarly, $\mathbf{a}_{UE}$ can be computed by substituting N_{BS} and γ_ℓ^{BS} in (4.11) with N_{UE} and γ_ℓ^{UE}, respectively.

We assume that the BS antenna gain in dB is

$$G_{BS} = G_{omni} + G_{BF} \tag{4.12}$$

where G_{omni} is the conventional antenna gain when no beamforming techniques are applied and G_{BF} is the beamforming gain. In this work, we adopt an RF beamforming where the gain is obtained by controlling phase and magnitude of the input signal to each antenna to form a directional beam in a particular direction. In order to reduce the system complexity, we assume that the BS can select the beam configuration within a predefined beam codebook with cardinality N_t that uniformly covers the azimuth directions around the BS. In particular, the codebooks at the transmitter and the receiver are formed by N_t and N_r weight vectors $\{\mathbf{v}_1, ..., \mathbf{v}_{N_t}\}$ $\{\mathbf{w}_1, ..., \mathbf{w}_{N_r}\}$ of size N_{BS} and N_{UE}, respectively. Each vector is computed as $\mathbf{v}_i = \mathbf{a}(\phi_i)$ and $\mathbf{w}_k = \mathbf{a}(\theta_k)$ where ϕ_i and θ_k are the azimuth angles for the i-th transmit RF beam and k-th receive RF beam. We assume a multiple-input-single-output (MISO) scenario, in which the beamforming gain in the direction of the FSS antenna is:

$$G_{BF} = 10 \log(\left|\mathbf{v}_i^T \mathbf{h}_{FSS}\right|^2) \tag{4.13}$$

where $\mathbf{v}_i$ is the beamforming precoding vector selected by the BS and $\mathbf{h}_{FSS}$ is the channel matrix between the BS and the FSS.

Recommendation [90] indicates that interference from fixed service systems should not cause the BER to exceed 10^{-4} for more than 0.03% of any month nor cause the BER to exceed 10^{-3} for 0.005% of any month. These interference allowances, in terms of percentage of system noise, can be converted into corresponding values of I/N. For this percentage of time, referred in the literature as "short term" interference, the corresponding I/N values are equal to -2.4 and 0 dB, respectively. To evaluate the level of interference at the FSS we

consider a "long term" interference criterion that refers to a percentage of time greater than 20%. In this case, recommendation [90] allows an interference level equivalent to 10% of the clear-sky satellite system noise that would give rise to a BER of 10^{-6}. The recommended I/N value is computed in [91] and it is equal to -10 dB.

4.2.1.1 Scenarios Considered

We evaluate the interference at the FSS using three different scenarios.

In the first scenario we consider a **single BS** equipped with one omnidirectional antenna to evaluate the impact of the BS position and the elevation angle on the interference at the FSS. In this case, the BS antenna gain is given only by the omnidirectional component.

In the second scenario, we evaluate the aggregate interference from **multiple omnidirectional BSs** deployed in circular tiers around the FSS with fixed inter-site distance. The interference at the FSS is given by the sum of all the BS contributions that depend on the transmitter positions and on the FSS elevation angle. We define as protection distance d_p the distance from the FSS and the first tier of BSs. The scenario is depicted in Fig. 4.5.

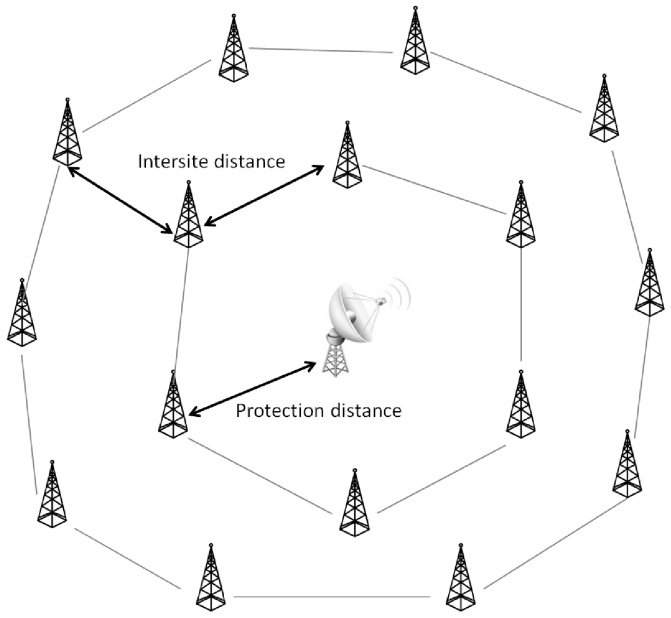

Figure 4.5. *Multiple BSs scenario*

In the third scenario, we consider **multiple directional BSs**. In this case, the BSs, deployed as in the previous scenario, are equipped with multiple antennas and an RF beamforming scheme is adopted to serve the single antenna UEs. The users are randomly dis-

tributed within the BS coverage area and each BS selects one user at a time. The precoding beam vector is selected by each BS within the predefined beam codebook to maximize the SNR at the UE selected. We assume that the user scheduling and the beamforming selection are performed in a distributed manner among the BSs without any cooperation or signalling for interference coordination.

4.2.2 Cooperative scheduling algorithms

In this section we describe the cooperative scheduling algorithm proposed for the multiple directional BSs scenario. The aim of this algorithm is to improve the BSs-FSS coexistence reducing the minimum d_p required to satisfy the standard interference limit threshold at the FSS. The main idea is to coordinate the user transmission in order to regulate the interference at the FSS and at the same time preserve the user average spectral efficiency. The interactions among the BSs can be modelled using a game theoretic framework. In particular, by modelling the scenario as an exact potential game, it is possible to ensure that a pure Nash equilibrium can be reached [83] [84]. A characteristic of a potential game is that any unilateral change of utility, $U(s_i, s_{-i})$, corresponds to a difference of a potential function, $F(s)$, for every player and for every choice of the other players. The potential function models the information associated with the improvement paths of a game instead of the exact utility of the game. Our scenario can be modelled in a normal form game $\Gamma = \{N, \{S_i\}_{i\in N}, \{U_i\}_{i\in N}\}$, where each player corresponds to a BS, N is the set of players and therefore the number of BSs and $S_i = \{1, 2, ..., K\}$ is the set of strategies of player i. Considering that K users are deployed within the coverage area of a player i, the strategy played by i consists of the selection of a specific user within the K deployed in its area. For every player i in Γ, the utility function U_i is a function of strategy s_i selected by player i, and the strategies of the other players, globally denoted as s_{-i}.

In our algorithm we assume that the actions of the players are taken sequentially by randomly selecting one player in each algorithm iteration. The procedure terminates when the algorithm converges to a stable scheduling configuration. We also assume that each BS has a global knowledge of the system parameters that is exploited to optimize the utility function, and that the channel conditions are constant during each algorithm realization. When a BS is selected, the user that maximizes the BS's utility function is scheduled. We

emphasize that, if the game considered corresponds to an exact potential game, the equilibrium convergence is guaranteed and the configuration of the users scheduled is stable. We define three different approaches based on three different utility functions: a maximum rate approach (MaxRate), a minimum interference approach (MinInt) and finally an algorithm based on the linear combination of the previous ones (LinComb).

The aim of the first algorithm is to maximize the mean spectral efficiency of the users considering within the utility function the signals received by the selected user and the intercell interference. In this case, we define the utility U_i^{MR} (where "MR" stands for "Maximum rate") of player i given a certain strategy s_i as

$$U_i^{MR}(s_i, s_{-i}) = p_{ji} \left|\mathbf{v}_i^T \mathbf{h}_{ji}\right|^2 - \sum_{n=1, n\neq i}^{N} p_{jn} \left|\mathbf{v}_n^T \mathbf{h}_{jn}\right|^2 - \sum_{m=1, m\neq j}^{M} p_{mi} \left|\mathbf{v}_i^T \mathbf{h}_{mi}\right|^2$$

where j is the user scheduled by BS i when strategy s_i is adopted and p_{ji} is the power at user j transmitted from i. The utility function is composed by three terms. The first term represents the power received by the user scheduled by i, the second term indicates the inter-cell interference received by user j and, the third term represents the interference generated by i on the users scheduled by the other BSs.

Conversely, the aim of the MinInt algorithm is to minimize the FSS interference. In this case the utility function of user i is denoted as U_i^{MI} and is

$$U_i^{MI}(s_i, s_{-i}) = -\xi(I/N) \tag{4.14}$$

where $\xi(I/N)$ is a function of the interference generated by the BSs to the FSS. In particular the I/N rate is defined as

$$I/N = \sum_{n=1, n\neq i}^{N} I_n - N \tag{4.15}$$

where I_n is defined in (4.7) and N is the noise level in dB. The function $\xi(I/N)$ is designed in order to penalize the strategies that generate large interference at the FSS and to provide more flexibility to the users selection if the FSS interference is lower than the recommended threshold. $\xi(I/N)$ is set as

$$\xi(I/N) = \begin{cases} 0 & \text{if } \; I/N < I/N_0 \\ \dfrac{I}{1 - e^{-(I/N - I/N_0)}} & \text{if } \; I/N \geq I/N_0 \end{cases}$$

where I/N_0 is fixed to a value lower than the recommended I/N threshold, -12 dB, in order to regulate the interference at the FSS.

Finally, we define the LinComb algorithm where the effects on the users and on the FSS are considered together. In this case, the utility function is:

$$U_i(s_i, s_{-i}) = p_{ji} \left|\mathbf{v}_i^T \mathbf{h}_{ji}\right|^2 - \sum_{n=1, n\neq i}^{N} p_{jn} \left|\mathbf{v}_n^T \mathbf{h}_{jn}\right|^2 - \sum_{m=1, m\neq j}^{M} p_{mi} \left|\mathbf{v}_i^T \mathbf{h}_{mi}\right|^2 - \beta\xi(I/N)$$

where β is an adjusting parameter.

For all the algorithms it is possible to define an exact potential function that leads to a specific potential game. The proof is reported in Appendix A.3.

4.2.3 Performance Evaluation

In this section, we describe the results obtained for the scenarios presented in the previous sections. We assume that the total downlink bandwith is 500 MHz and the BSs allocate the power uniformly over this bandwith. The pathloss model is given exploiting the results presented in [75] on the mmWave band. Assuming a system effective noise temperature `T` equal to 300 K the one-sided noise power spectral density value results equal to $N_0 = \texttt{kT} = -143.82$ dBW/MHz, where `k` is the Boltzmann constant. The detailed system parameters are reported in Table 4.2. All the evaluations have been performed using a customized MATLAB simulator.

4.2.3.1 Single omnidirectional BS

In Fig. 4.6, we evaluate the region around the FSS where a single omnidirectional BS can be placed without causing I/N to go above the recommended threshold. In particular, the graph shows the contour of the "-10 dB region" that represents the area where a single omnidirectional BS generates an amount of interference at the FSS higher than the regulatory requirements. We evaluate the regions obtained with a pico BS, $P_{BS} = 30$ dBm and with a macro BS, $P_{BS} = 43$ dBm, considering the FSS elevation angle α equal to $10°$ and $30°$. As expected, the -10 dB area extension is proportional to the BS power. Moreover, the interference depends on the FSS elevation angle, in particular the higher the α the lower the interference at the FSS.

Parameter	Value
Carrier frequency	18 GHz
Total downlink bandwidth	500 MHz
BS transmit power	30, 43 dBm
BS antenna height	20 m
BS omnidirectional antenna gain	6, 12 dBi
BSs intersite distance	500 m
BS inter-antenna distance	$\lambda/2$
BS beam codebook cardinality	16
FSS antenna main lobe gain	42.1 dBi
FSS antenna diameter	2.4 m
FSS antenna height	2 m
Elevation angle	10°, 30°
Pathloss model	61.39 + $10 \times 2.47 \log(d)$ [75]
Number of scatterers	3
Noise temperature	300 K
Number of users per BS	10
Recommended I/N level	-10 dB

Table 4.2. *Main system parameters*

4.2.3.2 Multiple omnidirectional BSs

In the next simulations, we evaluate the interference at the FSS when more omnidirectional pico BSs are deployed around the FSS. In the first simulation, we consider the worst case scenario when one BS within every tier of BSs is placed in the direction of the maximum FSS antenna gain, *i.e.*, $\vartheta = 0°$, and the others are placed accordingly with a fixed intersite distance d_i. Considering the expected cell coverage in next generation cellular networks [72] we assume $d_i = 500$ m. Fig. 4.7 shows the I/N obtained varying the protection distance and adopting three different values for the number of BS tiers, N_r, and two different elevation angles. We observe that, for $\alpha = 10°$, the interference at the FSS is very high and the I/N

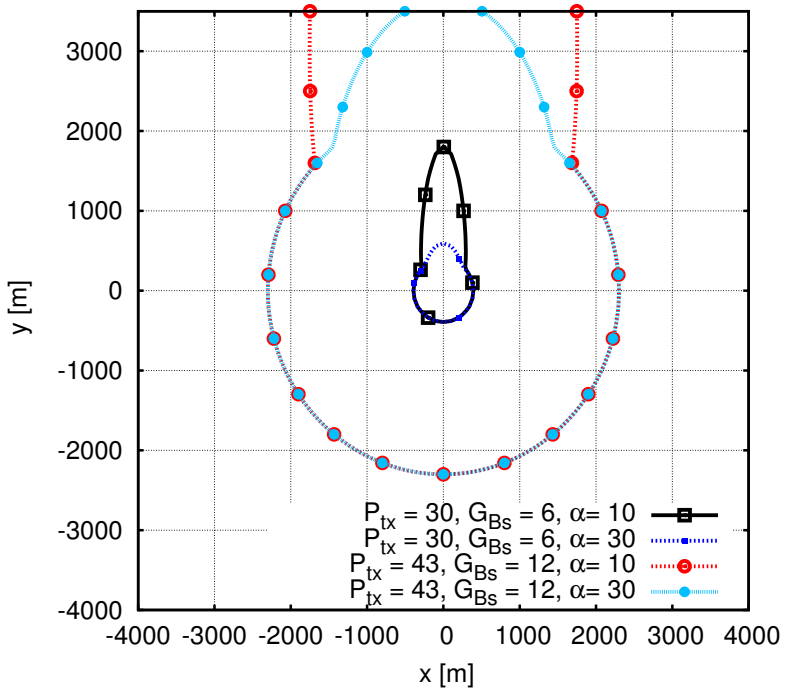

Figure 4.6. *-10 dB region with a single interferer*

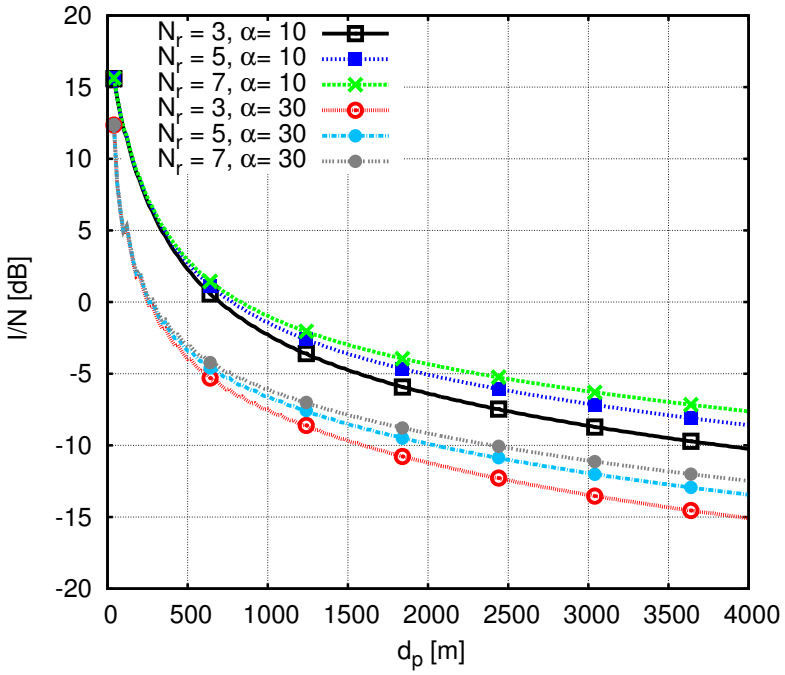

Figure 4.7. *Aggregate interference in the omnidirectional worst-case scenario*

level recommended by the standard is never achieved even for high d_p values. Increasing the elevation angle to 30° the recommended value is reached for $d_p = 2000$ m. As expected, considering more BSs circles the interference at the FSS increases but the effects of the more distant BSs circle become negligible due to the high pathloss. Then, in the next evaluations, we restrict the value of N_r to 3 or 5.

Fig. 4.8 shows the CDF of I/N when the BS are deployed randomly over the circles around the FSS. We consider five tiers of BSs and two fixed protection distances for each value of the elevation angle. The intersite distance between the BSs is fixed as in the previous simulation. The results are obtained via Monte Carlo simulation with several runs per configuration where in each run the BS positions are changed. Firstly, we note that since the radiation pattern shape depends on α, the higher the FSS elevation angle the lower the interference generated to the FSS and so the I/N level. In general, for the d_p values considered the interference requirement is never met.

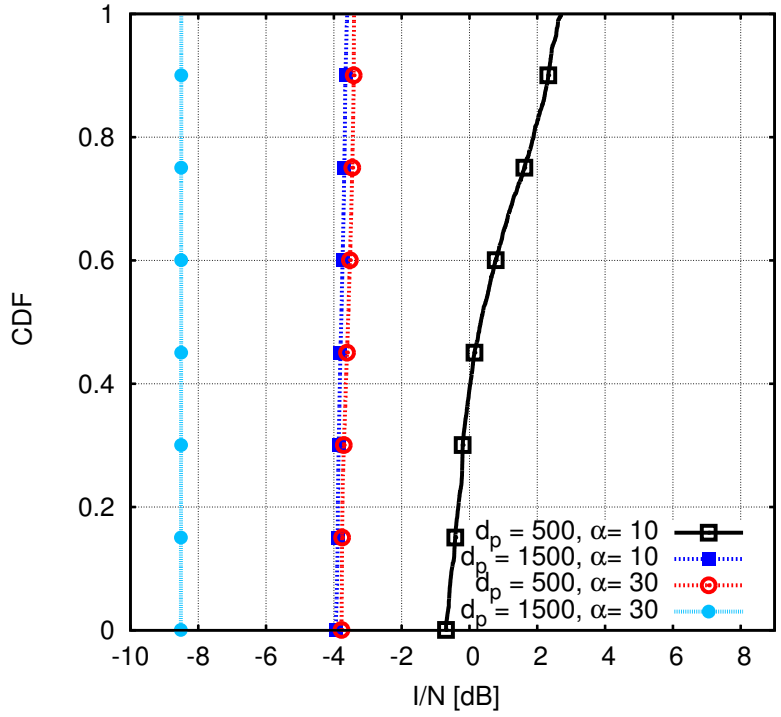

Figure 4.8. *Aggregate interference CDF with omnidirectional BSs*

4.2.3.3 Multiple directional BSs

In Figs. 4.9, 4.10 and 4.11 we evaluate the interference at the FSS exploiting an analog beamforming scheme at the BSs that maximizes the user capacity. We consider a random scheduling of the users. Fig. 4.9 shows the I/N obtained in the worst-case scenario by varying the protection distance and considering different numbers of antennas at the transmitter N_a, and different values of α. The number N_r of tiers of BSs around the FSS is fixed to three and the results have been obtained, as in the previous case, by Monte Carlo evaluations over different channel realizations and user selections. When the number of antennas is increased, the directional beams becomes narrower and the interference due to the side lobes decreases. Also, the interference towards the FSS decreases with the number of antennas at the BSs. Besides, we note that the interference due to a small elevation angle can be compensated by using a larger antenna array. In general, beamforming schemes can reach a considerable improvement in comparison with the omnidirectional BSs case. Fig. 4.10 shows the CDF of I/N when the number of antennas is set to 16 and the BSs are randomly placed around the FSS over three tiers. Using this configuration, we notice that it is possible to satisfy the standard recommendation constraints adopting a protection distance of 1500 m for an elevation angle equal to 30°. We emphasize that user scheduling and beam selection are completely unaware of the interference at the FSS since no communication is assumed between the devices. The results of a similar evaluation are reported in Fig. 4.11 increasing the number of antennas at the BSs to 64. We note that the required protection distance with $\alpha = 30^\circ$ is reduced to 500 m and the regulatory requirement can be satisfied also for $\alpha = 10^\circ$ with $d_p = 1500$ m. Fig. 4.12 shows the impact of the BSs intersite distance on the interference at the FSS. In this evaluation we set $N_a = 16$, $d_p = 1500$, $N_r = 3$ and $\alpha = 30$. As expected, decreasing the intersite distance, the BS density around the FSS increases, thus generating higher interference at the FSS. The BSs density is then another key parameter to design the network in order to preserve the FSS functionalities.

4.2.3.4 Cooperative scheduling algorithms

In the second part of this section we evaluate the performance reachable with a cooperative scheduling of the users. In particular, we study the results achievable by the LinComb algorithm in terms of I/N level at the FSS and mean spectral efficiency of the users. We

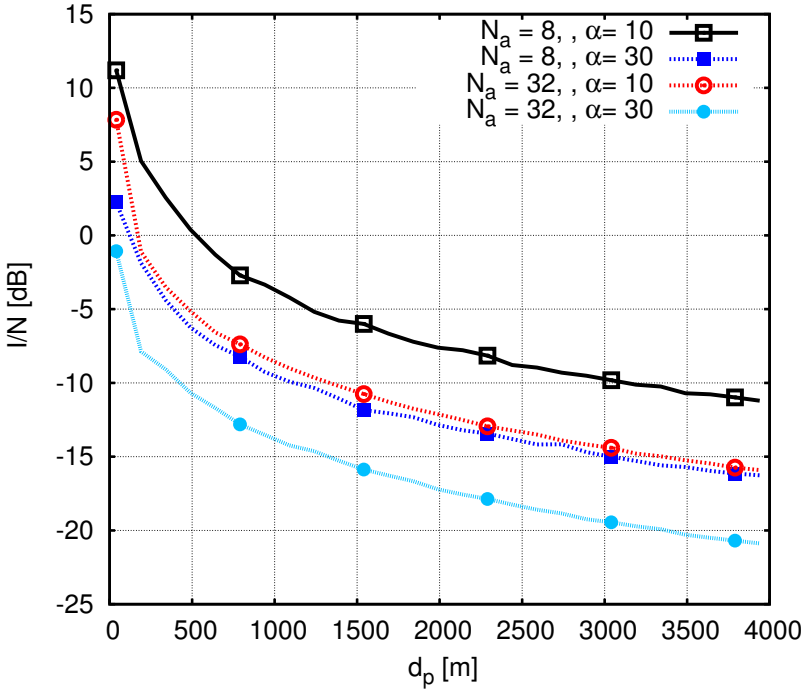

Figure 4.9. *Aggregate interference in the beamforming worst-case scenario*

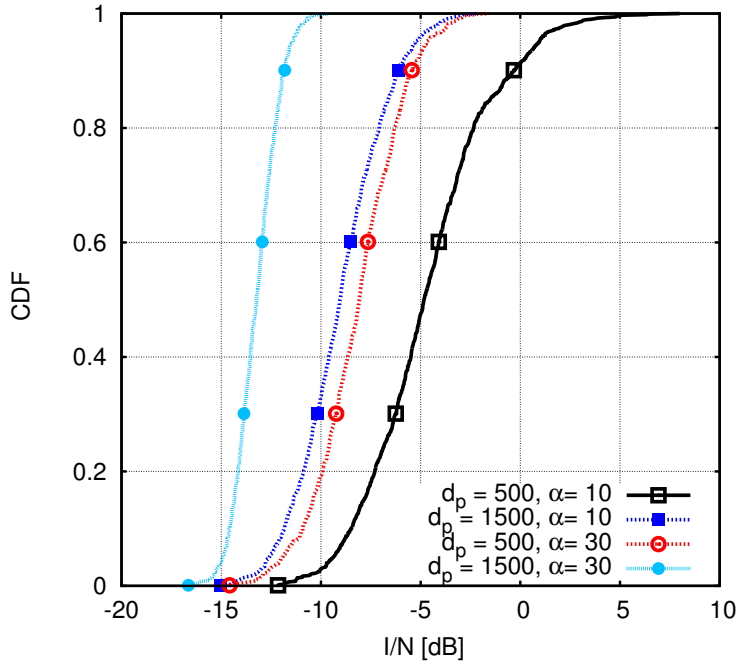

Figure 4.10. *Aggregate interference CDF considering BSs with* $N_a = 16$

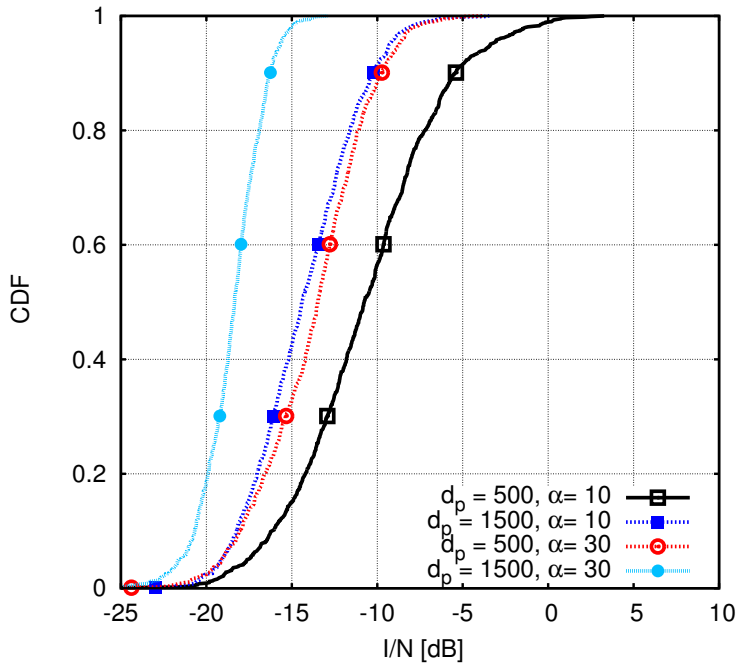

Figure 4.11. *Aggregate interference CDF considering BSs with* $N_a = 64$

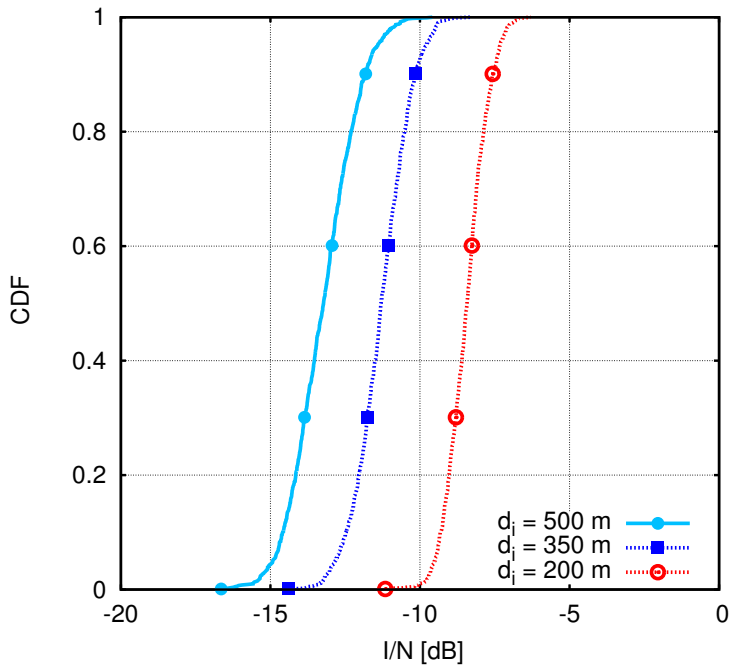

Figure 4.12. *Aggregate interference CDF considering different BSs intersite distances*

consider the third scenario presented in Section 4.2.1.1 and we assume that each BS has 10 users deployed randomly within the coverage area. The other system parameters are the same used to generate fig. 4.10.

Fig. 4.13 shows the evolution of the I/N level at the FSS for the different potential game algorithms proposed using the same configuration of users and starting from the same random set of scheduled users. As expected, the I/N level for the MinInt algorithm converges around I_0 since there is no reward for the BSs to schedule users that generate interference at the FSS. Conversely, the utility of the MaxRate algorithm is related just to the spectral efficiency of the users and the I/N level converges to a higher value. Finally, the LinComb algorithm achieves an intermediate I/N value. We emphasize that the converging values of the MinInt and LinComb algorithms can be modified selecting a different I_0 value.

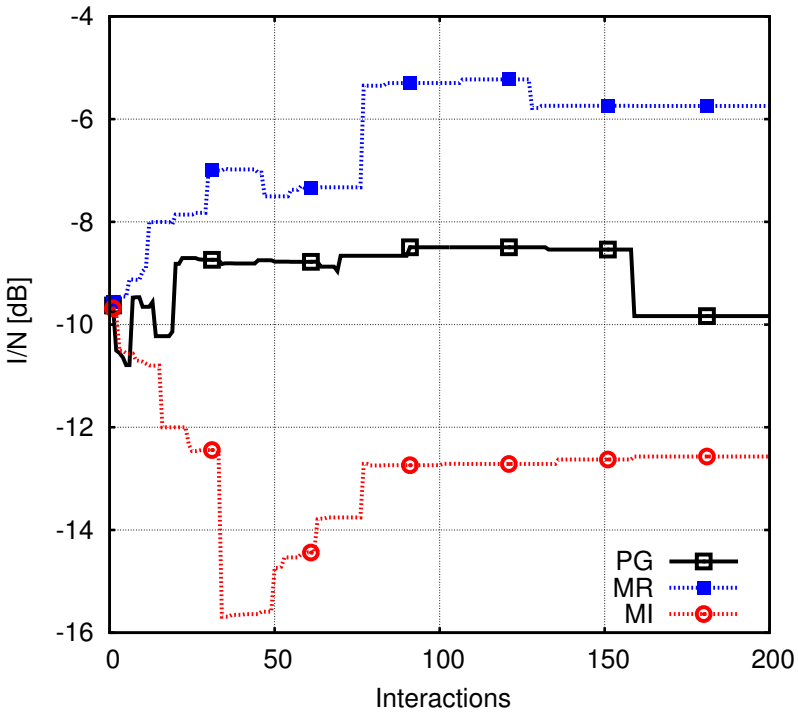

Figure 4.13. *I/N evolution for the different algorithms considered*

Fig. 4.14 describes the CDF of the I/N level at the FSS. The results have been obtained via Monte Carlo simulations using a different users configuration for each realization. As expected, the performance achieved by the MaxRate algorithm are above the limit imposed by regulations since there is no constraints on the interference at the FSS. Conversely, for the

MinInt algorithm the I/N level is maintained under the -10 dB threshold recommended by the standard. Using the LinComb algorithm the standard threshold is achieved for almost 60% of the user configurations getting a significant improvement in comparison with the MaxRate case.

Fig. 4.15 shows the CDF of the user spectral efficiency for the different algorithms considered. As expected, the MinInt and MaxRate algorithms obtained the worst and the best results, respectively. Conversely, the PG algorithm achieves a result very close to the MaxRate algorithm even though, as depicted in Fig. 4.14, the interference at the FSS is maintained at low values. Thus, the LinComb algorithm provides a good tradeoff between guaranteeing a high user spectral efficiency and achieving an acceptable interference level at the FSS. Besides, properly selecting the parameters I_0 and β, it is possible to regulate the BSs-FSS coexistence and to reduce the protection distance to increase the mmWave network coverage area.

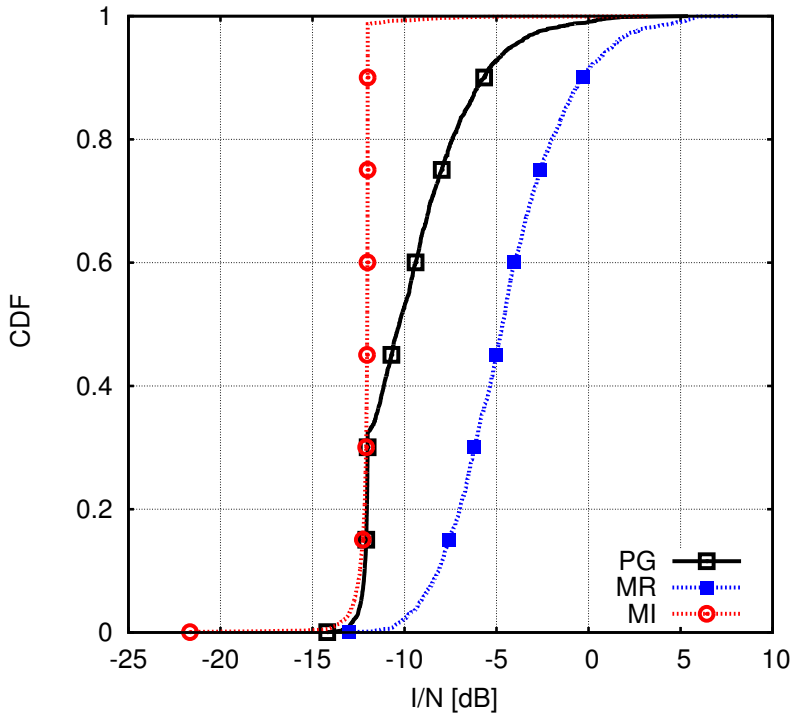

Figure 4.14. *I/N CDF for the different algorithms considered*

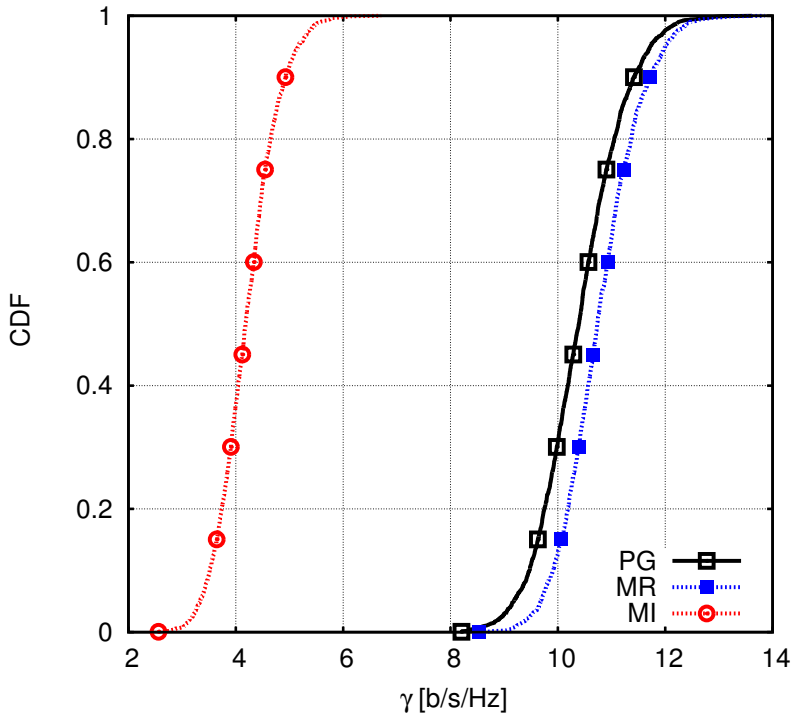

Figure 4.15. *ν CDF for the different algorithms considered*

Chapter 5

Heterogeneous Networks Mobility Management

While increasing the efficiency of the cellular networks, HetNets also raise several technical challenges related to user management [4]. An important aspect is related to the handover (HO) process of mobile users that, differently from the classical cellular networks, have to deal with cells of widely varying coverage areas. In general, the HO process, standardized by the 3GPP [92], is triggered by the UE, which periodically measures the Reference Symbols Received Power (RSRP) from the surrounding cells. When the difference between the RSRP of a neighboring cell and the serving cell is higher than a fixed HO hysteresis value (event A3 in [93]), the HO process starts, as exemplified in Fig. 5.1. If this condition holds for a period of time equal to the *Time-To-Trigger* (TTT) parameter, the HO is finalized and the UE connects to the BS with the strongest RSRP.

The static setting of the HO hysteresis and TTT values adopted in traditional scenarios with only macrocells is no longer effective for HetNet systems, because of the large variety in cell characteristics [25]. With large values of TTT and hysteresis margin, the UE will likely experience a severe degradation of the RSRP during the TTT period when crossing a small cell, a problem that is generally referred to as *HO Failure* (HF). On the other hand, short TTT and low hysteresis margin may cause *HO Ping-Pong* (HPP), i.e., frequent HOs to/from the M-BS, which yields performance losses due to signaling overhead and handover times. Reducing HO failure and ping-pong rates are clearly conflicting objectives, and the HO policy needs to trade off the two aspects.

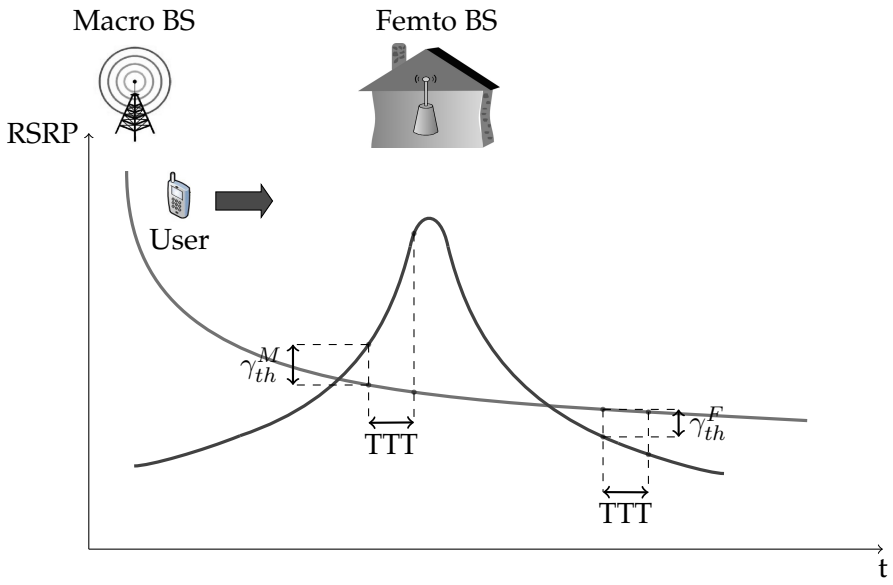

Figure 5.1. *Example of the decay of the power profile from the M-BS and F-BS as the UE moves away from the M-BS and towards the F-BS.*

Another challenge of HetNet management is the so called *Load Balancing* (LB), which consists in mitigating congestions in cellular networks by offloading users from overloaded cells to light loaded neighboring cells. This problem has been mostly addressed in homogeneous networks, with only macrocells. LB in HetNets is more involved due to the disparities in cell sizes and transmit powers. In order to achieve the desired efficiency from the deployment of small cells, hence, the handover decision needs also to be load-aware. Indeed, mobile users may be encouraged to switch to small BSs that are light loaded to get higher data rates, even if the measured RSRP gain is below threshold. As a consequence, macrocells will also have the possibility to better serve their remaining users.

In this work, we make a step forward towards the design of context-aware HO policies by first presenting a theoretical model that describes the evolution of the UE state along its trajectory, within a basic but representative HetNet scenario. Second, we determine the expression of the average UE performance as a function of the HO parameters and other contextual parameters, such as the UE speed, the power profiles of the macro/pico/femto BSs, the cell load factors, and the channel model. The mathematical framework we developed can accommodate different performance metrics, such as the HO failure rate, the ping-pong rate, or the average Shannon capacity, which is the one actually considered in this work. The mathematical model is then used to design a context-aware HO policy (CAHP)

that selects the HO parameters to maximize the performance metric with respect to the UE environment and channel conditions.

In particular, we advanced the idea of modelling the handover process by means of a non-homogeneous Markov chain, and we exploited the model to define a context-aware HO policy that was shown to improve the average performance of a mobile UE with respect to the context-agnostic policies. Furthermore, upon such a base, this we extend the context-aware HO policy to take into account the traffic load of the different cells. This is obtained by dynamically changing the HO hysteresis values to be considered in the HO process according to the load information broadcasted by the cells. Moreover, in Appendix A.5 we sketch a possible generalization of the model to an HetNet scenario with multiple femtocells.

A similar work has been proposed in [94], where the authors develop a mathematical model for the HO procedure and derive a closed-form expression of the UE outage probability. Their policy selects the TTT and margin parameters in order to minimize the specific metric of HF rate. However, they do not consider the problem of load balancing among cells and, moreover, make the assumption that the UE trajectory with respect to the position of the BSs is known to the UE. Our work, instead, proposes a more general model, and defines a context-aware HO strategy based on the more realistic assumption that the UE's trajectory with respect to the location of the BSs is unknown and that the cells are loaded.

5.1 Prior Work

Recent surveys on self-organizing networks (SON) [95] and on mobility management in HetNets [96] clearly show that a proper configuration of system parameters is both crucial for the overall throughput and also challenging due to the heterogeneity of the network. Several solutions in the literature consider to adapt some HO parameters to the UE mobility conditions. In [97], for instance, authors propose an algorithm that, while keeping constant TTT and hysteresis margin, adaptively modifies the Cell Individual Offset (CIO) parameter, which is a margin to be added to the RSRP used for load management purposes. Here the authors show that an UE can detect changes in its mobility pattern by monitoring the changes of the type of HO failure events (e.g., too early/late HO events, HO failures, or HO to the wrong cell) and, hence, can adjust the specified CIO parameter to minimize both the HO failure and the ping-pong rates.

In [98] an extensive simulation campaign is conducted in SONs to compute Radio Link Failure (RLF)[1] rate for different UE speeds and types of handover, i.e., macro-to-macro and macro-to-pico handover. The proposed policy selects the TTT parameter that guarantees the RLF rate is below a certain threshold. The reference [99] analyzes the Cell Range Expansion (CRE) technique that consists in enlarging the small cell coverage in order to balance the users load. The authors simulate the effect of both CRE bias and hysteresis margin on the HO failure and ping-pong rates, while fixing the TTT parameter.

A different approach is presented in [99] where the HO decision is based on a mobility prediction algorithm that estimates the residence time of the UE on the possible target cell. The proposed policy allows the UE to switch to the target cell only when the estimated time is above a certain threshold. A similar procedure is considered in [100] where a mobility state estimation algorithm groups UEs into three speed classes and assigns a fix TTT value to each of them, such that high speed UEs avoid the HO to pico cells, while lower speed UEs perform HO in order to minimize their RLF rate.

In these works, however, all users are assumed to have full access to the whole amount of cell resources, irrespective of the current traffic load of each cell, which is unrealistic. The load balancing problem has been studied in [101], where the authors analyze the impact of the CRE parameter on the system capacity through the CDF of the SINR. The CRE parameter is adjusted to control the number of off-loaded users and, hence, to guarantee that the overall capacity is maximized. However, [101] assumes static users and does not take into account the handover that involves mobile users. The authors in [102], instead, propose a joint algorithm that, on the one hand, tunes TTT and hysteresis parameters to optimize the handover performance metric (defined as a weighted sum of RLF, PP and HF) and, on the other hand, adapts the handover margin to achieve a load balancing condition.

Although these solutions improve the efficiency of HO in HetNets with respect to the standard static setting of the HO parameters, to the best of our knowledge a mathematical model that describes the HO performance as a function of the scenario parameters, such as the pathloss coefficients, the UE speed, and the cell load factors, is still lacking.

[1] According to the standard [92], a RLF is declared when the user SINR remains below a certain threshold Q_{out} for the entire duration of the T310 timer (usually 1 s).

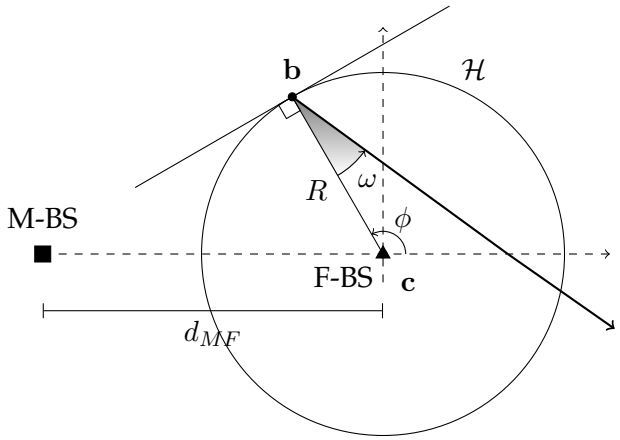

Figure 5.2. *Reference scenario: macrocell BS – M-BS (■), femtocell BS – F-BS (▲), and HO line $\mathcal{H}$ approximated as a circle of radius R and center* **c**. *Linear trajectory followed by a UE when entering the femtocell at point* **b** *with incidence angle ω.*

5.2 System Model

For the sake of simplicity, we focus on a basic scenario consisting of a macro BS (M-BS) and a femto BS (F-BS) placed at distance d_{MF}, and using the same frequency band. Despite its simplicity, this model still presents the fundamental issues involved in the HO process in HetNets and, hence, is representative of the targeted scenario. In any case, the approach we propose in this manuscript can be generalized to more complex scenarios with multiple overlapping femtocells, though at the cost of a more involved notation and argumentation. For this reason, we prefer to relegate the discussion of the multi femtocell case to Appendix A.5.

For convenience, we define the UE's trajectory with respect to a reference circle $\mathcal{H}$ of radius R centered at the F-BS. We assume that the UE moves at constant speed v, following a straight trajectory. With reference to the polar coordinate system depicted in Fig. 5.2, the trajectory is then uniquely identified by the angular coordinate ϕ of point **b** where the UE crosses the border $\mathcal{H}$, and by the incidence angle ω formed by the trajectory with respect to the radius passing through **b**. We assume that the UE can enter the femtocell from any point and with any angle, so that the parameters ϕ and ω are modeled as independent random variables with uniform distribution in the intervals $[0, 2\pi]$ and $[-\pi/2, \pi/2]$, respectively.

In the remainder of this section we describe the channel model, the HO process and the target performance metric considered in this work.

5.2.1 Propagation model

At time t, a mobile UE at position $\mathbf{a}$ measures an RSRP $\Gamma_M(\mathbf{a}, t)$ from the M-BS, and $\Gamma_F(\mathbf{a}, t)$ from the F-BS.

We assume a path-loss plus fading propagation model [103], according to which the RSRP from the h-BS, with $h \in \{M, F\}$, is given by

$$\Gamma_h(\mathbf{a}, t) = \Gamma_h^{tx}\, g_h(\mathbf{a})\, \alpha_h(t)\,, \tag{5.1}$$

where Γ_h^{tx} is the transmit power of the h-BS, $g_h(\mathbf{a})$ is the pathloss gain, which depends only on the distance of point $\mathbf{a}$ from the h-BS, while $\alpha_h(t)$ is the fast-fading channel gain at time t. We assume that the fading is Rayleigh distributed, i.e., $\alpha_h(t)$ is an exponential random variable with unit mean and coherence time

$$T_c = \sqrt{\frac{9}{16\pi}}\frac{1}{f_d} = \sqrt{\frac{9}{16\pi}}\frac{c}{v f_c}\,, \tag{5.2}$$

where f_d and f_c are the Doppler and the carrier frequencies, respectively, c is the speed of light, and v is the UE's speed. Due to fading, channel fluctuations can cause the HO process to be improperly triggered, thus generating the ping-pong effect. The duration of the channel outage is a well studied metric in the literature to model this phenomenon (see e.g., [104]).

Since the considered scenario is interference-limited, we can neglect the noise term and approximate the SINR $\gamma_h(\mathbf{a}, t)$ experienced by an UE connected to the h-BS at time t and in position $\mathbf{a}$ as[2]

$$\gamma_h(\mathbf{a}, t) = \bar{\gamma}_h(\mathbf{a})\xi_h(t)\,, \quad h \in \{M, F\}\,; \tag{5.3}$$

where

$$\bar{\gamma}_M(\mathbf{a}) = \frac{\Gamma_M^{tx}\, g_M(\mathbf{a})}{\Gamma_F^{tx}\, g_F(\mathbf{a})}\,, \quad \bar{\gamma}_F(\mathbf{a}) = \frac{\Gamma_F^{tx}\, g_F(\mathbf{a})}{\Gamma_M^{tx}\, g_M(\mathbf{a})}\,, \tag{5.4}$$

are the deterministic components of the SINR, while

$$\xi_M(t) = \frac{\alpha_M(t)}{\alpha_F(t)}\,, \quad \xi_F(t) = \frac{\alpha_F(t)}{\alpha_M(t)}\,, \tag{5.5}$$

account for the random variation due to fading.

[2]The model can be extended to account for the interference from other cells, Appendix A.5, though for the sake of simplicity we neglect other interference sources.

5.2.2 Handover performance model

The HO process is driven by the UE's instantaneous RSRP. If the difference between the RSRP of the serving and the target cell drops below the HO threshold γ_{th}, the TTT timer is initialized to a certain value T and the countdown starts. Whenever the RSRP difference returns above the HO threshold, however, the countdown is aborted and the HO procedure is interrupted. Conversely, if it remains below the threshold for the entire interval T, then the UE disconnects from the serving BS and connects to the new BS. This switching process takes a time T_H that accounts for the network procedures to connect the UE to the target BS. We remark here that the above condition on the RSRP difference can be translated to an equivalent condition on the SINR experienced by the UE where the power received from the target cell is the interference. Hence, we will use this latter notation in the following.

5.2.3 Mean trajectory performance

For any given point $\mathbf{a}$, we can then define the connection state S of the UE to be M, F or H depending on whether the UE is connected to the **M**-BS, the **F**-BS or is temporarily disconnected because **H**anding over from one to the other.

Given an arbitrary straight path ℓ, we define the mean trajectory performance as

$$\mathcal{C}_\ell = \frac{1}{|\ell|} \int_\ell \sum_{S\in\{M,F,H\}} C_S(\mathbf{a}) \chi_{\mathbf{a}}(S) \mathrm{d}\mathbf{a}\,; \tag{5.6}$$

where $|\ell|$ is the trajectory's length, $\int_\ell$ is the line integral along the trajectory, $\chi_{\mathbf{a}}(S)$ is 1 if the UE's state at point $\mathbf{a}$ is S and zero otherwise, while $C_S(\mathbf{a})$ is the performance experienced by the UE at point $\mathbf{a}$ along the trajectory, given that it is in state $S \in \{M, F, H\}$.

Since the UE can follow any trajectory, we average the mean trajectory performance along all the straight lines of length L that enter the femtocell with random incidence angle, thus obtaining[3]

$$\mathcal{C}_L = \frac{1}{L\pi} \int_{-\pi/2}^{\pi/2} \int_0^L \sum_{S\in\{M,F,H\}} C_S(\mathbf{a}(x,\omega)) \chi_{\mathbf{a}(x,\omega)}(S) \mathrm{d}x\, \mathrm{d}\omega\ , \tag{5.7}$$

with $\mathbf{a}(x,\omega)$ being the point at distance x from $\mathbf{b}$ along the trajectory with incidence angle ω.

[3]For the symmetry of the problem, the entrance point $\mathbf{b}$ is irrelevant. Moreover L is chosen to be large enough to allow the UE to be eventually connected back to the M-BS.

Now, the term $\chi_{\mathbf{a}(x,\omega)}(S)$ is random, depending on the evolution of the SINR in the previous time interval of length T. Taking the expectation of 5.7 with respect to the random variables $\xi_h(t)$, $h \in \{M, F\}$, defined in 5.5, we hence get

$$\bar{\mathcal{C}}_L = \frac{1}{L\pi} \int_{-\pi/2}^{\pi/2} \int_0^L \sum_{S \in \{M,F,H\}} \bar{C}_S(\mathbf{a}(x,\omega)) \mathrm{P}_S[\mathbf{a}(x,\omega)] \mathrm{d}x \, \mathrm{d}\omega \,, \tag{5.8}$$

where $\bar{C}_S(\mathbf{a}(x,\omega))$ is the average performance at point $\mathbf{a}(x,\omega)$, given that the UE's state at point $\mathbf{a}(x,\omega)$ is S, whose probability is

$$\mathrm{P}_S[\mathbf{a}(x,\omega)] = \mathbb{E}\, \chi_{\mathbf{a}(x,\omega)}(S) \,. \tag{5.9}$$

We focus on the average Shannon capacity experienced by the UE while crossing the femtocell. Hence, for $S \in \{M, F\}$ we define

$$\begin{aligned} \bar{C}_S(\mathbf{a}) &= \mathbb{E} \log_2 \left(1 + \gamma_S(\mathbf{a}, t)\right) \\ &= \log_2 \left(\bar{\gamma}_S(\mathbf{a})\right) \, \frac{\bar{\gamma}_S(\mathbf{a})}{\bar{\gamma}_S(\mathbf{a}) - 1} \,; \end{aligned} \tag{5.10}$$

where the expression in the last row is derived in the Appendix A.4. In order to account for the various costs of the handover process (energy, time, signaling, etc), we assume zero capacity when the UE is switching from one BS to the other, i.e.,

$$\bar{C}_H(\mathbf{a}) = 0 \,. \tag{5.11}$$

Unfortunately, the computation of 5.9 is very complex because of the time correlation of the fading process. To overcome this problem, we replace the continuous time model with a slotted-time model, where the UE's trajectory is observed at time epochs spaced apart by the fading coherence time T_c. In this way, at each slot we can approximately assume an independent fading value. Note that the sampling time, i.e., slot duration, varies with the UE's speed, as for 5.2. Nonetheless, the distance covered by the UE in a time slot is constant and equal to

$$\Delta_c = vT_c = \sqrt{\frac{9}{16\pi}} \frac{c}{f_c} \,. \tag{5.12}$$

In the following, we will refer to the space interval Δ_c, which represents the spatial granularity of our model, as *space slot*.

We can then define the *average capacity* $\bar{\mathcal{C}}_L$ with respect to this sampled space as

$$\bar{\mathcal{C}}_L = \frac{1}{\pi} \int_{-\pi/2}^{\pi/2} \frac{1}{N_L} \sum_{k=1}^{N_L} \sum_{S \in \{M,F,H\}} \bar{C}_S(\mathbf{a}_k(\omega)) \mathrm{P}_S[\mathbf{a}_k(\omega)] \, \mathrm{d}\omega \tag{5.13}$$

where

$$N_L = \left\lceil \frac{L}{\Delta_c} \right\rceil \tag{5.14}$$

is the total number of sample points along the trajectory, and $\mathrm{P}_S[\mathbf{a}_k(\omega)]$ is the probability that the UE is in state $S \in \{M, F, H\}$ at sample point $\mathbf{a}_k$ along its trajectory. In the next section, we describe a Markov model to compute the probabilities $\mathrm{P}_S[\mathbf{a}_k(\omega)]$.

5.3 Markov analysis of the HO performance

In this section we model the HO process by means of a *non homogeneous* discrete time Markov Chain (MC). To begin with, we denote by N_T and N_H the number of space slots covered by the UE in time T and T_H, respectively, i.e.,

$$N_T = \left\lceil \frac{vT}{\Delta_c} \right\rceil \ , \quad N_H = \left\lceil \frac{vT_H}{\Delta_c} \right\rceil \ . \tag{5.15}$$

At every step, the UE moves along its trajectory, and the SINR changes accordingly. As explained in the previous section, the HO process is started whenever the SINR drops below a certain threshold γ_{th}. We then define M_j and F_j, with $j \in \{0, \ldots, N_T\}$, as the MC state that is entered when the UE is connected to the M-BS or F-BS, respectively, and the SINR has remained below γ_{th} for j consecutive steps. Furthermore, we define H_j and $\tilde{H}_j$, $j \in \{1, \ldots, N_H\}$, as the MC states entered when the UE performs the macro-to-femto and femto-to-macro handover, respectively.

Assume that, at step k, the MC is in state M_j. In the following step, the MC evolves from M_j to M_{j+1} if $\gamma_M(\mathbf{a}_k, kT_c) < \gamma_{th}^M$, otherwise the MC returns to M_0 since the TTT counter is reset. Conversely, if the SINR remains below threshold when the MC is in state M_{N_T}, the UE starts the HO process to the F-BS and the MC enters state H_1. In the following N_H steps the MC deterministically crosses all the handover states H_j and ends up in state F_0, regardless of the channel conditions. At this point, the UE is connected to F-BS, and the evolution of the MC is conceptually identical to that seen for the M_j states.

A graphical representation of the non homogeneous discrete time MC is shown in Fig. 5.3, with the transition probabilities that will be explained below.

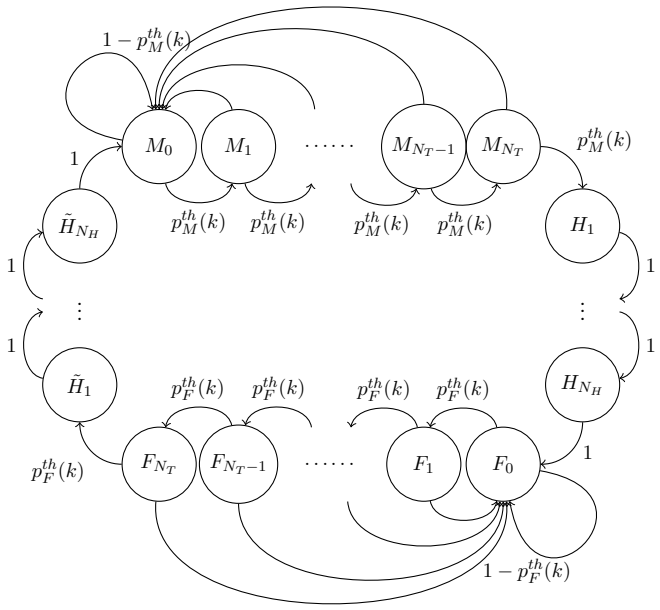

Figure 5.3. *Non homogeneous discrete time Markov chain referred to a scenario with arbitrary N_T and N_H. The transition probabilities are given by 5.17 and 5.18.*

5.3.1 Transition probabilities and transition matrix

The cumulative distribution function of the random variable ξ_h, given in 5.5 as the ratio of two independent and identically distributed exponential random variables, is equal to

$$\mathrm{P}[\xi_h \leq x] = \frac{x}{x+1}\,, \quad x \in [0, +\infty]\,. \tag{5.16}$$

Using 5.4 and 5.16, the transition probability from state M_j to M_{j+1}, with $j \in \{0, \ldots, N_T\}$, at step k, is given by

$$p_M^{th}(k) = \mathrm{P}\left[\gamma_M(\mathbf{a}_k, kT_c) < \gamma_{th}^M\right] = \frac{\gamma_{th}^M}{\gamma_{th}^M + \bar{\gamma}_M(\mathbf{a}_k)}\,. \tag{5.17}$$

Similarly, the transition probability from F_j to F_{j+1} is equal to

$$p_F^{th}(k) = \mathrm{P}\left[\gamma_F(\mathbf{a}_k, kT_c) < \gamma_{th}^F\right] = \frac{\gamma_{th}^F}{\gamma_{th}^F + \bar{\gamma}_F(\mathbf{a}_k)}\,. \tag{5.18}$$

Note that 5.17 and 5.18 vary along the UE trajectory because of the pathloss, so that the MC is indeed non-homogeneous.

Without loss of generality, we can arrange the states according to the order $\{M_j\}$, $\{H_j\}$, $\{F_j\}$, and $\{\tilde{H}_j\}$, and in increasing order of the index j within the same set of states. The

system transition matrix $\mathbf{P}(k)$ at the k-th step can then be expressed with the following sub block structure

$$\mathbf{P}(k) = \begin{bmatrix} \mathbf{M}(k) & \mathbf{V}_M^H(k) & \mathbf{0} & \mathbf{0} \\ \mathbf{0} & \mathbf{H}(k) & \mathbf{V}_H^F(k) & \mathbf{0} \\ \mathbf{0} & \mathbf{0} & \mathbf{F}(k) & \mathbf{V}_F^{\tilde{H}}(k) \\ \mathbf{V}_{\tilde{H}}^M(k) & \mathbf{0} & \mathbf{0} & \tilde{\mathbf{H}}(k) \end{bmatrix} \tag{5.19}$$

where the submatrices $\mathbf{M}(k)$, $\mathbf{F}(k)$, $\mathbf{H}(k)$, and $\tilde{\mathbf{H}}(k)$ are the square transition matrices within the sets $\{M_j\}$, $\{F_j\}$, $\{H_j\}$, and $\{\tilde{H}_j\}$, respectively, while $\mathbf{V}_X^Y(k)$ are the rectangular transition matrices from the set X to the set Y. All the other blocks are null and represented by the symbol $\mathbf{0}$. From the previous analysis, $\mathbf{M}(k)$ is given by

$$\mathbf{M}(k) = \begin{bmatrix} 1 - p_M^{th}(k) & p_M^{th}(k) & 0 & \cdots & 0 \\ 1 - p_M^{th}(k) & 0 & p_M^{th}(k) & \cdots & 0 \\ \vdots & \vdots & \vdots & \ddots & 0 \\ 1 - p_M^{th}(k) & 0 & 0 & \cdots & p_M^{th}(k) \\ 1 - p_M^{th}(k) & 0 & 0 & \cdots & 0 \end{bmatrix} . \tag{5.20}$$

$\mathbf{F}(k)$ is the same as $\mathbf{M}(k)$ with $p_F^{th}(k)$ in place of $p_M^{th}(k)$, while

$$\mathbf{H}(k) = \tilde{\mathbf{H}}(k) = \begin{bmatrix} 0 & 1 & 0 & \cdots & 0 \\ 0 & 0 & 1 & \cdots & 0 \\ \vdots & \vdots & \vdots & \ddots & 0 \\ 0 & 0 & \cdots & \cdots & 1 \\ 0 & 0 & \cdots & \cdots & 0 \end{bmatrix} . \tag{5.21}$$

Finally,

$$\mathbf{V}_H^F(k) = \mathbf{V}_{\tilde{H}}^M(k) = \begin{bmatrix} \mathbf{0} & \mathbf{0} \\ 1 & \mathbf{0} \end{bmatrix} , \tag{5.22}$$

and

$$\mathbf{V}_M^H(k) = \begin{bmatrix} \mathbf{0} & \mathbf{0} \\ p_M^{th}(k) & \mathbf{0} \end{bmatrix} , \; \mathbf{V}_F^{\tilde{H}}(k) = \begin{bmatrix} \mathbf{0} & \mathbf{0} \\ p_F^{th}(k) & \mathbf{0} \end{bmatrix} . \tag{5.23}$$

Once the transition matrix is defined, the state probability vector $\mathbf{p}(k)$ at the k-th step is given by

$$\mathbf{p}(k) = \mathbf{p}(0) \prod_{i=0}^{k-1} \mathbf{P}(i) , \tag{5.24}$$

where $\mathbf{p}(0)$ is the state probability vector at the starting point of the UE trajectory. Assuming that the UE starts its path when connected to the M-BS, we set the initial probabilities to 1 for M_0 and 0 for all the other states, so that

$$\mathbf{p}(0) = \begin{bmatrix} 1 & 0 & \cdots & 0 \end{bmatrix} . \tag{5.25}$$

We can then compute the probability that the UE is in state $S \in \{M, F, H\}$ at any given point $\mathbf{a}_k$, $k \in \{1, \ldots, N_L\}$, as the sum of the probabilities of the states $\{M_j\}$, $\{F_j\}$, and $\{H_j\} \cup \{\tilde{H}_j\}$, respectively, at step k, i.e.,

$$\mathrm{P}_S[\mathbf{a}_k] = \sum_{i \in \{S_j\}} p_i(k) \, , \tag{5.26}$$

where $p_i(k)$ is the i-th entry of the state probability vector 5.24.

5.4 Handover Decision accounting for Cells Load

In this section we consider the handover decision problem when macro and femtocells are partially loaded. In this case, handing over towards the BS with the strongest RSRP may actually yield poorer performance because the traffic load of the new cell. As in [105], we assume that the BSs include an indication of their current traffic load in the pilot signals, so that the UEs know the average fraction of available resources for each surrounding cell. This information shall then be considered in the HO strategy, in order to select the cell with the best tradeoff between signal quality and traffic load.

Let $\lambda_S \in [0, 1]$, $S \in \{M, F\}$, denote the fraction of available resources in the cell served by S-BS. Although our model can accommodate any other scaling law, for the sake of simplicity we assume that the average performance experienced by an UE when connected to such a BS will be simply scaled by the factor λ_S. We hence define the load-scaled average capacity of the UE in state $S \in \{M, F\}$ as follows

$$\bar{C}_S^{load}(\mathbf{a}_k) = \lambda_S \bar{C}_S(\mathbf{a}_k) = \lambda_S \log_2(\bar{\gamma}_S(\mathbf{a}_k)) \frac{\bar{\gamma}_S(\mathbf{a}_k)}{\bar{\gamma}_S(\mathbf{a}_k) - 1} \, , \tag{5.27}$$

while, as usual, we assume zero capacity during handover, i.e.,

$$\bar{C}_H^{load}(\mathbf{a}_k) = 0 \, . \tag{5.28}$$

Accordingly, the average load-scaled capacity $\bar{\mathcal{C}}_L^{load}$ along the UE trajectory is given by

$$\bar{\mathcal{C}}_L^{load} = \frac{1}{\pi} \int_{-\pi/2}^{\pi/2} \frac{1}{N_L} \sum_{k=1}^{N_L} \sum_{S \in \{M,F,H\}} \bar{C}_S^{load}(\mathbf{a}_k(\omega)) \mathrm{P}_S^{load}[\mathbf{a}_k(\omega)] \, \mathrm{d}\omega \tag{5.29}$$

where $\mathrm{P}_S^{load}[\mathbf{a}_k(\omega)]$ is the probability that at point $\mathbf{a}_k$ the UE is in state $S \in \{M, F, H\}$. Clearly, this probability depends on the HO policy, which shall be adjusted to account for the load conditions of the cells.

A simple way to reach this goal, with minimal impact on the HO mechanism, is to maintain the standard SINR-based HO procedure considered in the previous section, and acting on the Cell Individual Offset (CIO) of the cells, which shall be modified to account for the different traffic loads. This is equivalent to define, for each cell S, a threshold $\gamma_{th}^{S,load}$ that depends on the current traffic loads of the macro and femtocells, respectively.

The choice of the thresholds determines the characteristics of the load-aware HO algorithm. A reasonable approach is to adapt the threshold to the cell loads in such a way that the relative performance gain experienced by the UE when changing BS is constant. Now, averaging over the fading phenomena and assuming both macro and femtocells are unloaded ($\lambda_M = \lambda_F = 1$), the HO from M-BS to F-BS is triggered when the SINR drops below the threshold γ_{th}^M. According to 5.10, the ratio between the average capacity of the UE in state M and F at this threshold-crossing point $\mathbf{a}_{k^*}$ is given by

$$\frac{\bar{C}_M(\mathbf{a}_{k^*})}{\bar{C}_F(\mathbf{a}_{k^*})} = \frac{\log_2(\gamma_{th}^M)\frac{\gamma_{th}^M}{\gamma_{th}^M-1}}{\log_2(1/\gamma_{th}^M)\frac{1/\gamma_{th}^M}{1/\gamma_{th}^M-1}} = \gamma_{th}^M \,, \tag{5.30}$$

where $\bar{\gamma}_M(\mathbf{a}_{k^*}) = \gamma_{th}^M$ and $\bar{\gamma}_F(\mathbf{a}_{k^*}) = 1/\gamma_{th}^M$. We can then set $\gamma_{th}^{M,load}$ in such a way that the ratio between the load-scaled capacities given by (5.27) at the new threshold-crossing point $\mathbf{a}_{k^*}^{load}$ are still equal to γ_{th}^M, i.e.,

$$\frac{\bar{C}_M^{load}(\mathbf{a}_{k^*}^{load})}{\bar{C}_F^{load}(\mathbf{a}_{k^*}^{load})} = \gamma_{th}^M \,. \tag{5.31}$$

where $\bar{\gamma}_M(\mathbf{a}_{k^*}^{load}) = \gamma_{th}^{M,load}$ and $\bar{\gamma}_F(\mathbf{a}_{k^*}^{load}) = 1/\gamma_{th}^{M,load}$. Using (5.27) into (5.31) we finally get

$$\gamma_{th}^{M,load} = \gamma_{th}^M \frac{\lambda_F}{\lambda_M} \,. \tag{5.32}$$

Repeating the same reasoning for the femto-to-macro handover, we get

$$\gamma_{th}^{F,load} = \gamma_{th}^F \frac{\lambda_M}{\lambda_F} \,. \tag{5.33}$$

Using $\gamma_{th}^{S,load}$ in place of γ_{th}^S in 5.17 and 5.18, we can then resort to the MC model described in the previous section to compute the average trajectory performance achieved by the load-aware HO policy. The model can then be utilized to investigate the optimal choice of the TTT parameter, as it will be explained in the next section.

5.5 Context-Aware HO Policy (CAHP)

The mathematical model developed in the previous sections can be used to derive a *Context-Aware HO Policy* (CAHP). The context parameters that the model is built upon consist of the transmit powers of the BSs (Γ_M^{tx} and Γ_F^{tx}), the path loss coefficients (which determine the distance-dependent path gains $g_M(\mathbf{a})$ and $g_F(\mathbf{a})$), the inter-BS distance d_{MF}, the carrier frequency f_c, and the UE speed v. In addition, the traffic load of the cells can be considered for the traffic-aware CAHP. Given these parameters, it is then possible to use the models 5.13 and 5.29 to find the value TTT that maximizes the estimated average performance experienced by the UE when crossing the area. The CAHP, hence, consists in using the optimal TTT value for the current context parameters, which are supposed to be either known by the UE or estimated from the RSRP received from the different BSs.

In the remaining of this section we investigate the average UE capacity 5.13 when varying the context parameters, in order to gain insights on the shape of the CAHP when cells traffic load is neglected. In the following section, we compare by simulation the performance of our CAHP against the standard handover process using static TTT values (FIX) and we extend the analysis to the model described in Section 5.4, where it is considered the user loads at the cells.

We assume a scenario composed by a M-BS with transmission power of $46\ \mathrm{dBm}$ and a F-BS with transmission power of $24\ \mathrm{dBm}$ [106]. The BSs are placed $500\ \mathrm{m}$ apart. Furthermore, we set $T_H = 200\ \mathrm{ms}$, $\gamma_{th}^M = \gamma_{th}^F = 1\ \mathrm{dB}$, while T is varied with a granularity of $10\ \mathrm{ms}$.

Fig. 5.4 shows the analytical average capacity $\bar{\mathcal{C}}_L$ given by 5.13 for different speeds, as a function of T. We note that the curves show a similar trend for all speed values. The sharp capacity drop for low T values is due to the ping-pong effect, which is indeed alleviated when using longer T values. In particular, the longer the channel coherence time (i.e., the lower the speed v), the larger the T required to avoid the ping pong effect. For high T values, all curves reach an asymptotic value that corresponds to the average trajectory capacity achievable when handover is not performed. The optimal T shall then trade off between the risk of ping-pong effect and the HO delay. Note that, for very high speeds of the UE, the maximum capacity corresponds to the asymptotic capacity. In this case, the optimal policy simply consists in avoiding the HO, since the performance loss incurred during the HO process is not compensated by the capacity gain obtained by connecting to the F-BS.

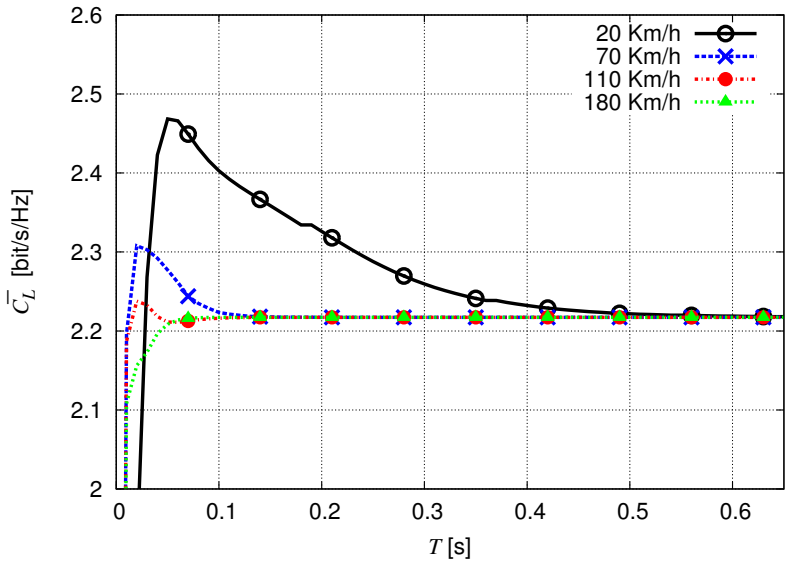

Figure 5.4. *Analytical average trajectory capacity obtained for different speeds, as a function of the TTT.*

Fig. 5.5 shows the optimal T values obtained by the analytical model for different speeds and scenarios. In practice, we vary the pathloss coefficients of the macro and femto BSs to change the channel profile and the femtocell coverage area, which is "small" for $\eta_F = 2, \eta_M = 4$ (radius of 9 m, left most bar), "medium", for $\eta_F = 2.5, \eta_M = 4.5$ (radius of 11 m, middle bar), and "large", for $\eta_F = 3, \eta_M = 5$ (radius of 13 m, right most bar). As predictable, the speed threshold above which the optimal policy is to skip HO depends on the femtocell range. In particular, for large cells, the losses due the HO are balanced by the higher capacity obtained by connecting to the F-BS. Therefore, skipping HO is convenient only when the UE speed is quite high. For lower speeds, instead, the optimal T is the minimum value to avoid ping-pong events due to fast fading and, hence, only depends on the channel coherence time that, in turn, depends on the UE's speed, but is independent of the size of the cells.

5.6 Performance Evaluation

In this section we evaluate the performance achieved by the CAHP approach through Montecarlo simulations. In particular, we compare the mean capacity obtained by CAHP against the capacity of FIX policies that use constant TTT values, with $T \in \{0.100\,\text{s}, 0.256\,\text{s}, 0.512\,\text{s}\}$, irrespective of the UE speed, and of the other channel parameters. In the simulation

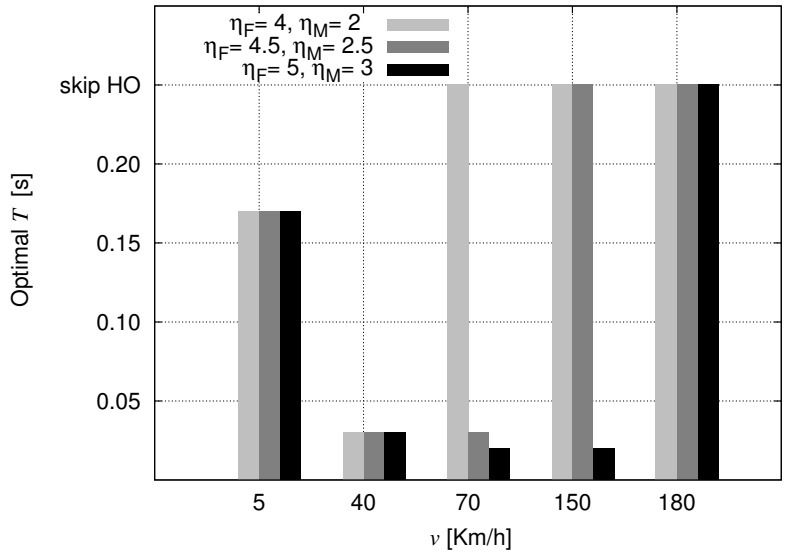

Figure 5.5. *Optimal T for different UE's speeds v and channel parameters according to CAHP approach.*

we consider path loss coefficients $\eta_F = 2.5$ and $\eta_M = 4.5$ for F-BS and M-BS, respectively, and the fast fading model presented in Section 5.2.

Fig. 5.6 shows the average trajectory capacity obtained in the simulations. At low speeds, the performance of the FIX policy suffers from the ping-pong effect due to low T values, while CAHP adopts a larger T that avoids HO triggering due to fast-fading fluctuations. Conversely, for higher speeds, CAHP outperforms the FIX policy by adopting sufficiently low T values to avoid the ping-pong effects, while not excessively delaying the switching to the F-BS. In particular, the higher the fixed T value, the lower the speed beyond which HO is never performed, and the higher the capacity loss in comparison with CAHP that, instead, performs handover. We note that, at high speeds, all curves asymptotically converge to the same value corresponding, as in the analytical model, to the average trajectory capacity achieved when the UE remains always connected to the M-BS. The optimal HO policy consists therefore in not performing the handover to the F-BS, to avoid the loss due to the two T_H in a short time interval. In this case, all the policies with sufficiently large T obtain the same results. Note that the asymptotic capacity given by simulations slightly differs from that given by the Markov model, as reported in Fig. 5.4. This small discrepancy is likely due to the simplifying assumption of the analytical model, which considers a perfectly homogeneous scenario around the femtocell center $\mathbf{c}$. The simulations, instead,

consider the actual location of both BSs and the actual power received at any given point by each of them.

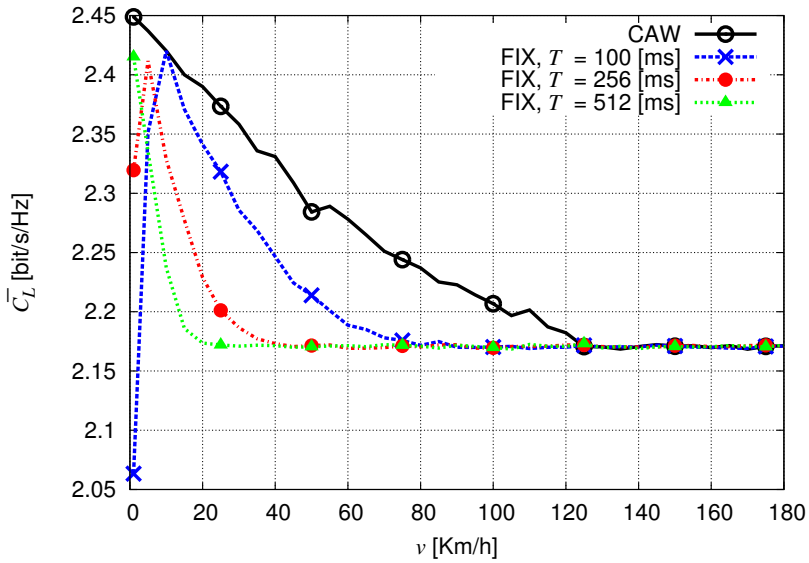

Figure 5.6. *Average capacity trajectory obtained with different approaches, as a function of the UE speed.*

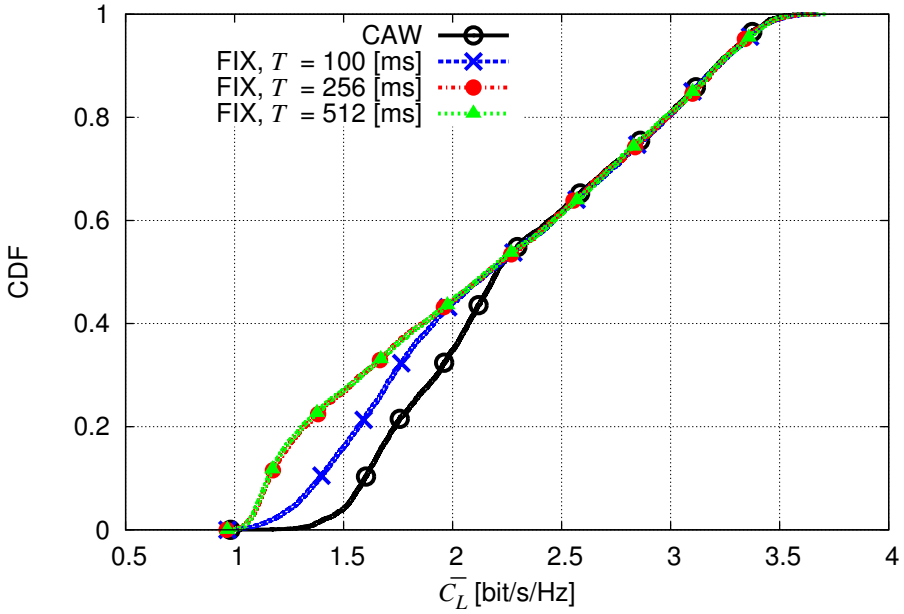

Figure 5.7. *Average trajectory capacity CDF for different approaches.*

Fig. 5.7 describes the CDF of the average trajectory capacity for a UE speed of v =

40 Km/h. We note that the improvement provided by CAHP is concentrated in the lower part of the CDF. These values correspond to the trajectories that cross the femtocell area close to its center, i.e., to the location of the F-BS. In this region, a small T makes it possible to exploit the signal from the F-BS and to gain up to 50% in capacity in comparison with the case with larger T. On the contrary, the higher part of the CDF corresponds to trajectories that cross the femtocell far from the center, so that the average trajectory capacity is basically unaffected by T because HO is skipped in most cases.

The above results have been obtained by assuming that both macro and femtocell were unloaded. In the following we instead consider the case where cells capacity is partially taken by other users. The pathloss coefficients from M-BS and F-BS are fixed to 4.5 and 2.5, respectively. Fig. 5.8 shows the analytical average trajectory capacity (5.29) as function of T, and with UE's speed $v = 20$ Km/h, when varying the load factor λ_M of the macrocell in the set $\lambda_M \in \{0.2, 0.5, 0.7, 1\}$, while keeping the femtocell unloaded ($\lambda_F = 1$). We can observe that the curves in Fig. 5.8 have the same shape, but are scaled according to λ_M. In particular, the asymptotic capacity scales proportionally to λ_M. In fact, when T is large enough, the UE does not perform handover and remains always connected to the macrocell, and its resulting average trajectory capacity equals that of the macrocell, which is scaled by a factor λ_M with respect to the unloaded case. We observe also that the T value that maximizes the average trajectory capacity is the same for every load condition. The situation however changes for higher UE speed, as can be seen from Fig. 5.9 which reports the average capacity of the UE when varying T, with $v = 150$ Km/h. Here, CAHP encourages the UE to switch to the femtocell for highly loaded macrocells ($\lambda_M = 0.2, 0.5$), while it avoids the handover when the macrocell is unloaded. This confirms the intuition that the threshold speed increases with the load of the macrocell.

Figs. 5.10 and 5.11 show the average trajectory capacity obtained through simulations when fixing $\lambda_F = 1$ and setting λ_M equal to 0.2 and 0.7, respectively. In order to quantify the performance achieved by the CAHP, we show also the capacity upper bound (Opt) computed through an exhaustive search of all possible HO policies, thus representing the best achievable performance for every user trajectory. Note that the computation of the optimal strategy requires to know in advance the fast fading gains at each point along the UE's trajectory and, hence, it is unfeasible in practical scenarios. As in the previous case, we com-

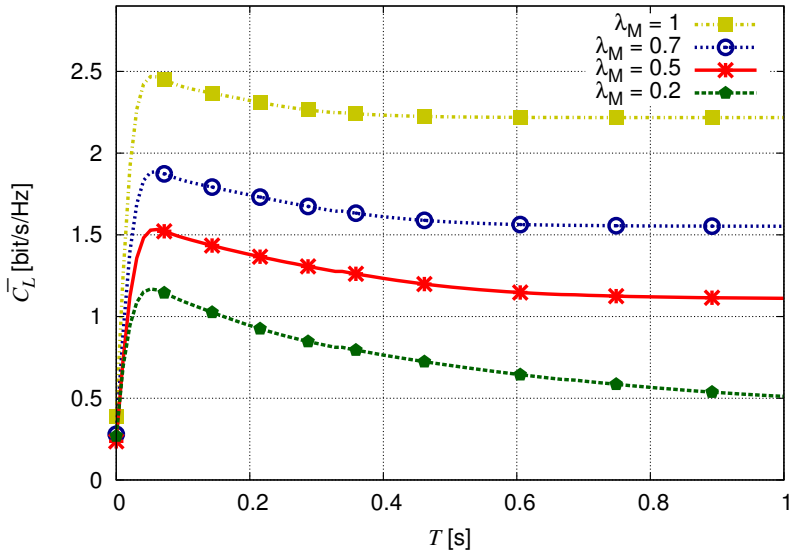

Figure 5.8. *Analytical average trajectory capacity obtained for different load conditions, as a function of* T*, with* $v = 20$ Km/h.

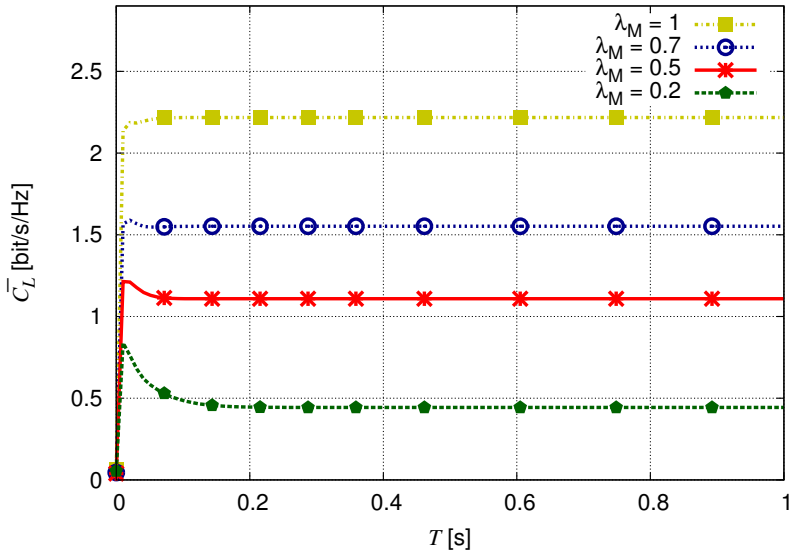

Figure 5.9. *Analytical average trajectory capacity obtained for different load conditions, as a function of* T*, with* $v = 150$ Km/h.

pare the performance achieved by the CAHP policy with two TTT-fixed policies, where the cell loads are not considered and T is set to 100 ms and 50 ms, respectively. As in Fig. 5.6, the CAHP approach achieves a substantial gain in comparison with the TTT-fixed policies for all the considered speeds. We notice that, since the capacity penalty due to T_H is larger

at high speeds, the gap with the Opt policy increases with the users velocity. Moreover, the gain provided by the CAHP policy grows when the cell load is unbalanced.

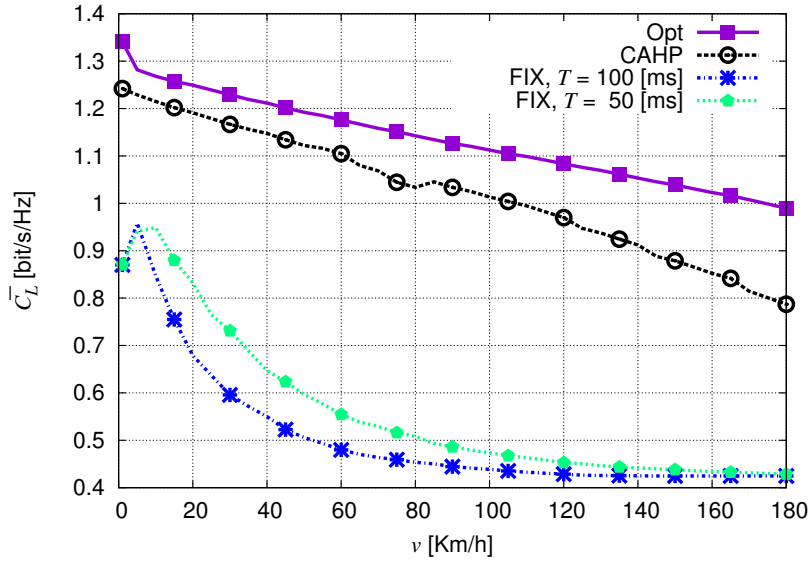

Figure 5.10. *Average trajectory capacity obtained with different approaches with $\lambda_M = 0.2$.*

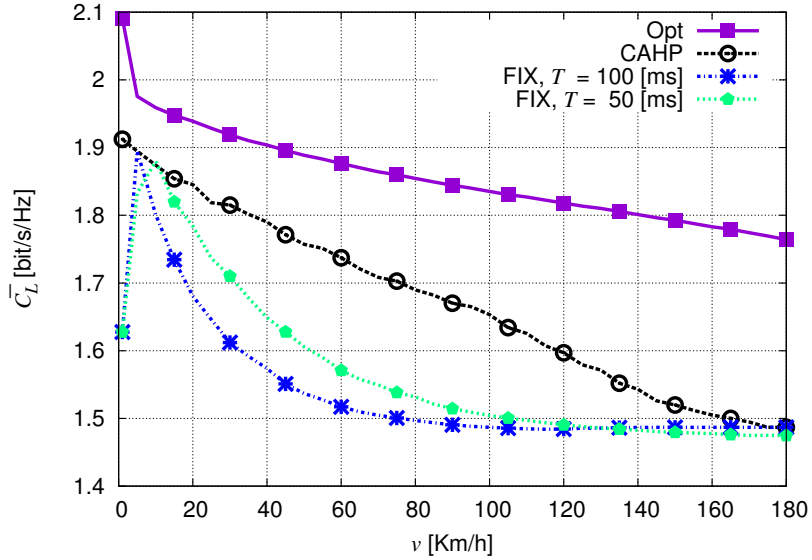

Figure 5.11. *Average trajectory capacity obtained with different approaches with $\lambda_M = 0.7$.*

This trend is analyzed in Fig. 5.12. In this simulation we set $v = 60$ Km/h, while λ_M is varied from 0.1 to 1 and $\lambda_F = 1$. As expected, the average trajectory capacity increases when the macrocell is unloaded since HO is performed less frequently because the macrocell pro-

vides good enough performance. When the load at the macrocell increases, the gap between the CAHP and the TTT-fixed policies increases. The CAHP gain is due to the capability of the CAHP approach to tune the TTT considering the cell loads. In particular, when the load at the macrocell is very high, the CAHP policy achieves more than 100% performance improvement with respect to the TTT-fixed policies.

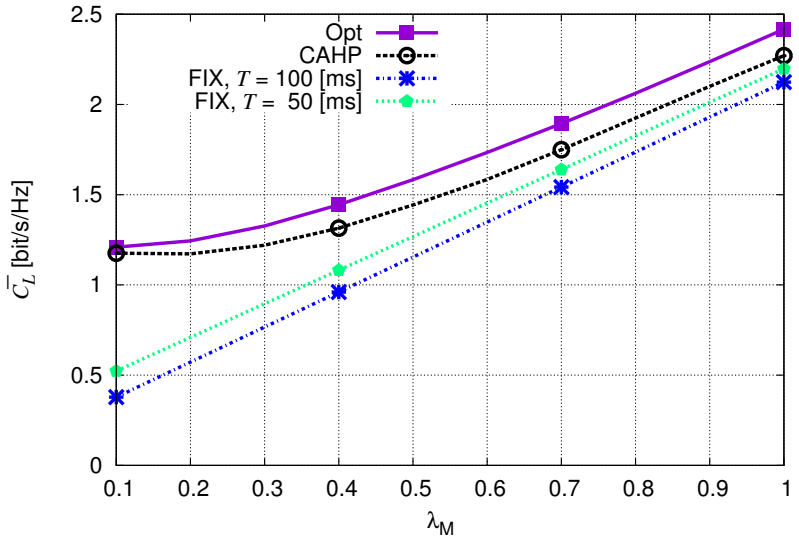

Figure 5.12. *Average trajectory capacity obtained with different approaches for* $v = 60\,\mathrm{Km/h}$ *and varying* λ_M *from* 0.1 *to* 1.

Chapter 6

Conclusions

In this thesis we discussed several issues concerning interference management, spectrum sharing and user mobile management. We adopted simulative and analytical approaches to provide new algorithms for interference and mobility management and to analyze the performance of these approaches in a standard compliant environment. Starting from the newest paradigm of cellular network communications, i.e. spectrum sharing, MIMO, CoMP, mmWave communication, heterogeneous networks, we obtained new tools for the interference management trying to face the new challenges representing by the development of a new generation of cellular networks.

In the first part of the work, we described the implementation of a 2×2 MIMO system in the simulation of LTE networks, within the well known network simulator ns3. Several MIMO techniques were framed into our approach, and the results were compared and discussed. We extend our analytical/simulation integrated framework for the available rate regions of 2×1 MISO-IC and MISO-BC scenarios. This led to several evaluations of the theoretical maximum achievable rate and the actual throughput from the perspective of a realistic network scenario, and enabled us to confirm the validity of the analytical approach and also to quantify the performance of MISO systems applied to LTE. We evaluated throughput and fairness of several beamforming techniques that allow to reach specific points of the Pareto Boundary. We demonstrated how, in a realistic LTE scenario, the performance of the network can be improved adopting these beamforming approaches. Due to the inherent complexity of framing MIMO and MISO schemes in a comprehensive system view, the proposed simulative approaches appears as a very good candidate for researchers and

practitioners to gain understanding on this kind of technology.

We proposed a modular framework based on the definition of an ISR parameter to evaluate the spectrum sharing performance. Numerical results show that non orthogonal spectrum sharing leads to considerable gains, in spite of the presence of inter-cell interference that degrades the SINR perceived by the users as long as some interference suppression techniques, such as beamforming or MIMO transmission, are available. Starting from the definition of the ISR parameter, we investigated NOSS techniques through a statistical analysis and a simulation analysis of the spectral efficiency obtained with the use of several scheduling techniques in an LTE network. Non-orthogonal sharing appears to be a promising technique for the performance improvement in cellular networks, and a joint user scheduling among the operators can give further improvements in terms of spectral efficiency. From the results obtained, it also appears that the additional sharing of the infrastructure can, depending on the specific scheduling algorithm, further improve the overall performance of the network.

We also investigated the implementation of orthogonal spectrum sharing techniques by analyzing different practical aspects, namely, whether the spectrum allocation should track the traffic variations of the operators and how often, and how this impacts the performance, quantified in terms of both throughput and fairness. We obtained that spectrum sharing is generally beneficial for the system performance, especially when the traffic loads of the operators are heavily unbalanced. Specifically, a significant gain in terms of user fairness is achieved, while total throughput improvements, albeit present, are marginal if the system operates in saturation. However, these gains require a dynamic approach that updates the spectrum allocation according to the users demand, while just using average values does not always lead to comparable gains. Furthermore, we also tested how often this dynamic update should be performed, and the main conclusions is that an update period of the order of few seconds is sufficient to retain the full performance of the approach, and even the degradation by just updating with a period of tens of seconds can be acceptable, depending on how fast the scenario changes. Thus, the associated overhead to a dynamic monitoring is likely to be relatively low and can be beneficial to the whole spectrum sharing procedure.

In the second part of the thesis we extend the concept of spectrum sharing to two different scenarios. In the first case, we proposed a novel dynamic distributed clustering algo-

rithm for CoMP that adapts the cluster configuration to the user distribution according to a predefined average cluster size. We compare the throughput performance with other clustering solutions developed in the literature, using the LTE module of the ns3 simulator. Our approach decreases the signaling exchange while at the same time improving the network performance, in particular for the low-SNR users.

In the second case, we investigated the coexistence feasibility of FSSs and cellular BSs in a mmWave scenario. Firstly, we evaluated the I/N at the FSS considering standard parameters and different BS deployments and configurations. In particular, we studied single and aggregate interference scenarios with a random distribution of the BSs and the impact of the introduction of an RF beamforming scheme at the transmitters with the assumption of no interaction among FSS and BSs. Therefore, we extend the analysis using a novel cooperative scheduling algorithm based on a game theoretic framework. From the results obtained, it appears that exploiting the characteristics of the mmWave scenario, such as high pathloss and large antenna arrays, the coexistence of FSSs and BSs in the same area is possible. Moreover, parameters such as the BS density, the protection distance and the FSS elevation angle became crucial on the network deployment to guarantee the FSS functionalities.

Finally, we proposed a novel approach to optimize the handover procedure in HetNets by considering context parameters, as the user speed, the channel gains and the load information of the cells. We derived a novel analytical framework that makes use of a Markov chain to model the evolution of the UE state during the handover process. The model was then used to derive the handover strategy that maximizes the UE average capacity in different scenarios, as a function of the context parameters. By adding suitable offsets to the HO thresholds, we then adjusted the mathematical model and the CAHP algorithm to account for the traffic loads of the cells. Finally, we presented a number of simulation results to assess the performance obtained by the proposed policy in comparison with standard HO policies with fixed TTT. From this study it clearly emerges that context-awareness can indeed improve the handover process and significantly increase the performance of mobile UEs in HetNets.

Appendix A

Appendix

A.1 ISR Computation

Since $p_{zj}|\mathbf{w}_{zk}^{(ZF)H}\mathbf{h}_{zk}| = 0$,we can write

$$ISR_j(k) = \frac{\frac{p_{ij}|\mathbf{w}_{ij}^{(ZF)H}\mathbf{h}_{ij}|^2}{\sigma^2 + p_{zj}|\mathbf{w}_{zk}^{(ZF)H}\mathbf{h}_{zk}|^2}}{\frac{p_{ij}|\mathbf{w}_{ij}^{(MRT)H}\mathbf{h}_{ij}|^2}{\sigma^2}} = \frac{|\mathbf{w}_{ij}^{(ZF)H}\mathbf{h}_{ij}|^2}{|\mathbf{w}_{ij}^{(MRT)H}\mathbf{h}_{ij}|^2}$$

$$= \frac{\left|\left(\frac{\mathbf{P}_{\mathbf{h}_{ik}}\mathbf{h}_{ij}}{\|\mathbf{P}_{\mathbf{h}_{ik}}\mathbf{h}_{ij}\|}\right)^H \mathbf{h}_{ij}\right|^2}{\left|\frac{\mathbf{h}_{ij}}{\|\mathbf{h}_{ij}\|}^H \mathbf{h}_{ij}\right|^2}$$

$$= \frac{\left|\frac{\left(\left(\mathbf{I} - \mathbf{h}_{ik}\left(\mathbf{h}_{ik}^H\mathbf{h}_{ik}\right)^{-1}\mathbf{h}_{ik}^H\right)\mathbf{h}_{ij}\right)^H}{\|\left(\mathbf{I} - \mathbf{h}_{ik}\left(\mathbf{h}_{ik}^H\mathbf{h}_{ik}\right)^{-1}\mathbf{h}_{ik}^H\right)\mathbf{h}_{ij}\|}\mathbf{h}_{ij}\right|^2}{\|\mathbf{h}_{ij}\|^2}$$

Since $\mathbf{h}_{ik}^H\mathbf{h}_{ik} = \|\mathbf{h}_{ik}\|^2$ and applying the conjugate transpose operator we obtain that:

$$ISR_j(k) = \frac{\left|\mathbf{h}_{ij}^H\left(\mathbf{I} - \frac{\mathbf{h}_{ik}\mathbf{h}_{ik}^H}{\|\mathbf{h}_{ik}\|^2}\right)\mathbf{h}_{ij}\right|^2}{\|\left(\mathbf{I} - \frac{\mathbf{h}_{ik}\mathbf{h}_{ik}^H}{\|\mathbf{h}_{ik}\|^2}\right)\mathbf{h}_{ij}\|^2} \cdot \frac{1}{\|\mathbf{h}_{ij}\|^2}$$

$$= \frac{\left|\|\mathbf{h}_{ij}\|^2\|\mathbf{h}_{ik}\|^2 - \mathbf{h}_{ij}^H\mathbf{h}_{ik}\mathbf{h}_{ik}^H\mathbf{h}_{ij}\right|^2}{\|\mathbf{h}_{ij}\|\mathbf{h}_{ik}\|^2 - \mathbf{h}_{ik}\mathbf{h}_{ik}^H\mathbf{h}_{ij}\|^2} \cdot \frac{1}{\|\mathbf{h}_{ij}\|^2}$$

$$
\begin{aligned}
&= \frac{\left|-\mathbf{h}_{ij}^H \mathbf{h}_{ik}\right|^2}{\|\mathbf{h}_{ij}\|^2\|\mathbf{h}_{ik}\|^2} \cdot \frac{\left|\frac{\|\mathbf{h}_{ij}\|^2\|\mathbf{h}_{ik}\|^2}{-\mathbf{h}_{ij}^H\mathbf{h}_{ik}} + \mathbf{h}_{ik}^H\mathbf{h}_{ij}\right|^2}{\|\mathbf{h}_{ij}\|\|\mathbf{h}_{ik}\| - \frac{\mathbf{h}_{ik}\mathbf{h}_{ik}^H\mathbf{h}_{ij}}{\|\mathbf{h}_{ik}\|}\|^2} \\
&= \rho_{jk}^2 \cdot \frac{\left|\frac{\|\mathbf{h}_{ij}\|^2\|\mathbf{h}_{ik}\|^2}{-\mathbf{h}_{ij}^H\mathbf{h}_{ik}} + \mathbf{h}_{ik}^H\mathbf{h}_{ij}\right|^2}{\|\mathbf{h}_{ij}\|\|\mathbf{h}_{ik}\| - \frac{\mathbf{h}_{ik}\mathbf{h}_{ik}^H\mathbf{h}_{ij}}{\|\mathbf{h}_{ik}\|}\|^2} \\
&= \rho_{jk}^2 \cdot \left|\frac{\|\mathbf{h}_{ij}\|^2\|\mathbf{h}_{ik}\|^2}{\mathbf{h}_{ij}^H\mathbf{h}_{ik}} - \mathbf{h}_{ik}^H\mathbf{h}_{ij}\right|^2 \cdot \frac{\|\mathbf{h}_{ik}\|^2}{\|\mathbf{h}_{ij}\|\|\mathbf{h}_{ik}\| - \mathbf{h}_{ik}\mathbf{h}_{ik}^H\mathbf{h}_{ij}\|^2} \\
&= \rho_{jk}^2 \cdot \frac{\left(\|\mathbf{h}_{ij}\|^2\|\mathbf{h}_{ik}\|^2 - |\mathbf{h}_{ik}^H\mathbf{h}_{ij}|^2\right)}{|\mathbf{h}_{ij}^H\mathbf{h}_{ik}|^2} \cdot \frac{\left(\|\mathbf{h}_{ij}\|^2\|\mathbf{h}_{ik}\|^2 - |\mathbf{h}_{ik}^H\mathbf{h}_{ij}|^2\right)'\|\mathbf{h}_{ik}\|^2}{\|\mathbf{h}_{ij}\|\|\mathbf{h}_{ik}\| - \mathbf{h}_{ik}\mathbf{h}_{ik}^H\mathbf{h}_{ij}\|^2} \\
&= \rho_{jk}^2 \cdot \left(\frac{1}{\rho_{jk}^2} - 1\right) \cdot \frac{\left(\|\mathbf{h}_{ij}\|^2\|\mathbf{h}_{ik}\|^2 - \left|\mathbf{h}_{ik}^H\mathbf{h}_{ij}\right|^2\right)'\|\mathbf{h}_{ik}\|^2}{\|\mathbf{h}_{ij}\|\|\mathbf{h}_{ik}\| - \mathbf{h}_{ik}\mathbf{h}_{ik}^H\mathbf{h}_{ij}\|^2} = 1 - \rho_{jk}^2
\end{aligned}
$$

since:

$$
\frac{\left(\|\mathbf{h}_{ij}\|^2\|\mathbf{h}_{ik}\|^2 - \left|\mathbf{h}_{ik}^H\mathbf{h}_{ij}\right|^2\right)'\|\mathbf{h}_{ik}\|^2}{\|\mathbf{h}_{ij}\|\|\mathbf{h}_{ik}\| - \mathbf{h}_{ik}\mathbf{h}_{ik}^H\mathbf{h}_{ij}\|^2} = 1
$$

A.2 PDF of the sum of two Beta random variables

Consider a set of n independent and identically distributed random variables. The cdf of the maximum of those variables is given by:

$$
P\{\max(y_1, y_2, ..., y_n) \leq \alpha\} = [P\{y \leq \alpha\}]^n
$$

In our case, the cumulative distribution is described by a regularized incomplete beta function $I_x(a,b)$=$B_x(a,b)/B(a,b)$, so the related pdf $f_\rho(x)$ can be obtained as

$$
\begin{aligned}
\frac{\mathrm{d}\left[I(x))\right]^n tbh}{\mathrm{d}x} &= \frac{\mathrm{d}\left[B_x(a,b)/B(a,b)\right]^n}{\mathrm{d}x} = n\left(\frac{B_x(a,b)}{B(a,b)}\right)^{n-1} \frac{\mathrm{d}B_x(a,b)/B(a,b)}{\mathrm{d}x} \\
&= n\left(\frac{B_x(a,b)}{B(a,b)}\right)^{n-1} \frac{x^{a-1}(1-x)^{b-1}}{B(a,b)}
\end{aligned}
$$

A similar approach can be used for the case of a general beta variable whose cdf is

$$
\frac{B_x(\alpha,\beta,a,b)}{B(\alpha,\beta)}.
$$

By repeating the same procedure applied above, (3.11) can be derived.

A.3 Exact potential functions definition

In game theory, a game is said to be a potential game if the incentive of all players to change their strategy can be expressed using a single global function called the potential function. In particular, a game $\Gamma(\mathbf{N}, \mathbf{S}, U_i)$ is an exact potential game if there exists a function $F : \mathbf{S} \to \mathbb{R}$ such that for all $i \in \mathbf{N}$, all $s \in \mathbf{S}$ and all $s'_i \in \mathbf{S}_i$:

$$U_i(s_i, s_{-i}) - U_i(s'_i, s_{-i}) = F(s_i, s_{-i}) - F(s'_i, s_{-i}) \tag{A.1}$$

The function F is called an exact potential function for the game $\Gamma(\mathbf{N}, \mathbf{S}, U_i)$ [83].

In order to show that the problems presented in Section 4.2.2 can be treated as potential games, we have to define a potential function for each scenario considered.

Considering the set of BSs $\{1, ..., N\}$ and denoting as q the user scheduled by BS k with $k \in \{1, ..., N\}$, we can define $F(S)$ for the MaxRate algorithm as

$$\begin{aligned} F(S) &= F(s_k, s_{-k}) \\ &= \sum_{i=1}^{N} (p_{ji} \left|\mathbf{v}_i^T \mathbf{h}_{ji}\right|^2 - \alpha \sum_{n=1, n\neq i}^{N} p_{jn} \left|\mathbf{v}_n^T \mathbf{h}_{jn}\right|^2 - (1-\alpha) \sum_{m=1, m\neq j}^{M} p_{mi} \left|\mathbf{v}_i^T \mathbf{h}_{mi}\right|^2) \end{aligned}$$

with $0 < \alpha < 1$.

It is possible to isolate the terms depending on s_k as

$$\begin{aligned} F(S) &= p_{qk} \left|\mathbf{v}_k^T \mathbf{h}_{qk}\right|^2 - \alpha \sum_{n=1, n\neq k}^{N} p_{qn} \left|\mathbf{v}_n^T \mathbf{h}_{qn}\right|^2 - (1-\alpha) \sum_{m=1, m\neq q}^{M} p_{mk} \left|\mathbf{v}_k^T \mathbf{h}_{mk}\right|^2 \\ &+ \sum_{i=1, i\neq k}^{N} (p_{ji} \left|\mathbf{v}_i^T \mathbf{h}_{ji}\right|^2 - \alpha \sum_{n=1, n\neq i}^{N} p_{jn} \left|\mathbf{v}_n^T \mathbf{h}_{jn}\right|^2 - (1-\alpha) \sum_{m=1, m\neq j}^{M} p_{mi} \left|\mathbf{v}_i^T \mathbf{h}_{mi}\right|^2) \\ &= p_{qk} \left|\mathbf{v}_k^T \mathbf{h}_{qk}\right|^2 - \alpha \sum_{n=1, n\neq k}^{N} p_{qn} \left|\mathbf{v}_n^T \mathbf{h}_{qn}\right|^2 - (1-\alpha) \sum_{m=1, m\neq q}^{M} p_{mk} \left|\mathbf{v}_k^T \mathbf{h}_{mk}\right|^2 \\ &+ \sum_{i=1, i\neq k}^{N} (p_{ji} \left|\mathbf{v}_i^T \mathbf{h}_{ji}\right|^2 - \alpha p_{jk} \left|\mathbf{v}_k^T \mathbf{h}_{jk}\right|^2 - \alpha \sum_{n=1, n\neq i,k}^{N} p_{jn} \left|\mathbf{v}_n^T \mathbf{h}_{jn}\right|^2 - (1-\alpha) p_{qi} \left|\mathbf{v}_i^T \mathbf{h}_{qi}\right|^2 \\ &- (1-\alpha) \sum_{m=1, m\neq j,q}^{M} p_{mi} \left|\mathbf{v}_i^T \mathbf{h}_{mi}\right|^2) \end{aligned}$$

Let

$$Q(s_{-k}) = \sum_{i=1, i\neq k}^{N} (p_{ji} \left|\mathbf{v}_i^T \mathbf{h}_{ji}\right|^2 - \alpha \sum_{n=1, n\neq i,k}^{N} p_{jn} \left|\mathbf{v}_n^T \mathbf{h}_{jn}\right|^2 - (1-\alpha) \sum_{m=1, m\neq j,q}^{M} p_{mi} \left|\mathbf{v}_i^T \mathbf{h}_{mi}\right|^2)$$

Then

$$
\begin{aligned}
F(S) &= p_{qk}\left|\mathbf{v}_k^T\mathbf{h}_{qk}\right|^2 - \alpha\sum_{n=1,n\neq k}^{N} p_{qn}\left|\mathbf{v}_n^T\mathbf{h}_{qn}\right|^2 - (1-\alpha)\sum_{m=1,m\neq q}^{M} p_{mk}\left|\mathbf{v}_k^T\mathbf{h}_{mk}\right|^2 \\
&\quad - \sum_{i=1,i\neq k}^{N}(\alpha p_{jk}\left|\mathbf{v}_k^T\mathbf{h}_{jk}\right|^2 + (1-\alpha)p_{qi}\left|\mathbf{v}_i^T\mathbf{h}_{qi}\right|^2) + Q(s_{-k}) - \beta\xi(I-I_o) \\
&= p_{qk}\left|\mathbf{v}_k^T\mathbf{h}_{qk}\right|^2 - \sum_{n=1,n\neq k}^{N} p_{qn}\left|\mathbf{v}_n^T\mathbf{h}_{qn}\right|^2 - \sum_{m=1,m\neq q}^{M} p_{mk}\left|\mathbf{v}_k^T\mathbf{h}_{mk}\right|^2 + Q(s_{-k}) - \beta\xi(I-I_o)
\end{aligned}
$$

Since the term $Q(s_{-k})$ is independent of the strategy of BS k, if BS k changes the scheduled user from q to q' we obtain:

$$
\begin{aligned}
&F(s_k, s_{k-1}) - F(s'_k, s_{-k}) \\
&= p_{qk}\left|\mathbf{v}_k^T\mathbf{h}_{qk}\right|^2 - \sum_{n=1,n\neq k}^{N} p_{qn}\left|\mathbf{v}_n^T\mathbf{h}_{qn}\right|^2 - \sum_{m=1,m\neq q}^{M} p_{mk}\left|\mathbf{v}_k^T\mathbf{h}_{mk}\right|^2 - \beta\xi(I-I_o) \\
&- \left(p_{q'k}\left|\mathbf{v}_k^T\mathbf{h}_{q'k}\right|^2 - \sum_{n=1,n\neq k}^{N} p_{q'n}\left|\mathbf{v}_n^T\mathbf{h}_{q'n}\right|^2 - \sum_{m=1,m\neq q'}^{M} p_{mk}\left|\mathbf{v}_k^T\mathbf{h}_{mk}\right|^2 - \beta\xi(I'-I_o)\right)
\end{aligned}
$$

that is equal to $U(s_k, s_{-k}) - U(s'_k, s_{-k})$.

For the MinInt algorithm the potential function can be easily set equal to its utility function leading directly to a potential game. Finally, the potential function for the LinComb algorithm is the sum of the two potential functions considered before and the proof is straightforward.

A.4 Expectation of $\log_2(1+\bar{\gamma}\xi)$

From 5.16, the probability density function of ξ is given by

$$
f_\xi(x) = \frac{\mathrm{d}}{\mathrm{d}x}\mathrm{P}[\xi \leq x] = \frac{1}{(x+1)^2}\ , \quad x \in [0, +\infty]\ . \tag{A.2}
$$

Given $\bar{\gamma}$, the expectation of $\log_2(1+\bar{\gamma}\xi)$ is computed as

$$
\begin{aligned}
\int_0^{+\infty} \log_2\left(1+\bar{\gamma}x\right) f_\xi(x)\,\mathrm{d}x &= \int_0^{+\infty} \log_2\left(1+\bar{\gamma}x\right)\frac{1}{(x+1)^2}\,\mathrm{d}x \\
&= \frac{\bar{\gamma}}{\bar{\gamma}-1}\log_2\left(\frac{1+\bar{\gamma}x}{1+x}\right)\Bigg|_0^{+\infty} = \frac{\bar{\gamma}}{\bar{\gamma}-1}\log_2\left(\bar{\gamma}\right)
\end{aligned}
$$

where integration by parts was used to solve the integral.

A.5 Multicell extension

We here describe a possible extension of the proposed mathematical model to a scenario with multiple femtocells. We indicate with $\mathcal{F} = \{F_1, \ldots, F_N\}$ the set of N femtocells, placed within the macrocell coverage area. At every step of its trajectory, the UE can be connected either to one of the femtocells, or to the macrocell, or can be switching from the serving to the target cell. The average capacity along the whole trajectory preserves the form of 5.13, except for the UE state space, being now $\{M, H\} \cup \mathcal{F}$:

$$\bar{\mathcal{C}}_L = \frac{1}{\pi} \int_{-\pi/2}^{\pi/2} \frac{1}{N_L} \sum_{k=1}^{N_L} \sum_{S \in \{M,H\} \cup \mathcal{F}} \bar{C}_S(\mathbf{a}_k(\omega)) \mathrm{P}_S[\mathbf{a}_k(\omega)] \, \mathrm{d}\omega \,. \tag{A.3}$$

The average capacity $\bar{C}_S(\mathbf{a}_k(\omega))$ at point $\mathbf{a}_k$ is given in 5.10 and 5.11, and the SINR $\gamma_S(\mathbf{a}_k, kT_c)$ with respect to the S-BS, $S \in \mathcal{F} \cup M$, is now given by

$$\gamma_S(\mathbf{a}_k, kT_c) = \frac{\Gamma_S(\mathbf{a}_k, kT_c)}{\sum_{S' \neq S} \Gamma_{S'}(\mathbf{a}_k, kT_c)} \tag{A.4}$$

where each received signal has power as in 5.1.

The probability $\mathrm{P}_S[\mathbf{a}_k(\omega)]$ in (A.3) are defined as in Section 5.3 and computed from the Markov Chain described below.

The MC for the multi cells scenario is slightly more involved than the one for the single femtocell (see Fig. 5.3), but the principle of transition among states is kept unchanged. The main difference is that we here need to take into account a TTT counter for each of the possible target BSs; the counter that expires first determines the next serving BS.

The states of the MC can be split into two classes. The first one describes the *cell states*, depicted with rectangular boxes in Fig. A.1 and Fig. A.2, where the UE is connected to any of the $N + 1$ BSs and one or more TTTs can possibly start. We recall here that, according to the standard [92], the TTT from the UE serving cell $\mathcal{S}er$ towards the target cell $\mathcal{T}$ starts when the SINR

$$\gamma_{\mathcal{S}er,\mathcal{T}}(\mathbf{a}_k, kT_c) = \frac{\Gamma_{\mathcal{S}er}(\mathbf{a}_k, kT_c)}{\Gamma_{\mathcal{T}}(\mathbf{a}_k, kT_c)} \tag{A.5}$$

is below threshold. In other words, in a multi-cells scenario the trigger condition involves the received powers of just the serving and the target BS. The cell states are defined as the $(N+1)$-tuples $< c_M, c_1, \ldots, c_N >$, where

$$c_S = \begin{cases} \mathrm{C} & \text{if } S = \mathcal{S}er \\ t & \text{otherwise} \,. \end{cases} \tag{A.6}$$

Parameter C indicates the BS that the UE is currently attached to, while the number $t \in \{0, 1, \ldots, N_T\}$ indicates for how many consecutive steps the SINR $\gamma_{\mathcal{S}er,S}(\mathbf{a}_k, kT_c)$ has been below threshold, i.e., t represents the TTT counter for a possible handover to S-BS. The UE will be eventually connected to BS $S^* \neq \mathcal{S}er$ if $c_{S^*} = N_T$ and $\gamma_{\mathcal{S}er,S^*}(\mathbf{a}_k, kT_c)$ remains below threshold for one more step. Obviously, S^* is the state for which these conditions occur first.

The second class of states in the MC accounts for the handover procedures towards the new serving cell. In this case the *handover states*, depicted with circles in Fig. A.2, are defined by the pair $< S, h >$ where S specifies the BS to be connected to and $h \in \{1, \ldots, N_H\}$ is the counter of the handover time.

For the sake of conciseness, we do not replicate here the rigorous analysis presented in Section 5.3 for the single cell case. We prefer instead to give some intuition on how the MC evolves in this more general case.

The transitions among cell states are constrained by the fact that, if at the k-th step $c_S = t$, with $t < N_T$ and $S \neq \mathcal{S}er$, then in the following step, c_S could be either $t + 1$ if $\gamma_{\mathcal{S}er,S}(\mathbf{a}_k, kT_c) < \gamma_{th}^{\mathcal{S}er}$ or 0 otherwise, i.e., the counter to S-BS is reset if its SINR goes above threshold. See Fig. A.1 for an example of this transition in the case of $N = 2$ femtocells.

If instead $c_S = N_T$ and $\gamma_{\mathcal{S}er,S}(\mathbf{a}_k, kT_c) < \gamma_{th}^{\mathcal{S}er}$ the UE starts the handover process to S-BS and the MC evolves to the handover state $< S, 1 >$. As before, the MC crosses deterministically all the handover states $< S, h >$, $h = 2, \ldots, N_H$ and ends up in the cell state where $c_S = \mathrm{C}$ and $c_{S'} = 0$, $\forall S' \neq S$. See Fig. A.2 for an example of this transition in the case of $N = 2$ femtocells.

The probability $p_{\mathcal{S}er,S}^{th}(k)$ that the SINR $\gamma_{\mathcal{S}er,S}(\mathbf{a}_k, kT_c)$ is below threshold is computed as in (5.17) and (5.18), and is equal to

$$p_{\mathcal{S}er,S}^{th}(k) = \mathrm{P}\left[\gamma_{\mathcal{S}er,S}(\mathbf{a}_k, kT_c) < \gamma_{th}^{\mathcal{S}er}\right] = \frac{\gamma_{th}^{\mathcal{S}er}}{\gamma_{th}^{\mathcal{S}er} + \bar{\gamma}_{\mathcal{S}er,S}(\mathbf{a}_k)} \tag{A.7}$$

where

$$\bar{\gamma}_{\mathcal{S}er,S}(\mathbf{a}_k) = \frac{\Gamma_{\mathcal{S}er}^{tx}\, g_{\mathcal{S}er}(\mathbf{a}_k)}{\Gamma_S^{tx}\, g_S(\mathbf{a}_k)} \tag{A.8}$$

is the deterministic part of the SINR $\gamma_{\mathcal{S}er,S}(\mathbf{a}_k, kT_c)$.

Since the received powers from different cells are independent, the transition probabilities among the states of the MC are easily computed from (A.7) as the product of the probabilities with respect to all cells but the serving one, as can be seen from Fig. A.1 and Fig. A.2.

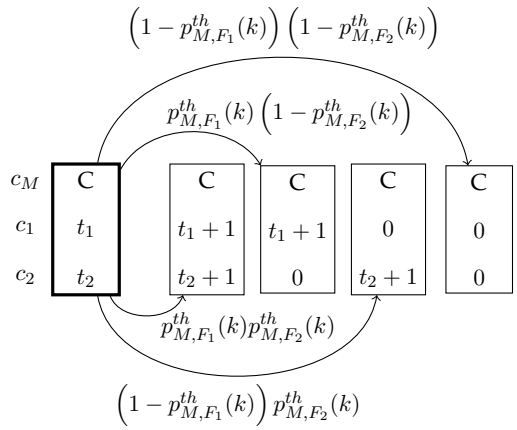

Figure A.1. *Transitions from cell state* $< \mathrm{C}, t_1, t_2 >$ *(in bold), where* $0 \leq t_1, t_2 < N_T$.

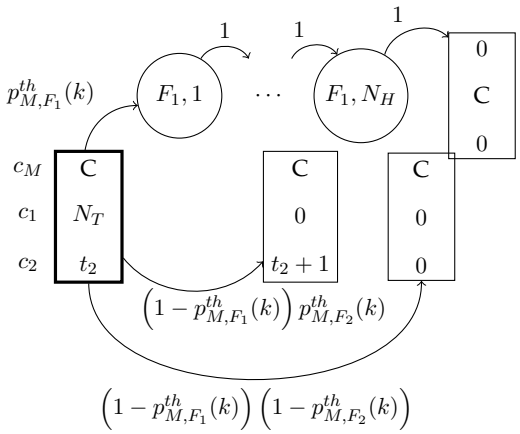

Figure A.2. *Transitions from cell state* $< \mathrm{C}, t_1, t_2 >$ *(in bold), where* $t_1 = N_T$ *and* $0 \leq t_2 < N_T$.

As a final comment, we note that the number of states N_{TOT} of the MC described above grows exponentially with the number of femtocells, since

$$N_{TOT} = (N+1)(N_T^N + N_H)\,. \tag{A.9}$$

However, the complexity of the model can be reduced by considering only transitions among neighboring cells.

List of Publications

The work presented in this thesis has appeared in the articles reported below.

Journal papers

[J1] **F. Guidolin**, L. Badia, M. Zorzi, "A Distributed Clustering Algorithm for Coordinated Multipoint in LTE Networks," *IEEE Wireless Communications Letters*, vol. 3, no. 5, pp. 517–520, Oct. 2014.

[J2] **F. Guidolin**, A. Orsino, L. Badia, M. Zorzi, "Network Analysis and Scheduling Policies for Next Generation Mobile Networks with Non-Orthogonal Spectrum Sharing," *Submitted to: IEEE Transactions on Wireless Communications*.

[J3] **F. Guidolin**, I. Pappalardo, A. Zanella, M. Zorzi, "Context-Aware Handover Policies in HetNets," *Submitted to: IEEE Transactions on Wireless Communications*.

Conference papers

[C1] **F. Guidolin**, L. Badia, M. Zorzi, "Implementation of 2 $\times$ 2 MIMO in an LTE module for the ns3 simulator," *IEEE CAMAD 2012*, pp. 281–285, 17–19 Sept. 2012.

[C2] L. Badia, R. Dal Re, **F. Guidolin**, A. Orsino, M. Zorzi, "A Tunable Framework for Performance Evaluation of Spectrum Sharing in LTE Networks," *IEEE WoWMoM 2013*, pp. 1–3, 4–7 June 2013.

[C3] **F. Guidolin**, A. Orsino, L. Badia, M. Zorzi, "Statistical Analysis of Non Orthogonal Spectrum Sharing and Scheduling Strategies in Next Generation Mobile Networks," *IEEE IWCMC 2013*, pp. 680–685, 1–5 July 2013

[C4] **F. Guidolin**, M. Carpin, L. Badia, M. Zorzi, "Performance evaluation of practical spectrum sharing techniques in LTE networks," *IEEE ISCC 2014*, 23–26 June 2014.

[C5] **F. Guidolin**, I. Pappalardo, A. Zanella, M. Zorzi, "A Markov-based framework for handover optimization in HetNets," *MedHocNet 2014*, pp. 134–139, 2–4 June 2014.

[C6] **F. Guidolin**, I. Pappalardo, A. Zanella, M. Zorzi, "Context-Aware Handover in HetNets," *EuCNC 2014.* **BEST STUDENT PAPER AWARD**

[C7] **F. Guidolin**, L. Badia, E. Karipidis, J. Lindblom, M. Zorzi, "A Framework for the Evaluation of MISO Beamforming Techniques in LTE Cellular Networks," *IEEE CAMAD 2014*, 1–3 Dec. 2014.

[C8] **F. Guidolin**, M. Nekovee, L. Badia, M. Zorzi, "A Study on the Coexistence of Fixed Satellite Service and Cellular Networks in a mmWave Scenario," *Accepted to: IEEE ICC 2015*.

[C9] **F. Guidolin**, M. Nekovee, L. Badia, M. Zorzi, "A Cooperative Scheduling Algorithm for the Coexistence of Fixed Satellite Services and 5G Cellular Networks," *Accepted to: IEEE ICC 2015*.

Bibliography

[1] 3GPP, "Evolved universal terrestrial radio acces (e- utra); physical layer procedures," TS36.213, version 8.5.0.

[2] Cisco, "Cisco visual networking index: Global mobile data traffic forecast update, 20132018," *White paper*, February 2014.

[3] N. Alliance, "Next generation mobile networks beyond HSPA & EVDO," *White paper 3.0*, December 2006.

[4] J. Andrews, "Seven ways that hetnets are a cellular paradigm shift," *IEEE Communications Magazine*, vol. 51, no. 3, pp. 136–144, March 2013.

[5] S.-E. Elayoubi, O. Ben Haddada, and B. Fourestié, "Performance evaluation of frequency planning schemes in ofdma-based networks," *IEEE Transactions on Wireless Communications*, vol. 7, no. 5, pp. 1623–1633, May 2008.

[6] M. Szydelko, "Business model analysis for spectrum sharing with the spectrum broker," in *IEEE International Symposium on Dynamic Spectrum Access Networks*, Oct 2012, pp. 378–388.

[7] T. Frisanco, P. Tafertshofer, P. Lurin, and R. Ang, "Infrastructure sharing and shared operations for mobile network operators: From a deployment and operations view," in *IEEE International Conference on Communications*, May 2008, pp. 2193–2200.

[8] P. Marques, J. Rodriguez, S. Delaere, P. Delahaye, B. Lecroart, M. Gundlach, D. Triantafyllopoulou, K. Moessner, and D. Noguet, "Shared use of radio spectrum in the

eu: From research projects to standards," in *IEEE International Conference on Communications Workshops*, June 2013, pp. 1249–1254.

[9] C. Gabriel. European commission gets behind spectrum sharing. [Online]. Available: http://www.rethink-wireless.com/2012/09/04/european-commission-behind-spectrum-sharing.htm

[10] The Saphyre project (fp7-ict-248001). [Online]. Available: http://saphyre.eu

[11] E. Jorswieck, L. Badia, T. Fahldieck, D. Gesbert, S. Gustafsson, M. Haardt, K.-M. Ho, E. Karipidis, A. Kortke, E. Larsson, H. Mark, M. Nawrocki, R. Piesiewicz, F. Römer, M. Schubert, J. Sykora, P. Trommelen, B. van den Ende, and M. Zorzi, "Resource sharing in wireless networks: The saphyre approach," in *Future Network and Mobile Summit*, June 2010, pp. 1–8.

[12] Directive 2002/21/EC of the European parliament and of the council of 7 March 2002 on a common regulatory framework for electronic communications networks and services.

[13] E. Jorswieck, L. Badia, T. Fahldieck, E. Karipidis, and J. Luo, "Spectrum sharing improves the network efficiency for cellular operators," *IEEE Communications Magazine*, vol. 52, no. 3, pp. 129–136, March 2014.

[14] B. Aazhang, J. Lilleberg, and G. Middleton, "Spectrum sharing in a cellular system," in *IEEE Eighth International Symposium on Spread Spectrum Techniques and Applications, 2004*, Aug 2004, pp. 355–359.

[15] L. Anchora, L. Badia, H. Zhang, T. Fahldieck, J. Zhang, M. Szydelko, M. Schubert, E. Karipidis, and M. Haardt, "Resource allocation and management in multi-operator cellular networks with shared physical resources," in *International Symposium on Wireless Communication Systems*, Aug 2012, pp. 296–300.

[16] R. Mochaourab and E. Jorswieck, "Optimal beamforming in interference networks with perfect local channel information," *IEEE Transactions on Signal Processing*, vol. 59, no. 3, pp. 1128–1141, March 2011.

[17] J. Laneman and G. Wornell, "Energy-efficient antenna sharing and relaying for wireless networks," in *IEEE Wireless Communications and Networking Confernce*, vol. 1, 2000, pp. 7–12 vol.1.

[18] D. Lee, H. Seo, B. Clerckx, E. Hardouin, D. Mazzarese, S. Nagata, and K. Sayana, "Coordinated multipoint transmission and reception in lte-advanced: deployment scenarios and operational challenges," *IEEE Communications Magazine*, vol. 50, no. 2, pp. 148–155, February 2012.

[19] Q. Wang, D. Jiang, G. Liu, and Z. Yan, "Coordinated multiple points transmission for lte-advanced systems," in *International Conference on Wireless Communications, Networking and Mobile Computing*, Sept 2009, pp. 1–4.

[20] M. Sawahashi, Y. Kishiyama, A. Morimoto, D. Nishikawa, and M. Tanno, "Coordinated multipoint transmission/reception techniques for lte-advanced [coordinated and distributed mimo]," *IEEE Wireless Communications*, vol. 17, no. 3, pp. 26–34, June 2010.

[21] B. Mondal, E. Visotsky, T. Thomas, X. Wang, and A. Ghosh, "Performance of downlink comp in lte under practical constraints," in *IEEE 23rd International Symposium on Personal Indoor and Mobile Radio Communications*, Sept 2012, pp. 2049–2054.

[22] A. Osseiran, F. Boccardi, V. Braun, K. Kusume, P. Marsch, M. Maternia, O. Queseth, M. Schellmann, H. Schotten, H. Taoka, H. Tullberg, M. Uusitalo, B. Timus, and M. Fallgren, "Scenarios for 5g mobile and wireless communications: the vision of the metis project," *IEEE Communications Magazine*, vol. 52, no. 5, pp. 26–35, May 2014.

[23] J. Bae, Y. S. Choi, J. S. Kim, and M. Y. Chung, "Architecture and performance evaluation of mmwave based 5g mobile communication system," in *International Conference on Information and Communication Technology Convergence*, Oct 2014, pp. 847–851.

[24] A. Apostolidis, L. Campoy, K. Chatzikokolakis, K.-J. Friederichs, T. Irnich, K. Koufos, J. Kronander, J. Luo, E. Mohyeldin, P. Olmos, T. Rosowski, H. Schotten, B. Singh, M. Tercero, O. Tirkkonen, and M. A. Uusitalo, "Intermediate description of the spectrum needs and usage principles," Metis project, D5.1 Deliverable, August 2013.

[25] D. Lopez-Perez, I. Guvenc, and X. Chu, "Mobility management challenges in 3gpp heterogeneous networks," *IEEE Communications Magazine*, vol. 50, no. 12, pp. 70–78, December 2012.

[26] Ns-3 network simulator. [Online]. Available: http://www.nsnam.org/

[27] G. Foschini and M. Gans, "On limits of wireless communications in a fading environment when using multiple antennas," *Wireless Personal Communications*, vol. 6, no. 3, pp. 311–335, 1998.

[28] H. Huang, C. B. Papadias, and S. Venkatesan, *MIMO Communication for Cellular Networks*. Springer, 2012.

[29] S. Catreux, P. Driessen, and L. Greenstein, "Data throughputs using multiple-input multiple-output (mimo) techniques in a noise-limited cellular environment," *IEEE Transactions on Wireless Communications*, vol. 1, no. 2, pp. 226–235, Apr 2002.

[30] S. Catreux, L. Greenstein, and V. Erceg, "Some results and insights on the performance gains of mimo systems," *IEEE Journal on Selected Areas in Communications*, vol. 21, no. 5, pp. 839–847, June 2003.

[31] J. Lindblom, E. Karipidis, and E. Larsson, "Closed-form parameterization of the pareto boundary for the two-user miso interference channel," in *IEEE International Conference on Acoustics, Speech and Signal Processing*, May 2011, pp. 3372–3375.

[32] E. Jorswieck, E. Larsson, and D. Danev, "Complete characterization of the pareto boundary for the miso interference channel," *IEEE Transactions on Signal Processing*, vol. 56, no. 10, pp. 5292–5296, Oct 2008.

[33] 3gpp lte toolbox and blockset. [Online]. Available: http://www.steepestascent.com/content/default.asp?page=s210

[34] Opnet lte specialized model. [Online]. Available: http://www.opnet.com/LTE/

[35] J. Ikuno, M. Wrulich, and M. Rupp, "System level simulation of lte networks," in *IEEE 71st Vehicular Technology Conference*, May 2010, pp. 1–5.

[36] G. Piro, N. Baldo, and M. Miozzo, "An lte module for the ns-3 network simulator," in *Proceedings of the 4th International ICST Conference on Simulation Tools and Techniques*, ser. SIMUTools '11, 2011, pp. 415–422.

[37] S. Alamouti, "A simple transmit diversity technique for wireless communications," *IEEE Journal on Selected Areas in Communications*, vol. 16, no. 8, pp. 1451–1458, Oct 1998.

[38] A. Ghosh, W. Xiao, R. Ratasuk, A. Rottinghaus, and B. Classon, "Multi-antenna system design for 3gpp lte," in *IEEE International Symposium on Wireless Communication Systems*, Oct 2008, pp. 478–482.

[39] Q. Li, G. Li, W. Lee, M. il Lee, D. Mazzarese, B. Clerckx, and Z. Li, "Mimo techniques in wimax and lte: a feature overview," *IEEE Communications Magazine*, vol. 48, no. 5, pp. 86–92, May 2010.

[40] R. Heath, S. Sandhu, and A. Paulraj, "Antenna selection for spatial multiplexing systems with linear receivers," *IEEE Communications Letters*, vol. 5, no. 4, pp. 142–144, April 2001.

[41] A. Paulraj, D. GORE, R. Nabar, and H. Bolcskei, "An overview of mimo communications - a key to gigabit wireless," *Proceedings of the IEEE*, vol. 92, no. 2, pp. 198–218, Feb 2004.

[42] G. Foschini, G. Golden, R. Valenzuela, and P. Wolniansky, "Simplified processing for high spectral efficiency wireless communication employing multi-element arrays," *IEEE Journal on Selected Areas in Communications*, vol. 17, no. 11, pp. 1841–1852, Nov 1999.

[43] 3GPP, "Spatial channel model for multiple input multiple output (mimo) simulations," TR 25.996 version 6.1.0, September 2003.

[44] I. Xirouchakis, "Spatial channel model for mimo simulations. a ray based simulator based on 3gpp tr 25.996 v.6.1.0." [Online]. Available: http://www.mathworks.com/matlabcentral/fileexchange/

[45] R. Pupala, L. Greenstein, and D. Daut, "Downlink throughput statistics in interference-limited cellular systems with multi-element antennas," *IEEE Transactions on Communications*, vol. 58, no. 1, pp. 311–317, January 2010.

[46] J. Lindblom and E. Larsson, "Does non-orthogonal spectrum sharing in the same cell improve the sum-rate of wireless operators?" in *IEEE 13th International Workshop on Signal Processing Advances in Wireless Communications*, June 2012, pp. 6–10.

[47] P. Mogensen, W. Na, I. Kovacs, F. Frederiksen, A. Pokhariyal, K. Pedersen, T. Kolding, K. Hugl, and M. Kuusela, "Lte capacity compared to the shannon bound," in *IEEE 65th Vehicular Technology Conference*, April 2007, pp. 1234–1238.

[48] [Online]. Available: http://code.nsnam.org/lanchora/ns-3-lte-SpectrumSharing.

[49] L. Anchora, M. Mezzavilla, L. Badia, and M. Zorzi, "A performance evaluation tool for spectrum sharing in multi-operator {LTE} networks," *Computer Communications*, vol. 35, no. 18, pp. 2218 – 2226, 2012. [Online]. Available: http://www.sciencedirect.com/science/article/pii/S0140366412002678

[50] X. Ge, X. Huang, Y. Wang, M. Chen, Q. Li, T. Han, and C.-X. Wang, "Energy-efficiency optimization for mimo-ofdm mobile multimedia communication systems with qos constraints," *IEEE Transactions on Vehicular Technology*, vol. 63, no. 5, pp. 2127–2138, June 2014.

[51] L. Anchora, L. Badia, E. Karipidis, and M. Zorzi, "Capacity gains due to orthogonal spectrum sharing in multi-operator lte cellular networks," in *International Symposium on Wireless Communication Systems*, Aug 2012, pp. 286–290.

[52] E. G. Larsson and P. Stoica, *Space-Time Block Coding for Wireless Communications*. Cambridge, U.K.: Cambridge Uni. Press, 2003.

[53] E. Larsson and E. Jorswieck, "Competition versus cooperation on the miso interference channel," *IEEE Journal on Selected Areas in Communications*, vol. 26, no. 7, pp. 1059–1069, September 2008.

[54] T. Yoo and A. Goldsmith, "On the optimality of multiantenna broadcast scheduling using zero-forcing beamforming," *IEEE Journal on Selected Areas in Communications*, vol. 24, no. 3, pp. 528–541, March 2006.

[55] L. Canzian, L. Badia, and M. Zorzi, "Promoting cooperation in wireless relay networks through stackelberg dynamic scheduling," *IEEE Transactions on Communications*, vol. 61, no. 2, pp. 700–711, February 2013.

[56] T. Pham and N. Turkkan, "Reliability of a standby system with beta-distributed component lives," *IEEE Transactions on Reliability*, vol. 43, no. 1, pp. 71–75, Mar 1994.

[57] P. Nuggehalli, M. Sarkar, and R. Rao, "Qos and selfish users: A mac layer perspective," in *IEEE Global Telecommunications Conference*, Nov 2007, pp. 4719–4723.

[58] L. Kleinrock, *Queueing Systems*. John Wiley & Sons, Inc., New York, NY, 1975, vol. 1.

[59] R. K. Jain, Dah-Ming Chiu, and W. Hawe, "A quantitative measure of fairness and discrimination for resource allocation in shared computer system," *ACM Transaction on Computer Systems*, 1984.

[60] A. Papadogiannis, D. Gesbert, and E. Hardouin, "A dynamic clustering approach in wireless networks with multi-cell cooperative processing," in *IEEE International Conference on Communications*, May 2008, pp. 4033–4037.

[61] J.-M. Moon and D.-H. Cho, "Formation of cooperative cluster for coordinated transmission in multi-cell wireless networks," in *IEEE Consumer Communications and Networking Conference*, Jan 2013, pp. 528–533.

[62] P. Baracca, F. Boccardi, and V. Braun, "A dynamic joint clustering scheduling algorithm for downlink comp systems with limited csi," in *International Symposium on Wireless Communication Systems*, Aug 2012, pp. 830–834.

[63] J. Gong, S. Zhou, Z. Niu, L. Geng, and M. Zheng, "Joint scheduling and dynamic clustering in downlink cellular networks," in *IEEE Global Telecommunications Conference*, Dec 2011, pp. 1–5.

[64] A. Papadogiannis, E. Hardouin, and D. Gesbert, "Decentralising multicell cooperative processing: a novel robust framework," *EURASIP Journal on Wireless Communication Networks*, February 2009.

[65] S. Zhou, J. Gong, Z. Niu, Y. Jia, and P. Yang, "A decentralized framework for dynamic downlink base station cooperation," in *IEEE Global Telecommunications Conference*, November 2009, pp. 1–6.

[66] Z. Khan, S. Glisic, L. DaSilva, and J. Lehtomäki, "Modeling the dynamics of coalition formation games for cooperative spectrum sharing in an interference channel," *IEEE Transactions on Computational Intelligence and AI in Games*, vol. 3, no. 1, pp. 17–30, March 2011.

[67] W. Saad, Z. Han, M. Debbah, and A. Hjorungnes, "A distributed coalition formation framework for fair user cooperation in wireless networks," *IEEE Transactions on Wireless Communications*, vol. 8, no. 9, pp. 4580–4593, September 2009.

[68] R. Irmer, H. Droste, P. Marsch, M. Grieger, G. Fettweis, S. Brueck, H.-P. Mayer, L. Thiele, and V. Jungnickel, "Coordinated multipoint: Concepts, performance, and field trial results," *IEEE Communications Magazine*, vol. 49, no. 2, pp. 102–111, February 2011.

[69] T. Rappaport, S. Sun, R. Mayzus, H. Zhao, Y. Azar, K. Wang, G. Wong, J. Schulz, M. Samimi, and F. Gutierrez, "Millimeter wave mobile communications for 5g cellular: It will work!" *IEEE Access*, vol. 1, pp. 335–349, 2013.

[70] W. Roh, J.-Y. Seol, J. Park, B. Lee, J. Lee, Y. Kim, J. Cho, K. Cheun, and F. Aryanfar, "Millimeter-wave beamforming as an enabling technology for 5g cellular communications: theoretical feasibility and prototype results," *IEEE Communications Magazine*, vol. 52, no. 2, pp. 106–113, February 2014.

[71] T. Kim, J. Park, J.-Y. Seol, S. Jeong, J. Cho, and W. Roh, "Tens of gbps support with mmwave beamforming systems for next generation communications," in *IEEE Global Communications Conference*, December 2013, pp. 3685–3690.

[72] S. Rangan, T. Rappaport, and E. Erkip, "Millimeter-wave cellular wireless networks: Potentials and challenges," *Proceedings of the IEEE*, vol. 102, no. 3, pp. 366–385, March 2014.

[73] M. Akdeniz, Y. Liu, M. Samimi, S. Sun, S. Rangan, T. Rappaport, and E. Erkip, "Millimeter wave channel modeling and cellular capacity evaluation," *IEEE Journal on Selected Areas in Communications*, vol. 32, no. 6, pp. 1164–1179, June 2014.

[74] T. Bai, V. Desai, and R. Heath, "Millimeter wave cellular channel models for system evaluation," in *International Conference on Computing, Networking and Communications*, Feb 2014, pp. 178–182.

[75] S. Hur, Y. J. Cho, K. Lee, J. H. Ko, and J. Park, "Millimeter-wave channel modeling based on measurements in in-building and campus environments at 28 ghz," *Korea*, 2014.

[76] CoRaSat project, "Service and market requirememts," D.2.1 Deliverable, Tech. Rep., October 2013.

[77] ITU-R M.2109, "Sharing studies between imt advanced systems and geostationary satellite networks in the fixed-satellite service in the 3400-4200 and 4500-4800 mhz frequency bands," Tech. Rep., 2007.

[78] ITU-R 4-5-6-7/TEMP/139-E, "Sharing and compatibility between imt system and fixed-satellite service network in 5850-6425 mhz frequency range," Tech. Rep., February 2007.

[79] S. Sharma, S. Chatzinotas, and B. Ottersten, "Satellite cognitive communications: Interference modeling and techniques selection," in *Advanced Satellite Multimedia Systems Conference and 12th Signal Processing for Space Communications Workshop*, Sept 2012, pp. 111–118.

[80] J.-W. Lim, H.-S. Jo, H.-G. Yoon, and J.-G. Yook, "Interference mitigation technique for the sharing between imt-advanced and fixed satellite service," *Journal of Communications and Networks*, vol. 9, no. 2, pp. 159–166, June 2007.

[81] D.-S. Oh, S. min Lee, D.-S. Ahn, and S. Kim, "A study on the separation distance for frequency sharing between gso network and terrestrial network in ka band," in *IEEE Vehicular Technology Conference*, May 2008, pp. 2967–2971.

[82] S. Sharma, S. Chatzinotas, and B. Ottersten, "Transmit beamforming for spectral coexistence of satellite and terrestrial networks," in *8th International Conference on Cognitive Radio Oriented Wireless Networks*, July 2013, pp. 275–281.

[83] D. Monderer and L. Shapley, "Potential games," *Games and Economic Behavior*, pp. 124–143, 1996.

[84] N. Nie and C. Comaniciu, "Adaptive channel allocation spectrum etiquette for cognitive radio networks," in *IEEE International Symposium on New Frontiers in Dynamic Spectrum Access Networks*, Nov 2005, pp. 269–278.

[85] S. Buzzi, G. Colavolpe, D. Saturnino, and A. Zappone, "Potential games for energy-efficient power control and subcarrier allocation in uplink multicell ofdma systems," *IEEE Journal of Selected Topics in Signal Processing,*, vol. 6, no. 2, pp. 89–103, April 2012.

[86] F.-W. Chen and J.-C. Kao, "Game-based broadcast over reliable and unreliable wireless links in wireless multihop networks," *IEEE Transactions on Mobile Computing*, vol. 12, no. 8, pp. 1613–1624, Aug 2013.

[87] ITU-R P.452-15, "Prediction procedure for the evaluation of interference between stations on the surface of the earth at frequencies above about 0.1 ghz," Tech. Rep., September 2013.

[88] ITU-R S.465, "Reference radiation pattern for earth station antennas in the fixed-satellite service for use in coordination and interference assessment in the frequency range from 2 to 31 ghz," Tech. Rep., January 2010.

[89] A. Alkhateeb, O. El Ayach, G. Leus, and R. Heath, "Hybrid precoding for millimeter wave cellular systems with partial channel knowledge," in *Information Theory and Applications Workshop*, February 2013, pp. 1–5.

[90] ITU-R SF.558-2, "Maximum allowable values of interference from terrestrial radio links to systems in the fixed-satellite service employing 8-bit pcm encoded telephony and sharing the same frequency bands," Tech. Rep., July 1986.

[91] ITU-R Rec. S.1432, "Apportionment of the allowable error performance degradation to fixed-satellite service (fss) hypothetical reference digital paths arising from time invariant interference for system operating below 30 ghz," Tech. Rep., January 2000.

[92] G. T. 36.839, "Evolved universal terrestrial radio access (e-utra); mobility enhancements in heterogeneous networks (release 11)," Tech. Rep. version 11.0.0, September 2012.

[93] G. T. 36.331, "Protocol specification; radio resource control," Tech. Rep. v.10.4.0, December 2011.

[94] Q. Liao, F. Penna, S. Stanczak, Z. Ren, and P. Fertl, "Context-aware handover optimization for relay-aided vehicular terminals," in *IEEE 14th Workshop on Signal Processing Advances in Wireless Communications*, June 2013, pp. 555–559.

[95] M. Peng, D. Liang, Y. Wei, J. Li, and H.-H. Chen, "Self-configuration and self-optimization in lte-advanced heterogeneous networks," *IEEE Communications Magazine*, vol. 51, no. 5, pp. 36–45, May 2013.

[96] D. Xenakis, N. Passas, L. Merakos, and C. Verikoukis, "Mobility management for femtocells in lte-advanced: Key aspects and survey of handover decision algorithms," *IEEE Communications Surveys Tutorials*, vol. 16, no. 1, pp. 64–91, First 2014.

[97] K. Kitagawa, T. Komine, T. Yamamoto, and S. Konishi, "A handover optimization algorithm with mobility robustness for lte systems," in *IEEE 22nd International Symposium on Personal Indoor and Mobile Radio Communications*, Sept 2011, pp. 1647–1651.

[98] Y. Lee, B. Shin, J. Lim, and D. Hong, "Effects of time-to-trigger parameter on handover performance in son-based lte systems," in *16th Asia-Pacific Conference on Communications*, Oct 2010, pp. 492–496.

[99] K. Kitagawa, T. Komine, T. Yamamoto, and S. Konishi, "Performance evaluation of handover in lte-advanced systems with pico cell range expansion," in *IEEE 23rd Inter-*

national Symposium on Personal Indoor and Mobile Radio Communications, Sept 2012, pp. 1071–1076.

[100] S. Barbera, P. Michaelsen, M. Saily, and K. Pedersen, "Improved mobility performance in lte co-channel hetnets through speed differentiated enhancements," in *IEEE Globecom Workshops*, December 2012, pp. 426–430.

[101] I. Guvenc, "Capacity and fairness analysis of heterogeneous networks with range expansion and interference coordination," *IEEE Communications Letters*, vol. 15, no. 10, pp. 1084–1087, October 2011.

[102] A. Lobinger, S. Stefanski, T. Jansen, and I. Balan, "Coordinating handover parameter optimization and load balancing in lte self-optimizing networks," in *IEEE 73rd Vehicular Technology Conference*, May 2011, pp. 1–5.

[103] A. Goldsmith, *Wireless Communications*. Cambridge University Press, New York, NJ, 2005.

[104] M. Zorzi, "Outage and error events in bursty channels," *IEEE Transactions on Communications*, vol. 46, no. 3, pp. 349–356, Mar 1998.

[105] Q. Ye, B. Rong, Y. Chen, M. Al-Shalash, C. Caramanis, and J. Andrews, "User association for load balancing in heterogeneous cellular networks," *IEEE Transactions on Wireless Communications*, vol. 12, no. 6, pp. 2706–2716, June 2013.

[106] R. Tanbourgi, S. Singh, J. Andrews, and F. Jondral, "Analysis of non-coherent joint-transmission cooperation in heterogeneous cellular networks," in *IEEE International Conference on Communications*, June 2014, pp. 5160–5165.

Acknowledgments

Questa tesi non ci sarebbe senza Leonardo Badia, Maziar Nekovee e Prof. Michele Zorzi. Grazie per il vostro prezioso supporto.

Desidero anche ringraziare tutti i miei colleghi e amici, senza di voi probabilmente non sarei arrivato a questo traguardo.

Infine un pensiero va ad Urska, grazie per essermi vicina in ogni mia scelta.